Evaluation of Low Noise Integration Concepts and Propulsion Technologies for Future Supersonic Civil Transports

Kishore Ramakrishnan, Umesh Paliath, Nikolai Pastouchenko, and Ivan Malcevic
GE Global Research, Niskayuna, New York

Anthony Pilon, John Morgenstern, and Michael Buonanno
Lockheed Martin, Palmdale, California

Michael Martinez and Muni Majjigi
GE Aviation, Evendale, Ohio

NASA STI Program . . . in Profile

Since its founding, NASA has been dedicated to the advancement of aeronautics and space science. The NASA Scientific and Technical Information (STI) Program plays a key part in helping NASA maintain this important role.

The NASA STI Program operates under the auspices of the Agency Chief Information Officer. It collects, organizes, provides for archiving, and disseminates NASA's STI. The NASA STI Program provides access to the NASA Technical Report Server—Registered (NTRS Reg) and NASA Technical Report Server—Public (NTRS) thus providing one of the largest collections of aeronautical and space science STI in the world. Results are published in both non-NASA channels and by NASA in the NASA STI Report Series, which includes the following report types:

- TECHNICAL PUBLICATION. Reports of completed research or a major significant phase of research that present the results of NASA programs and include extensive data or theoretical analysis. Includes compilations of significant scientific and technical data and information deemed to be of continuing reference value. NASA counter-part of peer-reviewed formal professional papers, but has less stringent limitations on manuscript length and extent of graphic presentations.

- TECHNICAL MEMORANDUM. Scientific and technical findings that are preliminary or of specialized interest, e.g., "quick-release" reports, working papers, and bibliographies that contain minimal annotation. Does not contain extensive analysis.

- CONTRACTOR REPORT. Scientific and technical findings by NASA-sponsored contractors and grantees.

- CONFERENCE PUBLICATION. Collected papers from scientific and technical conferences, symposia, seminars, or other meetings sponsored or co-sponsored by NASA.

- SPECIAL PUBLICATION. Scientific, technical, or historical information from NASA programs, projects, and missions, often concerned with subjects having substantial public interest.

- TECHNICAL TRANSLATION. English-language translations of foreign scientific and technical material pertinent to NASA's mission.

For more information about the NASA STI program, see the following:

- Access the NASA STI program home page at http://www.sti.nasa.gov

- E-mail your question to help@sti.nasa.gov

- Fax your question to the NASA STI Information Desk at 757-864-6500

- Telephone the NASA STI Information Desk at 757-864-9658

- Write to:
  NASA STI Program
  Mail Stop 148
  NASA Langley Research Center
  Hampton, VA 23681-2199

Evaluation of Low Noise Integration Concepts and Propulsion Technologies for Future Supersonic Civil Transports

Kishore Ramakrishnan, Umesh Paliath, Nikolai Pastouchenko, and Ivan Malcevic
GE Global Research, Niskayuna, New York

Anthony Pilon, John Morgenstern, and Michael Buonanno
Lockheed Martin, Palmdale, California

Michael Martinez and Muni Majjigi
GE Aviation, Evendale, Ohio

Acknowledgments

Level of Review: This material has been technically reviewed by NASA expert reviewer(s).

Available from

NASA STI Program	National Technical Information Service
Mail Stop 148	5285 Port Royal Road
NASA Langley Research Center	Springfield, VA 22161
Hampton, VA 23681-2199	703-605-6000

This report is available in electronic form at http://www.sti.nasa.gov/ and http://ntrs.nasa.gov/

Contents

List of Figures

List of Tables

Executive Summary

This report covers the entire effort of GE Global Research's NASA Prime Contract NNC15CA02C "Evaluation of Low Noise Integration Concepts and Propulsion Technologies for Future Supersonic Civil Transports". GE Global Research was supported by GE Aviation and Lockheed Martin in exploring the potential of wing shielding, flight path optimization, and jet noise technology to target aggressive community noise levels of 10 EPNdB lower than Chapter 14 for a future (mid-term) commercial supersonic transport aircraft. It builds on Phase II of the NASA sponsored 'N+2 NRA—System Level Experimental Validations for Supersonic Transport Aircraft' program (Ref. 1) (Lockheed Martin Prime Contract NNC10CA02C) and uses the same LM-1044 aircraft and GE propulsion system to perform noise and boom/performance assessments.

Our study shows that up to 10 EPNdB cum. noise benefit can be achieved with wing shielding. Flight path optimization through automatic throttle reduction at takeoff yields 3-4 EPNdB. Increasing approach glide slope from 3° to 4.5° gives another 4 EPNdB cum. Finally, jet noise reduction with an improved chevron design is expected to yield upwards of 2 EPNdB cum. These technologies are not necessarily additive but by judicious combination, community noise levels well below Chapter 14 may be achieved. And while the reduction in L/D is approximately 7 percent for this installation, improving nacelle fineness ratio could considerably mitigate the adverse impact.

A system level noise assessment is first performed to identify the potential of noise technologies as well as the dominant noise sources for high-fidelity analysis. The baseline system noise model developed in the prior program (Ref. 1) was updated to correctly account for fan, jet, and airframe noise sources on consistent trajectories at all three certification conditions. With the improved noise model, the aircraft is shown to nominally meet Chapter 4 regulation.

Using a fan noise suppression of 10 dB assumed from prior isolated CAA studies and jet noise suppressions derived from NASA's JSI code (Ref. 2), wing shielding is shown to attain benefits up to 10 EPNdB, similar to those published in subsonic studies (Ref. 3). Wing shielding also significantly reduces the importance of fan noise for the installation considered here. Noise sensitivity to thrust Programmed Lapse Rate (PLR) and cutback throttle as well as steeper landing approaches were also investigated. Takeoff trajectories were provided by Lockheed Martin and meet airplane safety and Takeoff Field Length (TOFL) requirements. The results of the analysis show that PLR is required to meet the sideline noise constraint for this aircraft. Significant noise reduction at approach can be realized if the airplane could be certified for a higher approach glide slope, with our study showing nearly 4 EPNdB reduction with an increase in glide slope from 3° to 4.5°.

Distortion ingested by the fan and resulting noise source increases were studied using installed steady CFD. A multistage fan was mated with the N+2 inlet and LM-1044 aircraft for this study. Installed CFD at the sideline condition was performed at two different engine positions for the outboard engines over the wing, with the most upstream location providing the best shielding within constraints of vehicle balance requirements. Fan inlet distortion was shown to increase noise, but not substantially at this condition. More detailed assessments at multiple angles of attack were performed for the most upstream engine location at Approach. The auxiliary door opening was maintained at the nominal level required for sideline thrust. For certain angles of attack and fan inlet mass flows, inlet lip separation led to significant distortion being ingested by the fan which could result in a fan noise increase on the order of 3 dB. The impact on fan operability was not evaluated.

However, wing shielding is expected to more than offset the increase in fan noise arising due to ingested distortion. This is confirmed by fan tone CAA of a simplified flow-through nacelle and wing surface at the Approach condition. For frequencies typical of fan blade passing fundamental and harmonics, shielding benefits are greater than 10 dB everywhere except the shallowest forward angles. These shallow angles would be most affected by spherical spreading for an observer below the aircraft flight path. Shielding benefits predicted using high fidelity analysis are thus better than the values assumed in the system noise assessments.

An LES analysis of the exhaust nozzle installed over the wing for one of the outboard engines was performed at sideline thrust to confirm the assumed shielding benefits for the system level noise studies. Farfield noise results were compared to an isolated nozzle as well as the shielding results predicted by the NASA JSI code (Ref. 2). The predictions closely track the JSI model but show higher benefit in the mid-high frequency range for all angles. Thus, the assumed shielding benefits derived from the JSI code are conservative, increasing confidence in the predicted shielded system noise levels.

Starting from the chevrons designed in the previous program (Ref. 1), variations of chevron count, penetration and position were explored for increased noise benefit. RANS flow fields of isolated chevron nozzles at the sideline condition were used to supply noise source information to the GENO code (Ref. 4) to predict farfield noise. Spectral differences between the baseline and chevrons were used to assess an EPNL benefit in conjunction with the assumed wing shielding benefits from the JSI code. A combination of increased chevron count and wing shielding are predicted to achieve approximately 1.2 EPNdB reduction relative to the baseline at sideline. Benefit at flyover and approach were not assessed, but with even with a fractional realization of the sideline benefits, over 2 EPNdB cum. of noise reduction is possible. Since the projected noise benefit is significant, acoustic testing of the improved chevrons with shielding is recommended in the NASA Glenn Research Center Aero-Acoustic Propulsion Laboratory (AAPL) facility.

Lockheed Martin performed sonic boom and cruise performance assessments on the installed geometry with the outboard engines at the most upstream location feasible within vehicle balance constraints. The analysis shows similar boom loudness potential for either engine location, with perhaps a dB or two better potential near the edge of the sonic boom carpet for engines over the wing. However, the L/D loss of engines over the wing was approximately 7 percent, primarily due to the loss of propulsion-induced lift of underwing nacelles. Preliminary estimates show that this penalty could be considerably mitigated by increasing the nacelle fineness ratio. A focused study that takes into consideration engine diameter and accessory placement trades is desirable.

In this study, we assessed benefits of noise technologies conceptually and verified shielding benefits using high fidelity analysis. The results of this study show that a future supersonic transport with quiet shaped sonic boom could achieve community noise levels below Chapter 14 with wing shielding, flight path optimization using takeoff thrust PLR and steeper approach along with improved jet noise technologies, accounting for realization of technology maturation. As a next step, performance and weight trades as well as the regulatory environment and safety considerations need to be assessed in more detail to determine the most practical combination of these solutions to the supersonic community noise challenge.

Evaluation of Low Noise Integration Concepts and Propulsion Technologies for Future Supersonic Civil Transports

Kishore Ramakrishnan, Umesh Paliath, Nikolai Pastouchenko, and Ivan Malcevic
GE Global Research
Niskayuna, New York 12309

Anthony Pilon, John Morgenstern, and Michael Buonanno
Lockheed Martin
Palmdale, California 93599

Michael Martinez and Muni Majjigi
GE Aviation
Evendale, Ohio 45215

1.0   Introduction

Community noise around airports generated by low bypass turbofan engines typical of supersonic aircraft is among the key technical barriers to viable commercial supersonic flight. Aircraft noise levels for subsonics have continuously decreased, driven in part by increasingly stringent regulations (see Figure 1) and in part by technological advances including increased bypass ratio. At the time of this writing, there is no special category for supersonics and any new aircraft are expected to comply with subsonic noise regulation. With Chapter 14 rules coming into effect soon, future aircraft will need to have sufficient noise margin to allow for increased stringency as well as uncertainties during development. This program explores wing shielding, flight path optimization, and exhaust nozzle chevrons to achieve community noise levels 10 EPNdB lower than Chapter 14 for a future (mid-term) commercial supersonic transport aircraft.

The deliverables of the current contract on Subtopic 2.2.2: Low Noise Technologies for Low Boom Aircraft: Achieving Chapter 14 minus 10EPNdB under NRA NNH14ZEA001N-HS1are as follows:

- Assessment of installation and propulsion noise reduction concepts to enable goal.
- Evaluate impact of noise technologies on sonic boom and cruise efficiency.
- List of technologies for further investigation/developments needed to meet or exceed goal.

The program was structured to first quantify noise benefits of various concepts (including shielding) at a system level and verify/refine these projections subsequently in Year 2. Program tasks by year are listed below:

Task/Year 1: System-level Study of Noise Reduction Concepts and their Impact on Cruise Performance

1.1 Baseline installed system noise quantification.
1.2 Conceptual system-level assessment of wing shielding and noise reduction technologies.
1.3 Initial assessment of fan distortion impact on sideline noise.
1.4 Initial assessment of cruise efficiency and sonic boom impact (Lockheed Martin).
1.5 Program management.
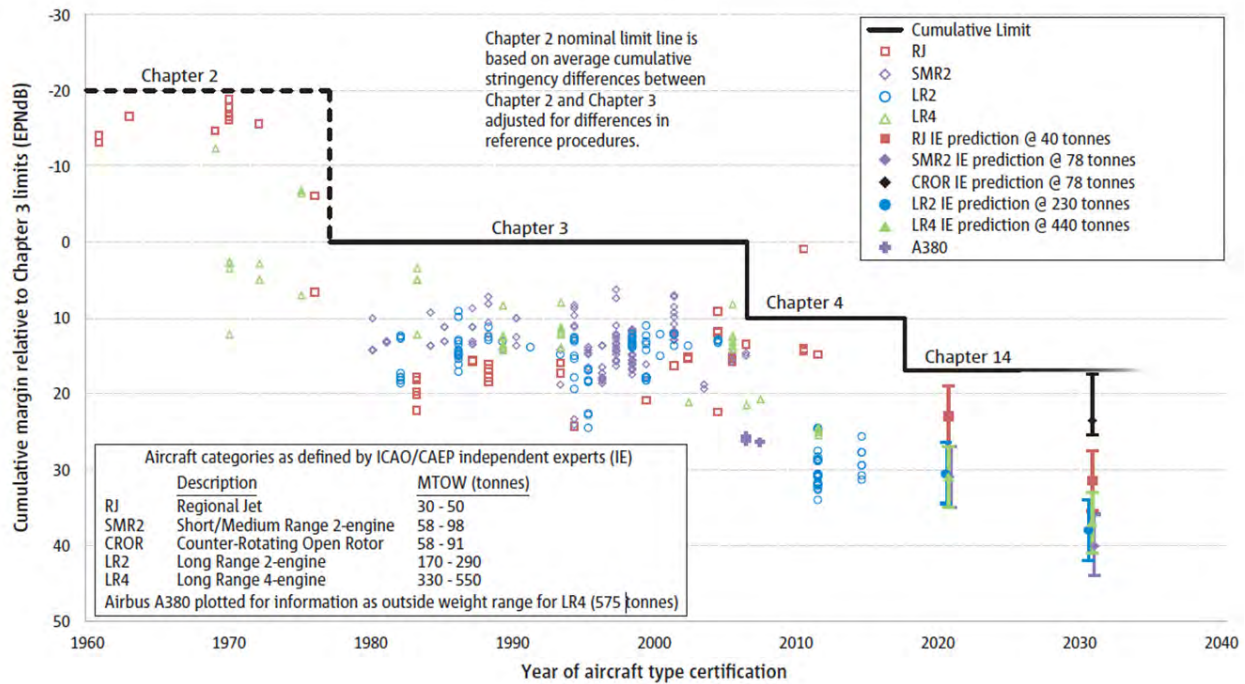
Figure 1.—Aircraft noise reduction over time (Source: European Annual Environmental Report 2016).

Based on the findings of the conceptual studies of Year 1, the second year's tasks were modified to focus on the key noise sources with shielding. Year 2 tasks are listed below.

Task/Year 2: High Fidelity Verification of Conceptual Benefits

2.1 Initial assessment of fan distortion impact at Approach.
2.2 Fan Tone CAA verification of wing shielding benefits.
2.3 LES verification of wing shielding benefits for exhaust noise.
2.4 Exploration of chevron design space for exhaust noise benefit.
2.5 Refined assessment of cruise efficiency and sonic boom impact (Lockheed Martin).
2.6 Aircraft noise sensitivity to trajectory (GE Aviation).
2.7 Program management.

The following sections document in detail the results of the work performed on these tasks to achieve the contract deliverables. Features of the propulsion system that are relevant to this program are summarized, drawing from the prior work (Ref. 1). Then, the system level noise studies are discussed. This includes the conceptual shielding studies (Task 1.2) as well as a summary of the trajectory sensitivity study (Task 2.6). Next, fan noise and installation studies are described. This includes engine placement studies performed in Year 1 to assess distortion effects on the fan at the sideline condition (Task 1.3) as well as Tasks 2.1 and 2.2. Jet exhaust noise studies (Tasks 2.3 and 2.4) are discussed next, following which Lockheed Martin's analysis of sonic boom and cruise performance of over-wing engine mounting are summarized. Finally, technology status and recommendations for future work are discussed. Details of the subcontractor tasks are discussed in the Appendix.

2.0 Propulsion System

2.1 Propulsion System Overview

No new propulsion system design work was performed in this contract. Noise relevant features of the propulsion system designed in the N+2 Ph2. Ext. program (Ref. 1) are summarized here.

The advanced Adaptive Cycle Engine (ACE) uses VAATE Phase II level technologies with a TRL 6 date of 2018. The engine architecture includes adaptive cycle features. For instance, since the exhaust system design is very important for supersonic vehicles for both performance and noise, the basic exhaust concept is a variable A8 and A9 (throat and exit area, respectively) through the use of a translating plug and cowl. The translating cowl also provides for a thrust reversing system.

A range of engine sizes and fan pressure ratios (FPR) were studied in Reference 1 and a FPR representing a compromise between noise and performance/weight was chosen. For the purposes of the current program therefore, variations to the cycle were not considered.

3.0 System Level Noise Assessments

3.1 Baseline Noise Assessment

The baseline system noise model from the N+2 Ph2. Ext. program in 2014 (Ref. 1) was refined to include: airframe noise, improved liner assumptions for fan noise attenuation, and spectral combination of component noise levels on consistent trajectories. After accounting for installation, the resulting baseline N+2 system noise margin is 10.2 EPNdB to Chapter 3 or 0.2 EPNdB to Chapter 4. This is well below the target of Chapter 14 minus 10 EPNdB for the program and well short of even nominally meeting Chapter 14. Thus, additional noise technologies being investigated in this program are crucial to meeting the noise goal.

3.1.1 Assumptions and Inputs

3.1.1.1 Trajectory

The N+2 Ph2 trajectory with PLR and deep cutback was used for the baseline system noise assessment previously. PLR can be thought of as a Variable Noise Reduction system (VNRS) that automatically reduces engine throttle during takeoff after obstacle clearance and before the takeoff cutback with the objective of reducing the peak sideline noise that generally occurs around 800 to 1000 ft above ground level.

For consistency with the N+2 Ph.2 Ext. program, the same trajectory (henceforth referred to as the baseline trajectory) is used in the noise analysis here, and the engine cycle conditions on which the fan and jet noise source models are based correspond to this trajectory, Figure 6 in Appendix B. Effect of different departure and landing trajectories on noise will be discussed in a separate section as well as in the GE Aviation and Lockheed Martin reports in the Appendix.

3.1.1.2 Noise Source Models: Airframe

Airframe noise was calculated by Lockheed Martin using ANOPP2. The predicted airframe EPNL at the certification conditions was then used to correct predictions of airframe noise using a GE generic airframe noise model. To ensure consistency with the Lockheed Martin calculation, the GE predicted spectra are calibrated to obtain the same EPNL as Lockheed Martin's prediction by applying a constant suppression value as a function of frequency and angle. Once calibrated, the GE airframe noise model is then flown along with the fan and jet noise components within our proprietary noise prediction codes to predict overall aircraft system noise. By this calibration process, consistency in airframe noise EPNLs is ensured.

3.1.1.3   Noise Source Models: Fan

Fan noise for this multistage fan was predicted using a GE Proprietary noise module "HiFan" (developed during the HSR program) which uses the Heidmann fan noise module (Ref. 5) akin to ANOPP2. This tool was used to estimate only the inlet radiated noise. Aft radiated fan noise was not assessed due to the dominance of jet and the possibility of lining the long length of the exhaust. Consistent with the CFD predictions from the N+2 Ph2 Ext. program, the source models show that the noise from the primary fan is dominant over the FLADE stream. Therefore, no changes were made to this source model, but inlet suppression due to acoustic treatment was applied when the sources were "flown" on the airplane flight path.

3.1.1.4   Noise Source Models: Jet

Jet noise source data are taken from NASA Glenn Research Center AAPL tests of the GE nozzles as part of the N+2 Ph2 Ext. program. Test data was acquired at various nozzle pressure ratios and forward flight Mach numbers and with chevrons. No attempt is made to baseline these source levels to a parent engine database or flight test data. This could be a refinement as part of a future study.

3.1.1.5   System Noise Analysis Process

The jet noise data from the AAPL facility is first scaled to a 1 ft lossless arc after correcting for wind tunnel shear layer refraction effects at the microphones. This is then scaled to full scale and atmospheric attenuation is accounted for. The full scale spectra are then flown along the trajectory and summed spectrally with the fan and airframe noise components to compute the aircraft system noise.

Ground reflection effects as well as Extra Ground Attenuation (EGA) and Doppler shift due to source motion are included. Corrections for fan liner attenuation or installation penalties are accounted for by user supplied suppression arrays on the noise components as a function of third octave band center frequencies and angle. No installation penalty is applied for the jet. EPNLs are obtained by integrating the PNLT time history of the entire aircraft system from the peak to 10 dB down levels in half second intervals and accounting for the duration correction.

3.1.2   Liner Attenuation

Figure 2 compares a publicly available modern high bypass ratio fan cross section to the N+2 inlet featuring fan tone CAA predictions from the N+2 Ph2. Ext. program. Comparing the cross sections shows that the area available for attenuation for a given duct area is potentially four times higher than a typical commercial engine assuming an effective treatment length of 80 percent of inlet area and including a centerbody liner. This significantly reduces fan noise at approach and flyover.
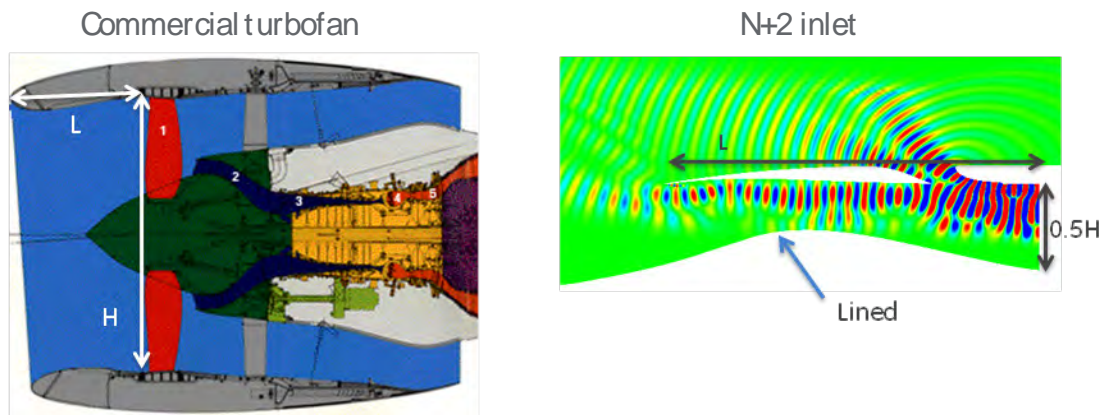
Figure 2.—Comparison of typical commercial and N+2 inlet cross sections.

3.1.3   Installation Effects

The following approach is used to quantify wing installation penalty for fan noise reflection for the under-wing engines:

1. Use N+2 Ph. 2 Ext. fan tone CAA directivity to determine over which angles the reflection penalty should be applied.
2. Construct fan radiation/reflection pattern for the under-wing engines, compute the angle subtended by the airframe to the noise radiating from the fan. All noise radiating upward from the fan encountering the airframe is assumed to reflect down towards the ground.
3. The over-wing engine is assumed to be fully shielded. No credit is taken for jet noise shielding of the over-wing engine and no penalties applied to jet noise for the under-wing engines although there may be some increase in noise for under-wing installation.

Figure 3 shows this schematically. Going a little further than10 dB below the peak lobe in the fan noise directivity, two lines representing the forward (30°) and aft (110°) limits of radiated noise are drawn from the origin on the engine axis. These lines are then revolved about the axis to where they intersect the fuselage and wing as shown in Figure 4. These surfaces represent the solid angle of the fan noise radiation that would encounter the airframe and reflect towards an observer on the ground. Interestingly, the angle subtended by the fuselage and wing is approximately 180° for both the forward and aft limits. Thus, half the noise radiated by the fan is reflected by the airframe. As a conservative approximation, it is assumed that all this reflected noise reaches the certification microphones with no corrections made for the reflected directivity.

The net result of this exercise is that fan noise increases by a factor of 4/3 or roughly 1.2 dB at each certification point. This is because fan noise for the two under-wing engines is doubled while the over-wing engine is fully shielded. Thus, fan noise from this 3-engine airplane is equivalent to that from a 4-engine airplane due to wing reflection and shielding.

- Account for fan noise reflection down to 10dB below peak radiation angle
- No jet noise reflection for below wing engine
- No jet noise shielding for above wing engine
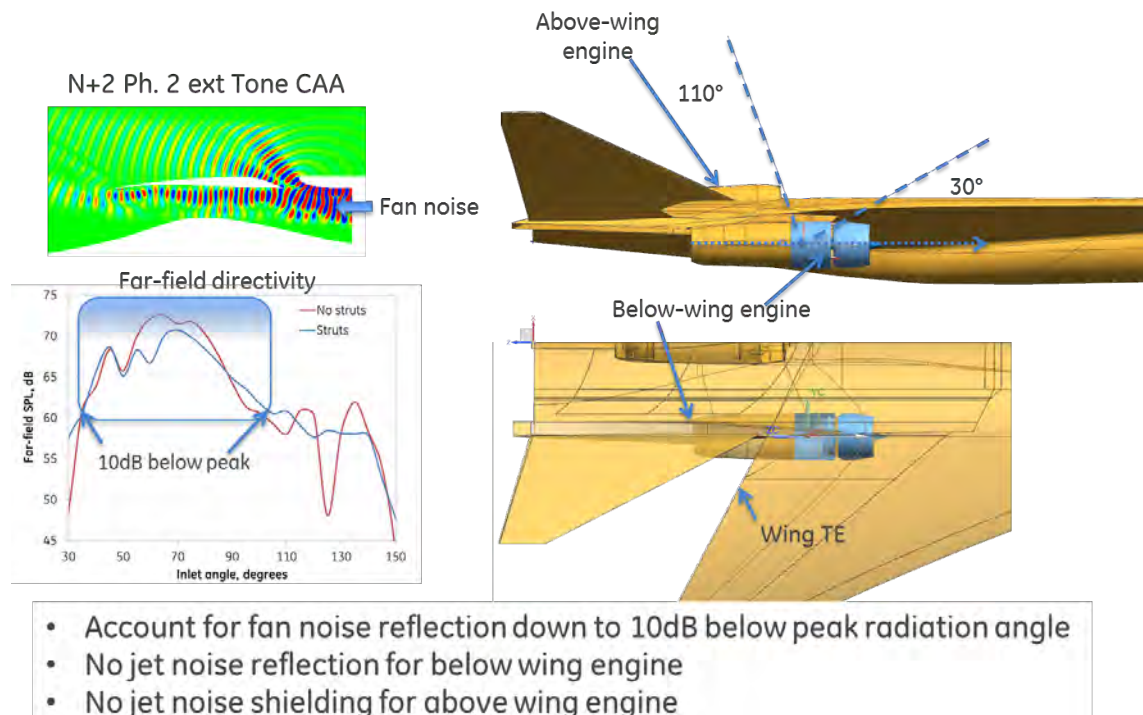
Figure 3.—Constructing installation penalties (1/2).
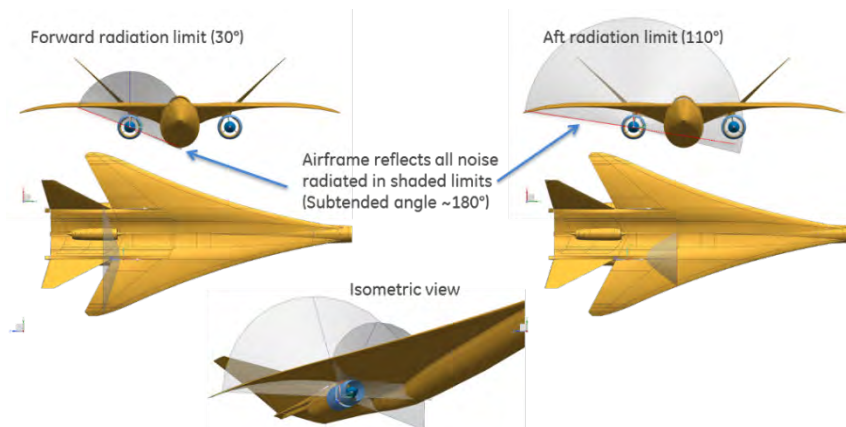
Figure 4.—Constructing installation penalties (2/2).
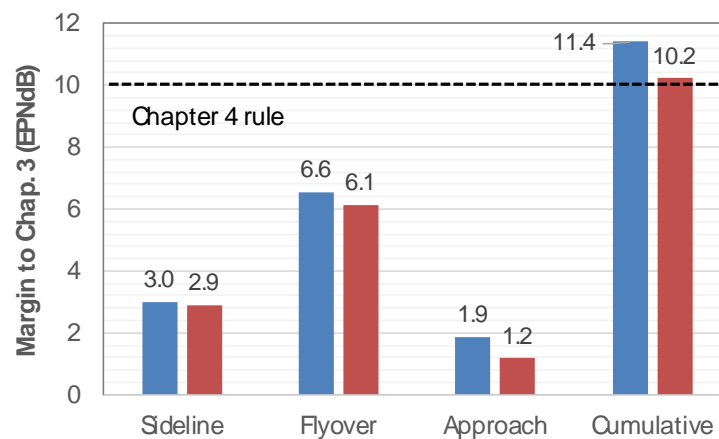
Figure 5.—Uninstalled (blue) and installed (red) baseline N+2
aircraft noise margin to Chapter 3.

3.1.4   Results of Baseline Installed System Noise Refinement

The N+2 Ph2 Ext. noise model was refined to include: airframe noise, improved liner assumptions for fan noise attenuation, and spectral combination of component noise levels on consistent trajectories. After accounting for installation, the resulting baseline N+2 system noise margin is 10.2 EPNdB to Chapter 3 or 0.2 EPNdB to Chapter 4.

At approach, fan noise is significant as expected, but jet noise can also be important due to the high thrust requirements at low speeds. Since no exhaust nozzle data was taken at the low pressure ratios typical of Approach, the data at flyover was extrapolated using a thrust correction as described in GE Aviation's report in the Appendix. The resulting margin to the rule is 1.9 EPNdB without installation penalty, and 1.2 EPNdB when the fan installation penalty is considered.

At flyover, airframe noise is not included since it is significantly below the propulsion noise sources. At sideline, overall noise levels are driven by jet noise as expected. Noise margins to the rule are shown in Figure 5. Note that the margin at sideline appears healthy, but this is due to the level of PLR used. It is shown in the trajectory sensitivity study that a takeoff without PLR results in the aircraft not meeting the sideline noise constraint.

Although uncertainties are present in the assessment, the predicted noise margin shows that this airplane would only just meet existing noise regulations even with PLR. Significant technology is thus needed to meet Chapter 14 noise regulations even nominally. This underscores the importance of wing shielding that is the focus of this program.

3.2   Wing Shielding Conceptual Study

In this section, an assessment of wing shielding benefit using the improved system noise model is described.

3.2.1   Over-Wing Engine Installation Considerations

Engine placement over the wing was guided by the key considerations listed below:

1. Maximize noise shielding benefit for both fan inlet and jet noise components:
   - Fan noise: Move engine aft
   - Jet noise: Move engine forward to maximize low frequency benefit but not so far as to cause the plume to interact with the trailing edge of the wing
2. Minimize impact to performance, stability and sonic boom:
   - Maintain engine nozzle TE to within 1D forward of reference N+2 under-wing engine. This is a credible starting point for potential redesign in a future program. A second, further aft position is considered as part of our shielding studies.
3. Minimize modifications to aircraft/engine geometry: No effort was made to redesign inlet or pylon or aircraft features for this conceptual study.

Note that turbine disk burst requirements for close placement of the three over-wing engines have not been considered yet since we are still in the acoustics feasibility phase. This must be accounted for if over-wing installation is selected as the future technology direction to go forward for a mid-term supersonic aircraft.

A baseline above-wing model is generated as shown in Figure 6 and Figure 7. A second engine configuration is shown in Figure 8. Important features of these models are listed below:

- No change in position of center engine
- Outboard (under-wing) engines rotated 180° and placed above wing
- Outboard engines moved forward (1D forward of reference engine) for the baseline over-wing position and moved aft 1D for the second position
- Outboard engines moved inboard to avoid the jet plume interacting with the tail
- Engine-wing offset for reference and over-wing model identical at pylon LE
- Pylon modified slightly to connect engines to wing smoothly for over-wing installation

Note that no changes have been made to the center engine. This engine is not modeled as part of the installed analysis in Section 4.0 or Section 5.1 either. Also, note that the details of the pylon attachment for the outboard engines are likely sub-optimal since there was no design effort to reduce pylon or attachment drag. This needs to be carefully considered in any follow-on redesign studies.
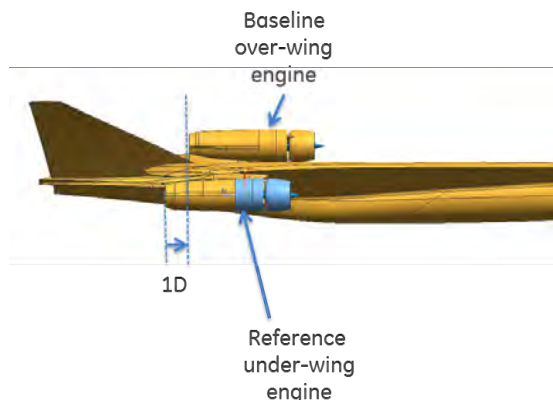
Figure 6.—Baseline above-wing engine model: Side view
with reference configuration.
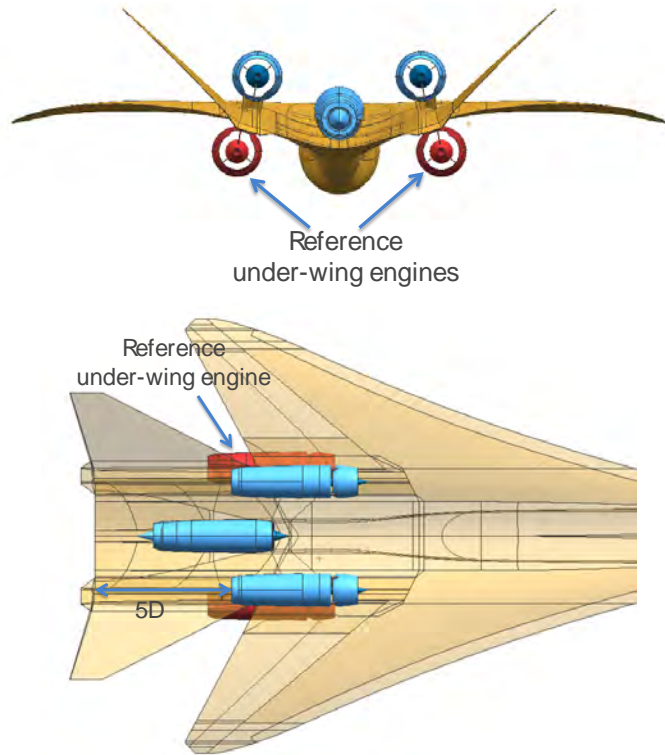
Figure 7.—Baseline above-wing engine model showing all three engines (reference engines included for comparison).
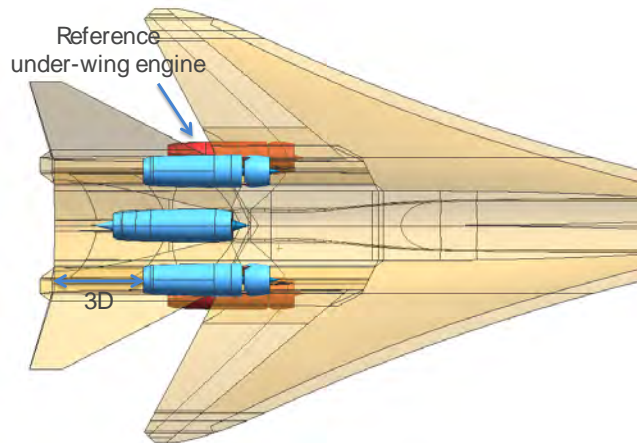
Figure 8.—Second above-wing engine model showing all three engines (reference engines included for comparison).

3.2.2 Fan Noise Shielding

As described in Section 3.1.3, fan noise for an over-wing engine is effectively shielded. A shielding suppression for fan noise of 10 dB per point is thus assumed. This will be subsequently verified by the high fidelity assessments in Section 4.3, however it is a reasonable assumption for this conceptual study.

3.2.3 Jet Noise Shielding Benefits

Figure 9 shows density gradients from an LES simulation of the cutback nozzle at a flight Mach of 0.3. As an approximate guideline, higher frequency sources are within 4.5 diameters of the nozzle exit while low frequency sources are located further downstream. So, the horizontal and vertical portions of the tail effectively shield high frequency sources. Low frequency benefits are likely to be limited at best.

The NASA JSI code (calibrated to data acquired for circular nozzles in the JSI tests) is used to estimate exhaust jet shielding benefits for the above-wing configuration. Shielding benefit is estimated using an equivalent mixed jet velocity for a reference circular nozzle. Shielding benefit for different engine placements is evaluated for both sideline and cutback conditions for various nozzle positions from the wing trailing edge.

For the purposes of the shielding calculation, X/D is the nondimensional distance in diameters of the nozzle from the wing TE and H/D is the nondimensional offset distance from the wing or tail surface. X/D = 5 corresponds to the baseline over-wing model shown in Figure 9 where the nozzle is located 5 diameters upstream of the wing TE. To account for forward flight effects, a simple x-correction for the shielding surface extent is derived by using the relative locations of the potential core at static and flight conditions (Figure 10 and Figure 11). This modified surface extent is used as input to the JSI code to obtain the shielding benefits as a function of frequency and angle. It should be noted that the presence of forward flight changes both the noise source spatial distribution as well as source strength. The current approach conceptually captures only the first effect.

In addition, the spreading rate of the jet predicted by RANS suggests that we do not expect any low frequency scrubbing noise penalty. To obtain a conservative estimate, shielding benefits are zeroed out for angles greater than 130°. The estimated shielding benefit with these assumptions is shown in Figure 12. LES simulations were performed in Year 2 of the program (reported in Section 5.0) to also account for changes in noise sources due to presence of wing surface and forward flight, and refine the shielding predictions used for system noise estimation.
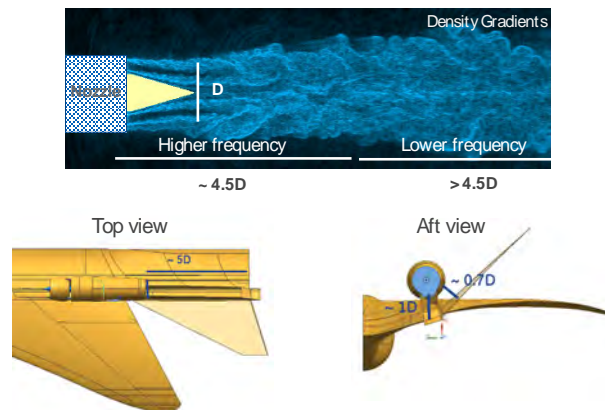
Figure 9.—LES simulation of cutback 3-stream nozzle with forward flight (M = 0.3) showing location of high frequency and low frequency sources. The baseline over-wing configuration is also shown to relate source locations to shielding benefits.
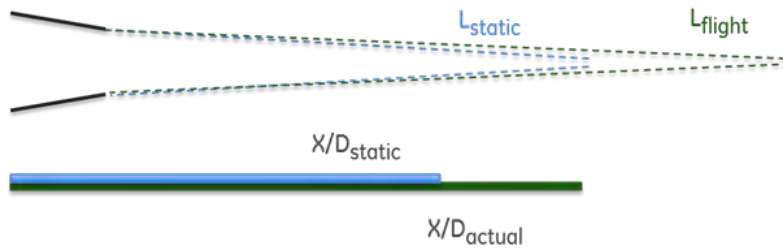
Figure 10.—Sketch to demonstrate how shielding surface extent at flight
condition is estimated based on jet potential core length ratio.
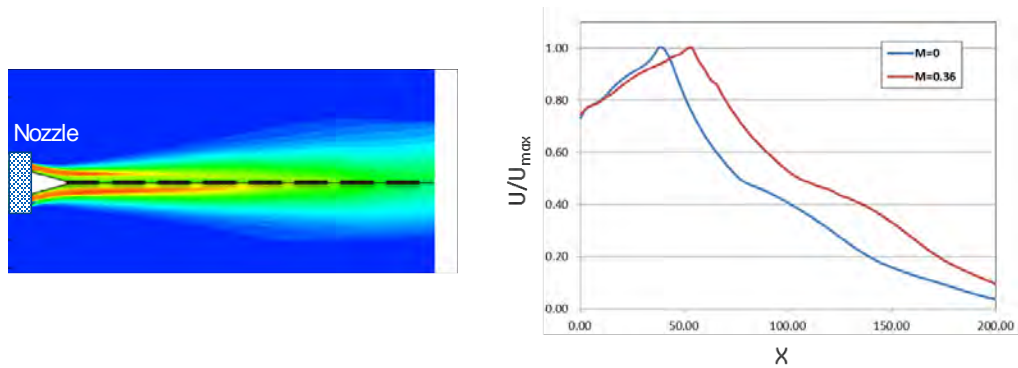
Figure 11.—CFX based RANS simulation of three stream nozzle at the sideline operating condition.
Axial velocity variation along centerline for cases with and without forward flight shown.
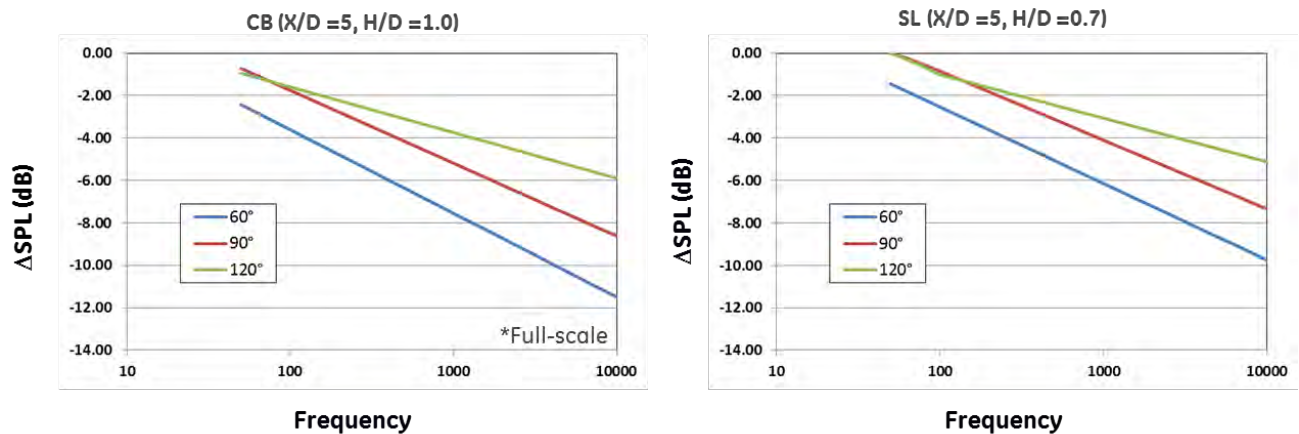
Figure 12.—Estimate of shielding benefit for engines located at X/D = 5 from wing TE using equivalent mixed out jet
velocity for cutback and sideline operating conditions.

3.2.4   Preliminary Estimate of Wing Shielding

Figure 13 shows the predicted system noise benefits for a HWB airframe from Thomas et al. (Ref. 3). They obtained nearly 10 EPNdB benefit for wing shielding for a high bypass ratio fan mounted two nozzle diameters upstream of the wing trailing edge. The system noise benefit was primarily attributed to reductions in the fan component. However, chevrons provided an additional 3.5 EPNdB cumulative noise benefit by shortening the jet exhaust potential core and increasing low frequency shielding benefit. The N+2 baseline over-wing model is located 5 nozzle diameters upstream of the wing trailing edge. Therefore, it is reasonable to expect significant reductions in system noise due to shielding.

Assuming a shielding noise benefit of 10 dB/point on fan noise and jet shielding suppressions derived from the NASA JSI tool, a cumulative noise margin of 24.2 EPNdB to Chapter 3 is predicted for engines in the baseline over-wing position, Figure 9. Recall that the baseline noise margin without installation penalty was 11.4 EPNdB cum. to Chapter 3. Thus, the shielding benefit of nearly 13 EPNdB cum. compares very favorably with published benefits from the Thomas et al. (Ref. 3) study.

Jet noise shielding benefits at sideline were lower than at flyover or approach because of the higher jet velocities and longer potential core. Also, fan noise benefits are not realized due to dominance of the jet. Still, a benefit of nearly 2 EPNdB is obtained with shielding at this condition, with more at flyover and approach, Figure 14. With shielding, the airplane now has over 7 EPNdB cum. margin to Chapter 14 for the baseline trajectory.
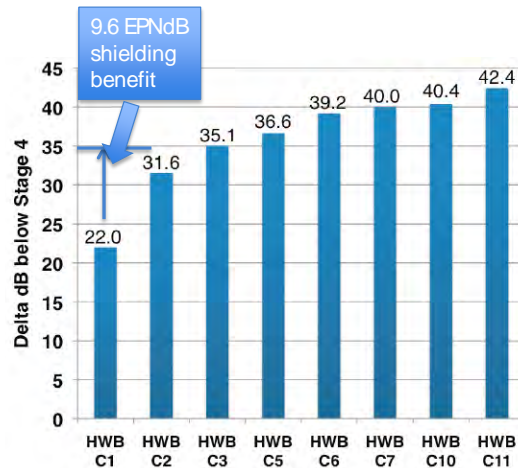
Figure 13.—Predicted system noise benefits for wing shielding for an HWB airframe (Ref. 3).
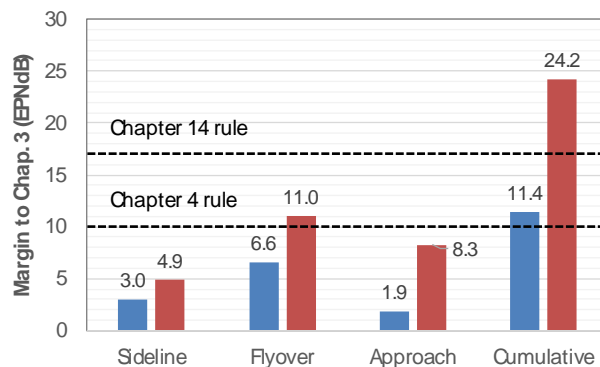
Figure 14.—Noise margins to rule for baseline shielding (exhaust nozzle located 5 diameters upstream of wing TE). Blue bars are installed levels without shielding, red bars are shielded levels.

Figure 7 shows the baseline over-wing engines with the outboard engines at five nozzle diameters upstream of the wing TE. The outboard engines were constrained at this position since any movement forward would adversely affect the vehicle's balance characteristics. However, as Figure 15 and Figure 16 show, there is still over 3 EPNdB to be gained by moving the engines another 2 nozzle diameters forward. In these shielding estimates, jet noise shielding for the approach condition was extrapolated linearly from 5D to 7D and interpolated to 3D, while fan noise in all cases was a flat 10 dB benefit per point/frequency/ angle. So, while additional shielding beyond 5D is not pursued because of the large system penalties, the large sensitivity illustrates that noise shielding should be an integral consideration as part of conceptual design.

Note that these results are nominal (50 percent confidence) preliminary design data with no implied guarantee or commitment on the part of GE.
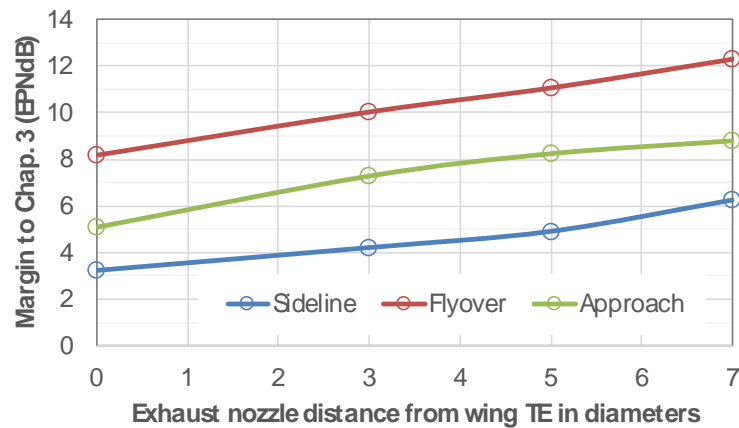
Figure 15.—Noise margin at certification conditions as a function of engine position from the wing trailing edge for wing shielding.
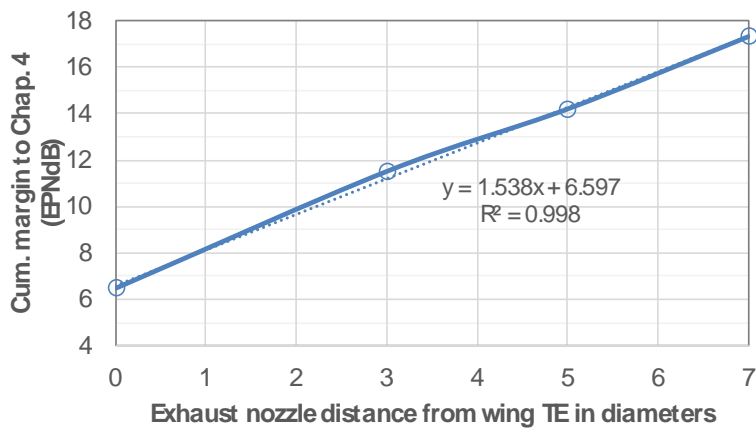
Figure 16.—Cumulative noise margin to Chapter 4 as a function of engine position from the wing trailing edge for wing shielding.

3.3   Trajectory Sensitivity Study

As part of the system noise assessment studies, we identified the need to perform a trajectory sensitivity study to assess the potential of flight path optimization to reduce noise. GE Aviation was subcontracted to perform this study with Lockheed Martin providing trajectories that met safety and Takeoff Field Length requirements. For this study, GE Aviation used the in-house community noise projection process that is employed for all GE proprietary noise assessments. Details of the trajectory sensitivity study are described in the GE Aviation report, but a summary is included below.

The trajectory study shows that both the increase of the Approach glideslope and the use of PLR for takeoff significantly reduces the noise of the N+2 aircraft. The best results on takeoff for this airplane and engine combination occur with improved takeoff combinations including PLR thrust reduction on climb out, until the standard initiated cutback occurs. The impact on Sideline noise improves from having a negative margin to the rule without PLR to having a positive margin to the rule for the PLR cases. In general, the PLRs lead to lower altitudes for the Flyover with Cutback point. However, by employing improved takeoff procedure combinations and flying faster, the PLR penalty on Flyover with Cutback can be reduced and potentially eliminated.

On Approach, the steeper the glideslope, the higher the airplane over the microphones, the lower the thrust required, and the lower the noise level. However, airframe noise may increase more than indicated in this study due to the need for devices to control the steep descent.

4.0   Installation and Fan Noise Analyses

4.1   Engine Placement Study at the Sideline Condition

The geometries shown in Section 3.2.1 are analyzed using steady RANS CFD at the sideline condition to assess distortion ingested by the fan as described below.

4.1.1   Mesh

A multiblock structured mesh for the engine above wing model was generated using ANSYS ICEMCFD Hexa. The takeoff condition at M = 0.38, 8.1° angle of attack for the baseline N+2 trajectory is analyzed. This is not the most critical condition for fan noise, however it is studied here to compare to the under-wing studies of the reference N+2 configuration. More studies at higher angles of attack are performed at the Approach condition in Section 4.2.

Key mesh details are listed below:

1. Mesh size: ~240 M nodes, Block count: ~800
2. Mesh topology: Same as reference N+2
3. Mesh practice (resolution, spacing, transition): Same as reference N+2
4. Target y+: 1, resolved boundary layer

Views of the surface mesh in different regions of the flow field can be seen in Figure 17 to Figure 24. For engine movement for the two over-wing positions, the topology remains the same and only a local re-projection of blocks is performed.
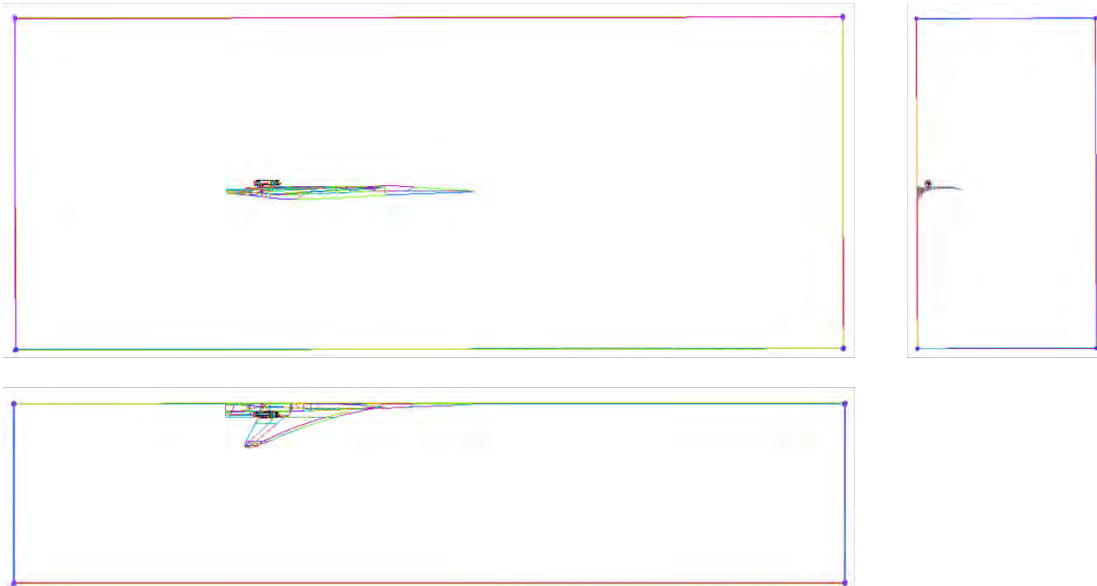
Figure 17.—Aircraft model with domain boundaries.
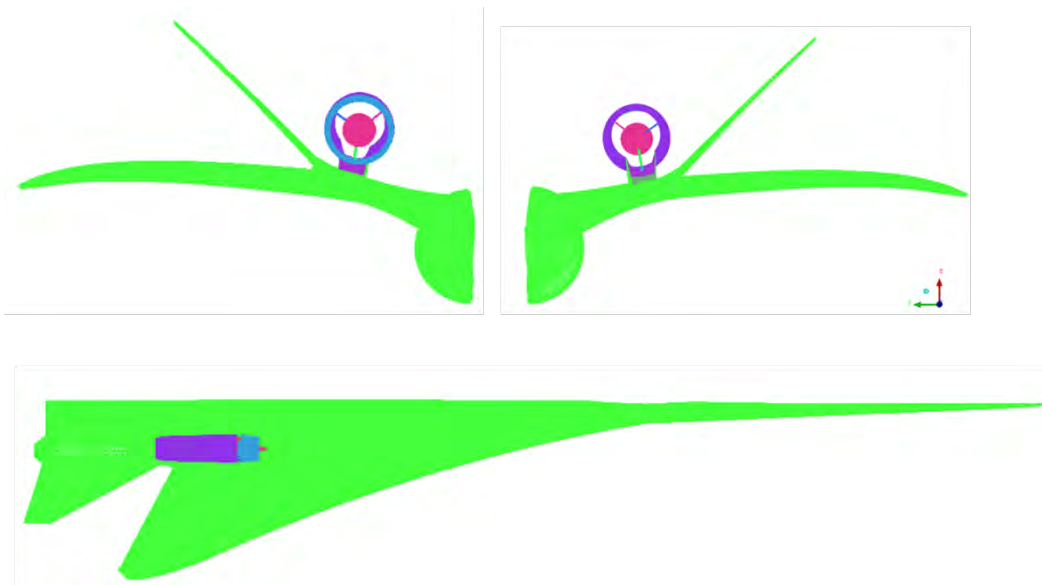
Figure 18.—Entire surface mesh.
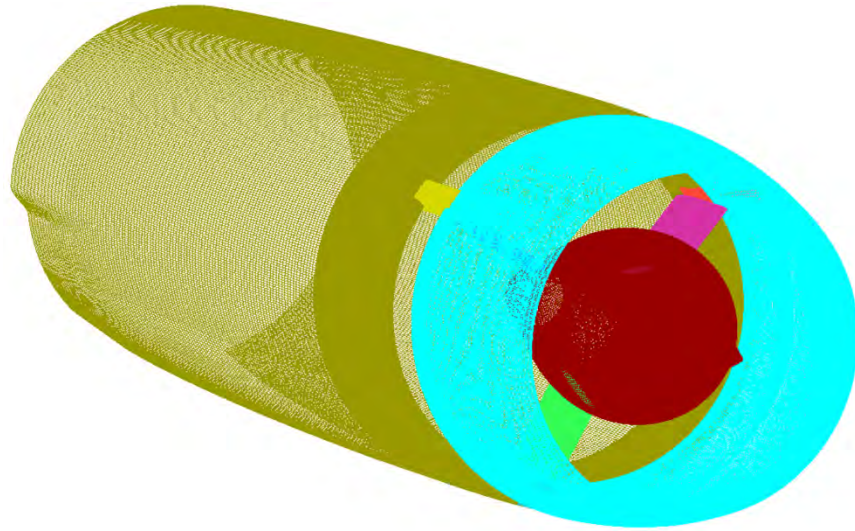
Figure 19.—Engine surface mesh.
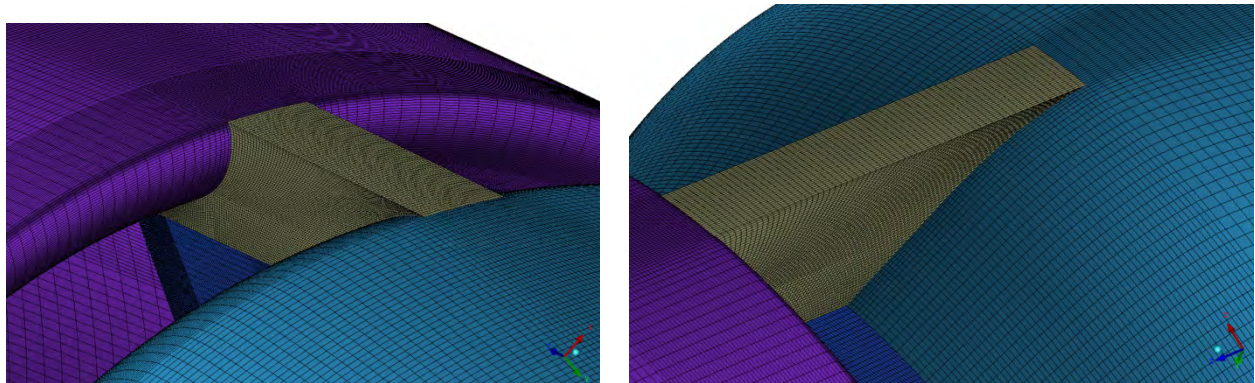
Figure 20.—Surface mesh: Door/hinge detail.
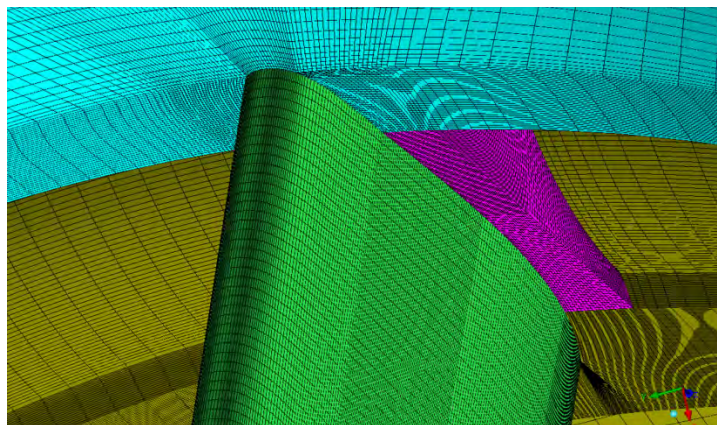
Figure 21.—Surface mesh: Strut/nacelle/hinge detail.
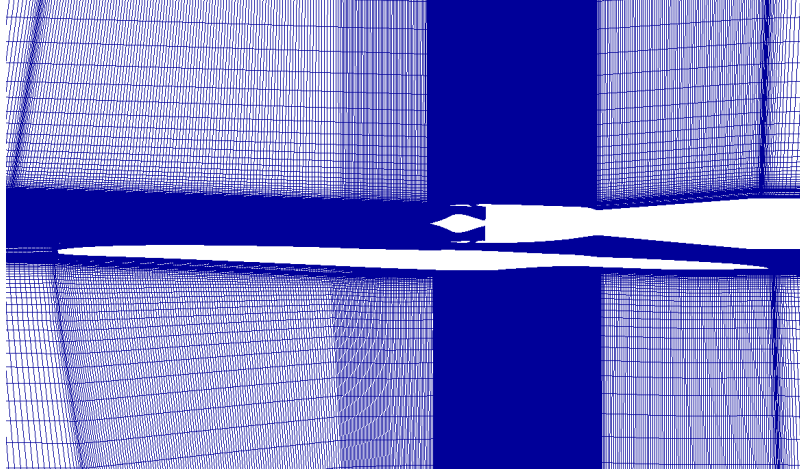
Figure 22.—Cut through volume mesh showing high resolution around the wing and engine.
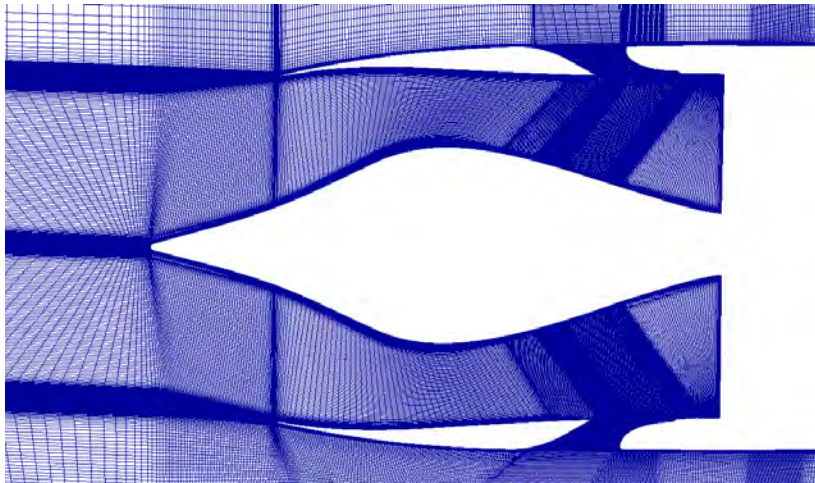
Figure 23.—Cut through volume mesh showing detail of nacelle and inlet mesh.
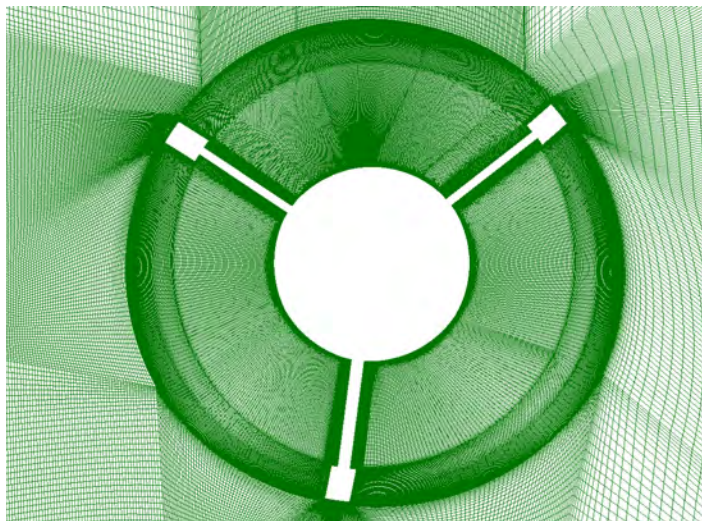
Figure 24.—Cut through volume mesh showing frontal view of inlet and centerbody mesh resolution.

4.1.2   CFD Analysis Procedure

The objective of the CFD analysis is to quantify the increase in fan noise due to increased distortion of the over-wing engine installation. Quantifying the distortion ingested by the fan is accomplished in two steps as follows: (a) Installed CFD analysis of the engine inlet and aircraft with the mass flow rate through the turbomachinery specified as a boundary condition at the interface plane, and (b) A distortion transfer analysis using the predicted distortion at the Turbomachinery interface plane and propagating to the fan face using a full wheel steady CFD analysis.

The center engine is not modeled as part of the analysis. Only one half of the aircraft is modeled and a symmetry boundary condition is used to account for the other half. Not modeling the center engine would change the flow seen by the outboard engines but the effect is expected to be somewhat lower than the effects of the fuselage and wing flow at high angle of attack. To accelerate the analysis, each block in the installed mesh (~240MM cells) is coarsened by a factor of 2 in each direction resulting in a grid that is approximately 30MM cells. The jet exhaust plume is modeled as an inviscid surface, like the procedure used in the N+2 Ph2 Ext. program. Errors in modeling jet plume position are not significant for the purposes of assessing fan distortion. It is also worth noting that the aircraft high lift devices are not modeled. Therefore, the current results are expected to represent a bad scenario in terms of fan distortion.

4.1.2.1   Fan geometry

A multistage fan geometry was selected in the previous N+2 program to perform detailed CFD and fan noise studies. It was chosen because there is no detailed engine geometry (other than flow path) for the GE engine for the N+2 study. However, the GE N+2 engine cycle is sized for a higher bypass ratio than the multistage fan considered in the study.

For this preliminary study of fan distortion noise at sideline (where fan noise is sub-dominant), we simply used the same operating conditions as used in the N+2 Ph2. Ext program where the fan is run at its design speed. In Section 4.2 where we simulate distortion noise at Approach, a more careful approach is used which considers the implications resulting from matching either pressure ratio or mass flow to the GE N+2 engine cycle conditions.

4.1.3   CFD Results—Baseline Shielded Configuration

Figure 25 shows a perspective view of the aircraft wing upper surface flow field with key features of interest. The wing leading edge vortex development is shown, but the vortex is not ingested by the fan. In the following figures, flow features of interest will be shown in more detail.

Figure 26 and Figure 27 show local separation near the pylon leading edge. This is caused by high incidence flow in the wing boundary layer as it sweeps past the pylon and migrates outward towards the tip. This is not unlike hub corner vortex separation observed in turbomachinery and can be remedied with some local redesign. Some of this high entropy fluid is ingested through the open auxiliary doors and enters the fan.

Figure 28 shows high losses in the aux door shear layer and the streamlines responsible. Again it is clear that none of the high entropy fluid from the wing leading edge vortex is ingested by the fan.

Note that since no high lift devices were modeled, the flow on the upper surface of the wing is likely to be more separated than reality. Thus, this analysis represents a sort of worst-case scenario in terms of fan distortion noise.
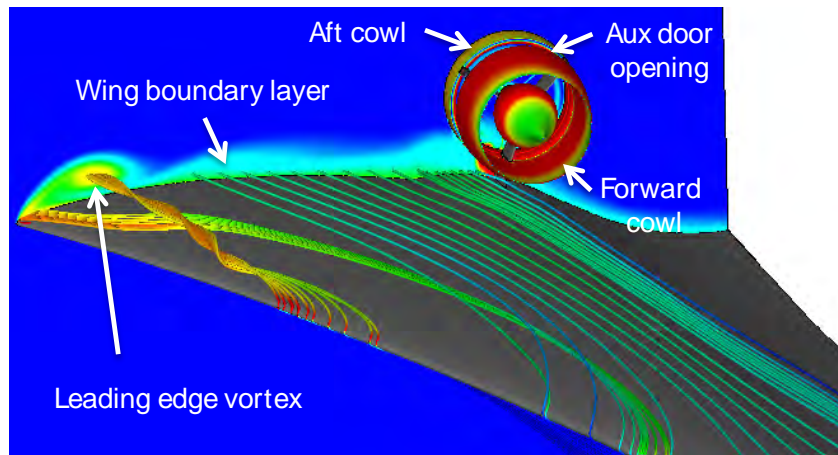
Figure 25.—Wing upper surface flow with streamlines colored by entropy.
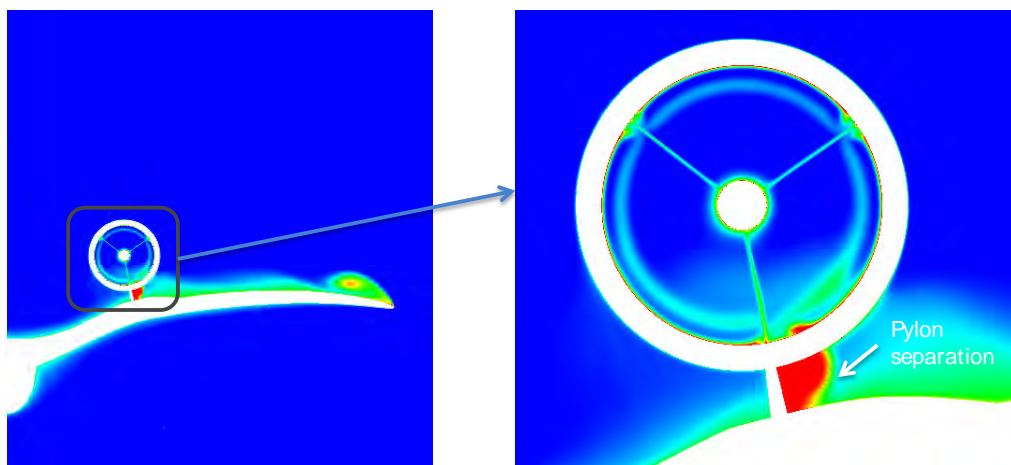
Entropy at AIP
(Aft looking fwd.)
AIP: Aero Interface Plane
between aircraft, turbomachinery

Figure 26.—Entropy at Aerodynamic Interface Plane (AIP) showing local separation at pylon leading edge.
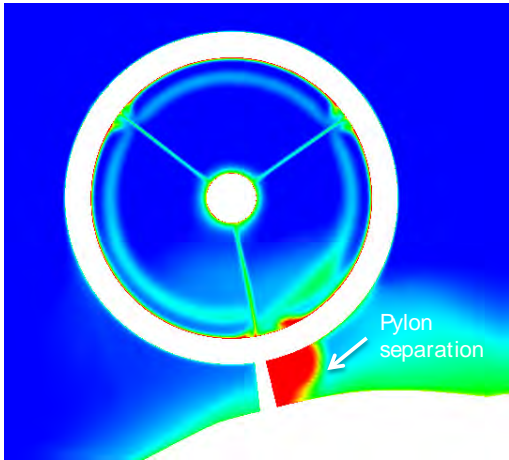
Entropy at AIP
(Aft looking fwd.)
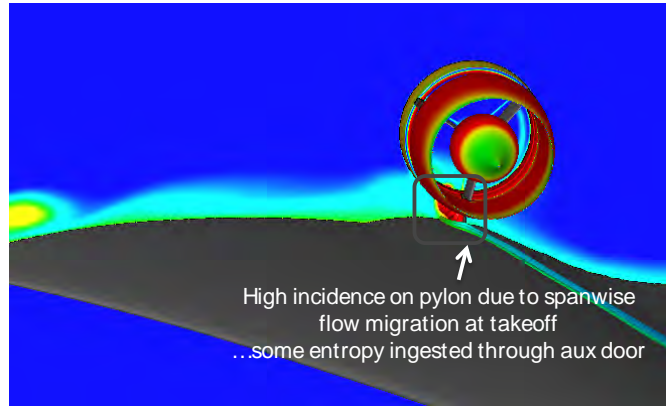
Figure 27.—Entropy at AIP showing streamlines responsible for pylon leading edge separation.
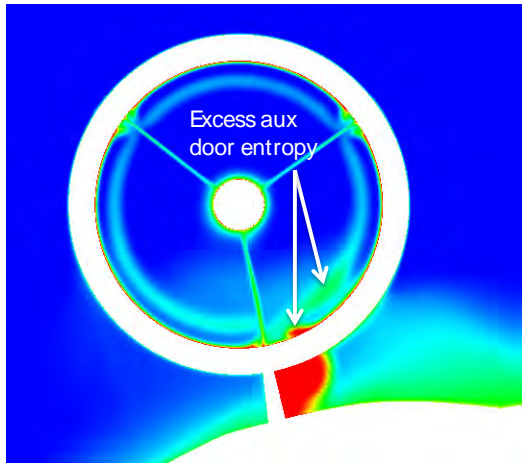
Entropy at AIP
(Aft looking fwd.)
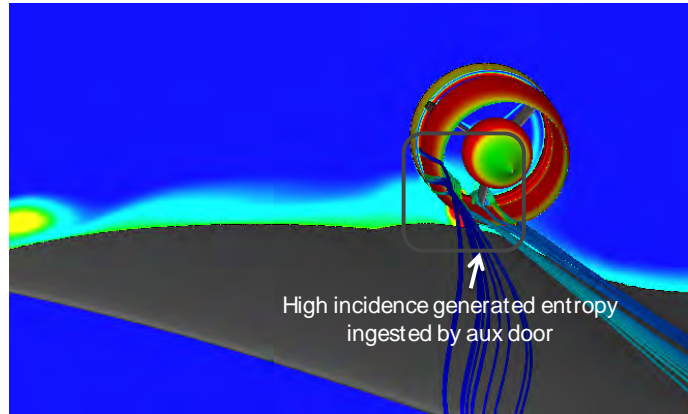
Figure 28.—Entropy at AIP showing streamlines responsible for high aux door shear layer loss.

4.1.4 CFD Analysis—Second Engine Position

Results of the CFD analysis for the second engine position (Figure 8) are shown in Figure 29. Again, the fan is sufficiently removed from the wing leading edge vortex and does not ingest it. However, due to the increased wing surface boundary layer, more vorticity and entropy will in general be ingested by the fan as the engine is moved further aft.

Figure 30 shows the entropy at the main rotor face for the baseline engine configuration. The IGV wakes are the dominant source of distortion to the fan, with the inlet strut wakes less noticeable. This shows that the strut wakes decay due to the long propagation distance and the IGVs are effective in reducing distortion. The swirl distortion entering the fan is shown in Figure 31 at two different spanwise locations. The change in flow angle relative to isolated conditions (baseline N+2) is hardly significant for the two over-wing installations. Hence distortion related noise is not expected to be significant for this operating condition and geometry shown.

Entropy at AIP
(Aft looking fwd.)

3D view of Entropy
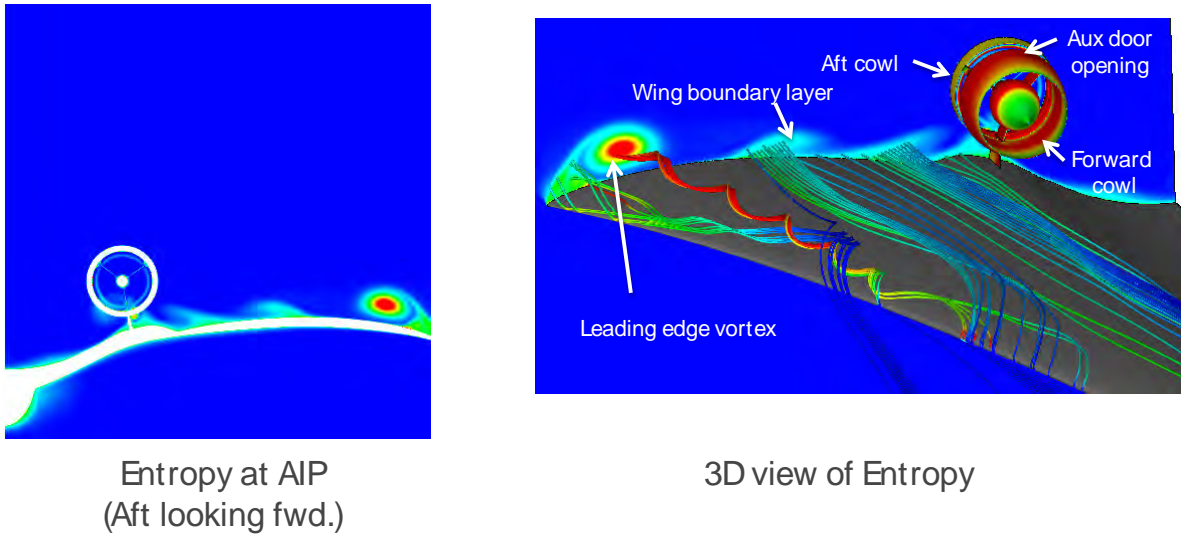
Figure 29.—Entropy and streamlines for second above-wing engine configuration.
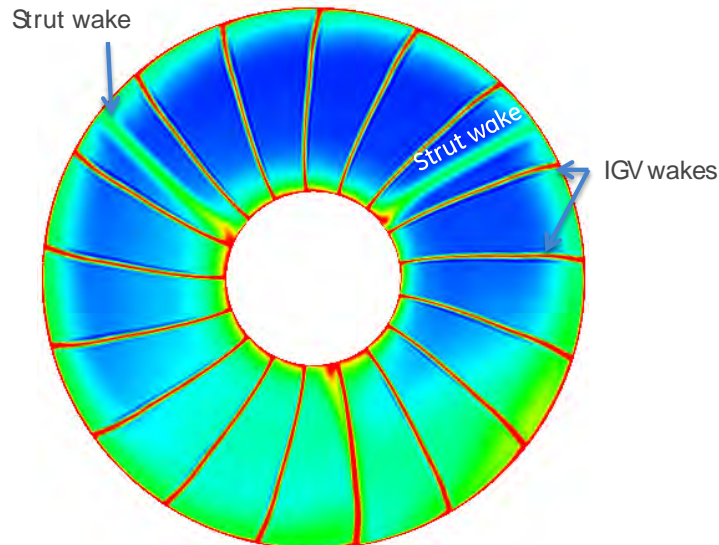
Figure 30.—Distortion at main rotor face (aft looking forward)
showing IGV and strut wakes.

4.1.5 Over-Wing Engine Mounting: CFD Summary and Other Considerations

In Figure 31, the increase in swirl distortion for even the second engine position (considered to be at higher risk for distortion) is observed to be small compared to the existing distortion pattern from the IGV wakes for the reference under-wing design. Thus, the added risk to fan distortion for over-wing mounting can be considered small for this geometry and operating condition. However, it is worth noting that this is only a preliminary assessment at takeoff where fan noise does not dominate. More analysis at the fan noise critical condition of Approach is described in Section 4.2.

The second point to bear in mind is that the over-wing engine is still podded. So, while distortion increase has been rather minimal, a clean-sheet redesign that may ingest the wing boundary layer is likely to incur some noise penalty. Finally, even though distortion may increase, shielding effectively eliminates fan noise for this aircraft. For other configurations, this may not necessarily be the case and distortion increases must be more carefully considered.

From a shielding benefit standpoint, the furthest upstream position (X/D = 5) is the most favorable and is used for further analysis going forward.

4.2 Fan Distortion and Noise at the Approach Condition

Fan noise source increase due to distortion ingested by the over-wing engines at Approach is now studied. In Section 4.1, the same study was conducted at takeoff and no appreciable noise increase was observed. But given the relative importance of fan noise at Approach and the increased angle of attack, it is important to re-evaluate this finding. The CFD analysis uses the same procedure, but the assessment of noise sources is more detailed.
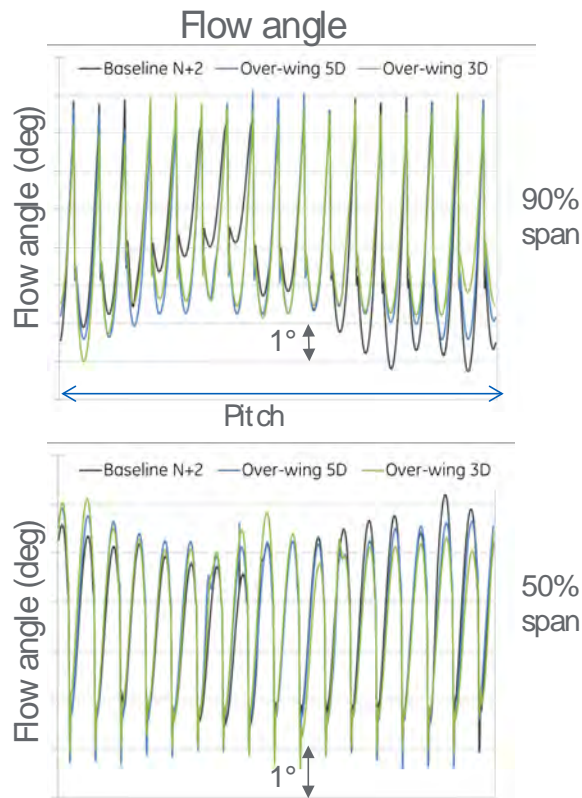
Figure 31.—Tangential flow angle at main rotor face.

4.2.1 Operating Conditions

A 3° glide slope at M = 0.25 flight speed is used for the approach calculations. Even at this condition, the fan tip speed is supersonic and shock-related noise is expected to be important.

Since the aircraft high lift devices are not modeled in the CFD analysis, the flow over the aircraft is simulated at three different angles of attack (6°, 8.1°, 11.7°) to assess noise sensitivity to inlet distortion. The latter is the actual angle of attack needed by the aircraft at Approach at M = 0.25 to sustain a 3° glide slope. For the intermediate angle of attack (chosen to be the same AoA as sideline), two different fan mass flows were simulated.

4.2.2 Fan Map

As mentioned previously, an existing multistage fan geometry is chosen for the CFD studies, resulting in a choice of parameters to match to the engine cycle for the current study. Since tip speed is the key driver for noise, it is maintained consistent between the cycle and the chosen fan. Additionally, either flow or fan pressure ratio can be matched, but not both. Therefore, we performed the analysis matching these parameters, one at a time (along with tip speed) to the engine cycle to obtain sensitivity to distortion for the 8.1° and 11.7° angles of attack. The results of these analyses are described in the following section.

Matching engine pressure ratio (in addition to tip speed) results in a mass flow that is higher than if the CFD is run to match engine mass flow. At higher mass flow, more distortion is ingested by the fan. Consequently, the increase in noise is expected to be higher. Thus, in the discussion below, we focus exclusively on the case where the fan pressure ratio matches the engine cycle.

4.2.3 Aircraft Flow Field

Figure 32 shows the entropy in the flow field at three different angles of attack along with streamlines seeded through flow features of interest for the case where the fan matches the engine pressure ratio. Entropy (aft-looking-forward) at the Aerodynamic Interface Plane (AIP) is shown below the 3D view for each angle of attack.
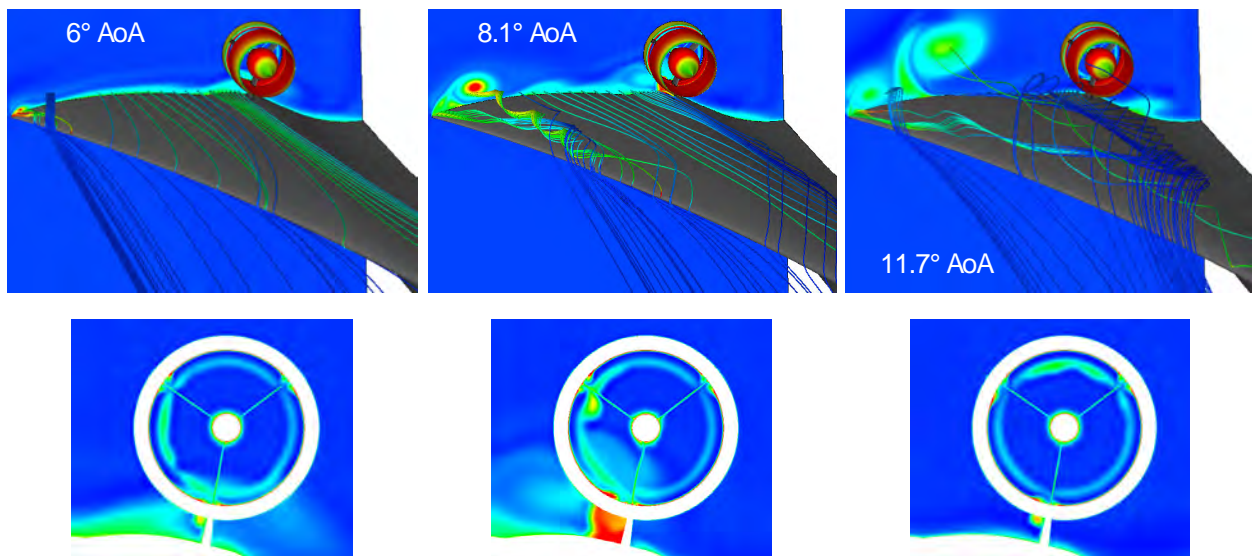
Figure 32.—Aircraft flow field at Approach speed at different angles of attack (no high lift devices modeled) showing development of the leading edge vortex and boundary layer on the wing upper surface. Entropy at the Aerodynamic Interface Plane (AIP) is shown below, aft-looking-forward.

Note the development of the leading edge vortex as the angle of attack increases—the vortex grows larger and sheds further inboard. This, combined with the induced velocity field of the vortex causes very different flow profiles at the AIP as shown in the Figure 32. There is a nonmonotonic trend with angle of attack, i.e., the flow ingested by the fan is very sensitive to the installation and operating conditions. The case at 8.1° AoA shows the largest distortion and it is instructive to examine this further, Figure 33.

In Figure 33(a) is the same as that shown in Figure 32, and (b) shows a view from the fuselage. The streamlines are colored by entropy in (b). A dramatic rise in entropy can be seen at the nacelle lip where the streamline color changes from dark blue (low entropy) to deep red (high entropy). This flow feature is shown in greater detail in Figure 34 where separation at the nacelle lip is observed as the root cause of entropy increase. This separation then recovers and is ingested by the fan as shown in the entropy contours at the AIP, resulting in noise increase.
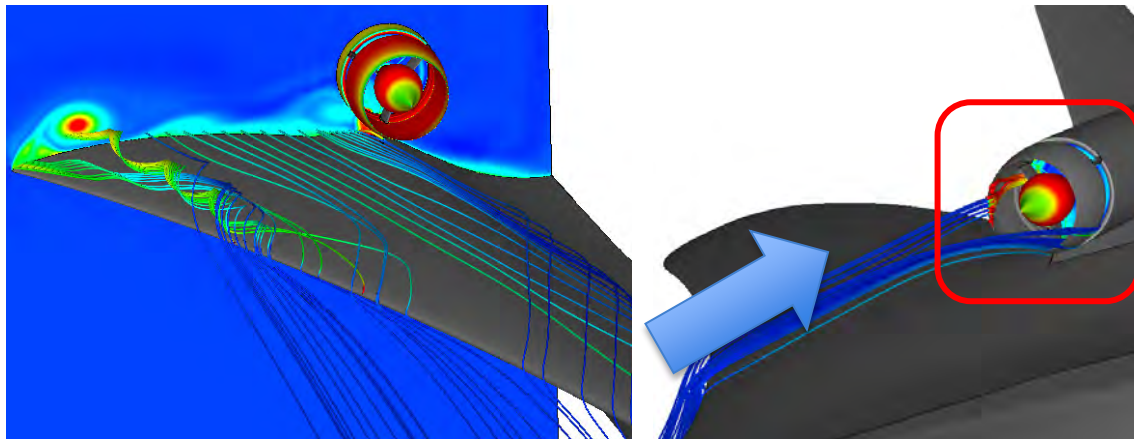
Figure 33.—(a) Aircraft flow field at 8.1° angle of attack (no high lift devices modeled) showing development of the leading edge vortex and boundary layer on the wing upper surface. (b) View from fuselage showing high entropy streamlines due to lip separation on outboard side of nacelle.
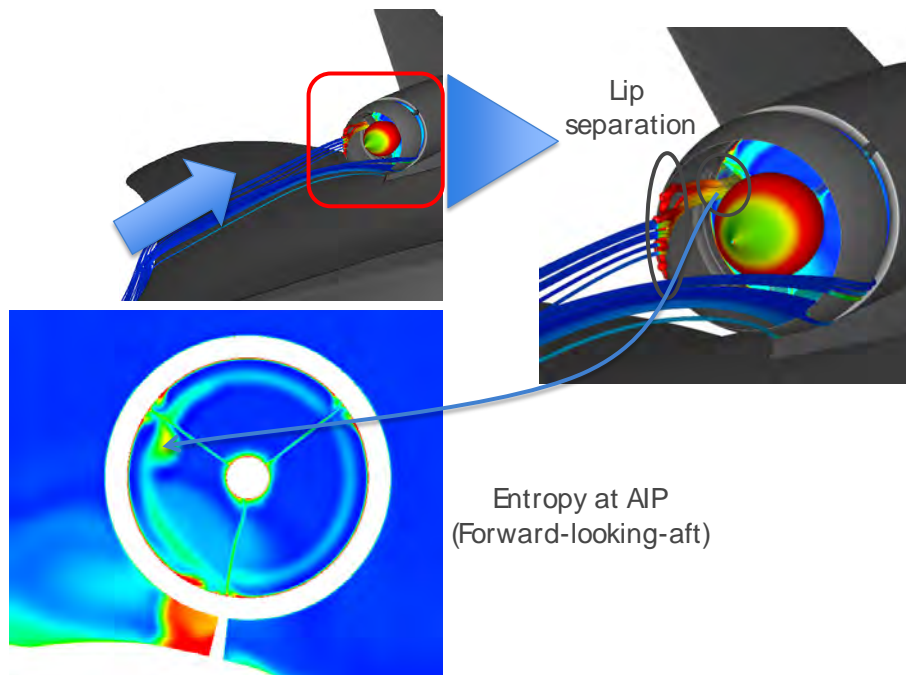
Figure 34.—Nacelle lip streamlines at 8.1° angle of attack and entropy at AIP.

4.2.4 Fan Face Distortion and Noise Increase

The distortion at the AIP is now propagated to the face of the main rotor using a steady, full annulus distortion transfer calculation. Figure 35 shows the entropy at the AIP and fan face for 8.1° AoA. Note that the entropy contours are now viewed aft-looking-forward.

Figure 35 shows the IGV and strut wakes, with the distortion due to nacelle lip separation observable within the circled red regions. This high entropy region interacts with the tip of the main fan where the Mach numbers are highest. To quantify the impact of the distortion, the vortical gust magnitude impinging on the fan is calculated in Figure 36. Since the flow exiting the IGV is predominantly axial, the upwash velocity responsible for noise generation is the component of the axial perturbation velocity that is perpendicular to the blade stagger.

Figure 36 shows the gust harmonic amplitude as a function of engine order at two different spanwise locations. When there is no distortion, only the IGV wakes and harmonics would be present, so the magnitude of the other gust harmonics gives an indication of the vortical energy present in the distortion pattern. Since the distortion profile varies radially, a more integrated measure is needed to quantify noise impact. One such measure is shown in Figure 37 where the gust strengths are integrated radially (accounting for area increase) across different spanwise extents. This integration is performed only over the nonIGV harmonics, i.e., the bars shown represent the difference in gust power arising from distortion alone.

Due to differences in the ingested distortion pattern for different angles of attack, the noise increase varies anywhere between 0.6 to 3.2 dB. As a worst case scenario therefore, we can expect 3.2 dB of noise increase due to distortion. Note that this increase is only an estimate of the vortical power in the distortion pattern. Conversion to acoustics and radiation are important factors that depend on the frequency and azimuthal mode content, but they are out of scope and therefore not accounted for in this simple assessment. It is likely that proper design would reduce the impact for a future product, but for the purposes of a conceptual study, this provides an upper bound on the importance of distortion for an above wing mounted engine.

Entropy at AIP
Aft-looking-forward

Entropy at main fan face
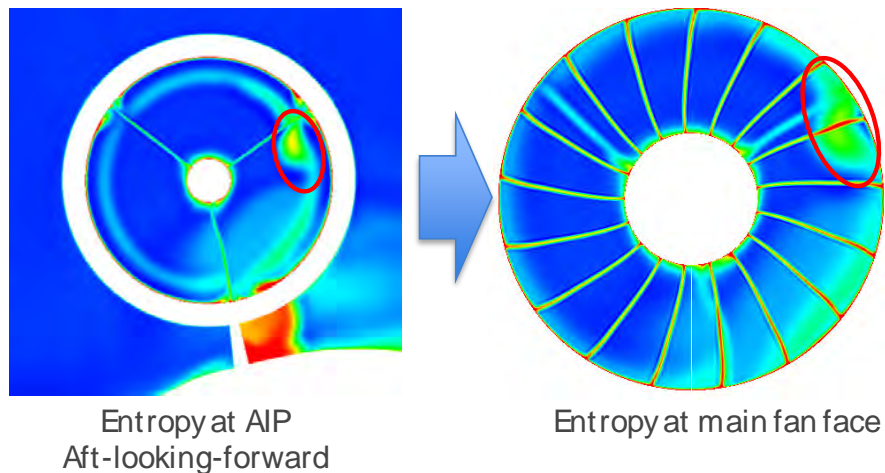
Figure 35.—Inlet distortion transfer to main fan face (aft-looking forward). IGV wakes visible as streaks of high entropy while the three strut wakes are weaker due to wake mixing and downstream convection from the AIP.
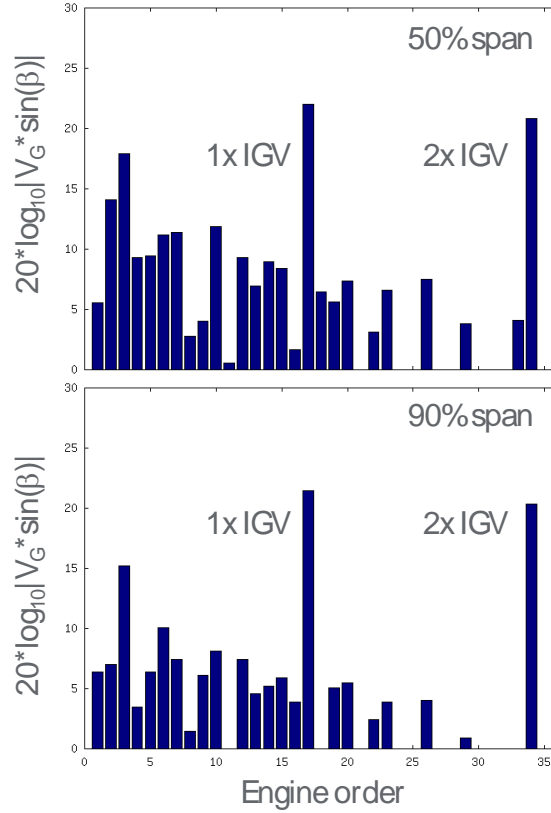
Figure 36.—Distortion gust upwash at fan face in dB. IGV wakes and engine order excitations due to the distortion are shown.
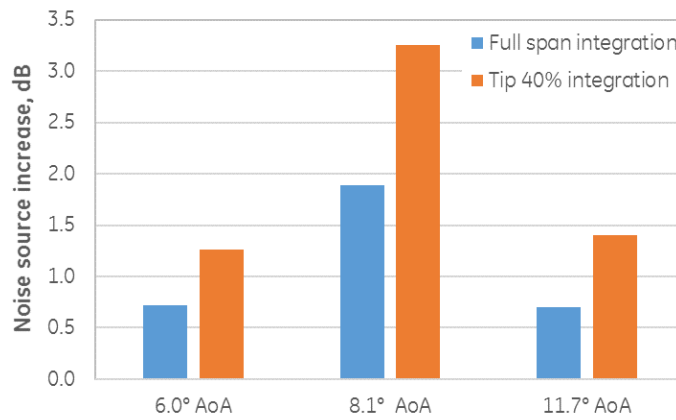
Figure 37.—Radially integrated source power increase due to distortion. Different angles of attack and radial integration extents shown. The worst-case scenario shows a potential for 3.2 dB tone noise increase due to distortion.

Broadband noise increase is assessed in a manner similar to tones but using circumferentially averaged turbulent kinetic energy (TKE) as the source indicator. Figure 38 shows the radial variation of circumferentially averaged TKE for the cases with and without distortion. Significant noise increase is possible due to additional TKE generated by the distortion. Radially integrating (accounting for area) over different spanwise extents yields the 1D metric shown in Figure 39. Full span integration shows approximately a 2.5 dB increase in turbulence sources due to distortion while integration over the tip 60 percent or tip 80 percent yields 2.7 dB. Hence, the upper bound for broadband noise increase is taken to be 2.7 dB.

Thus, using this simplified approach to source quantification, we see that there is a potential for nearly 3 dB of fan noise increase in both tones and broadband due to distortion, resulting in reduced shielding benefit for over-wing installation. This penalty is not present for the under-wing engines since the lower surface of the wing straightened the flow into the engine as shown in the N+2 Ph.2 Ext. program.
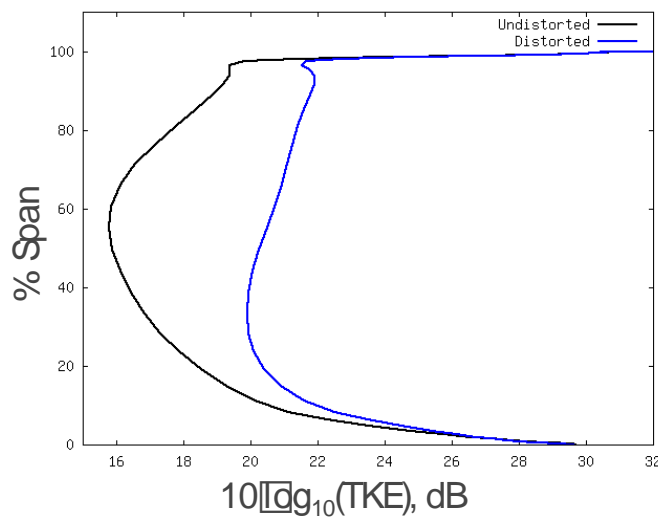
Figure 38.—Circumferentially averaged TKE profiles at main fan face.
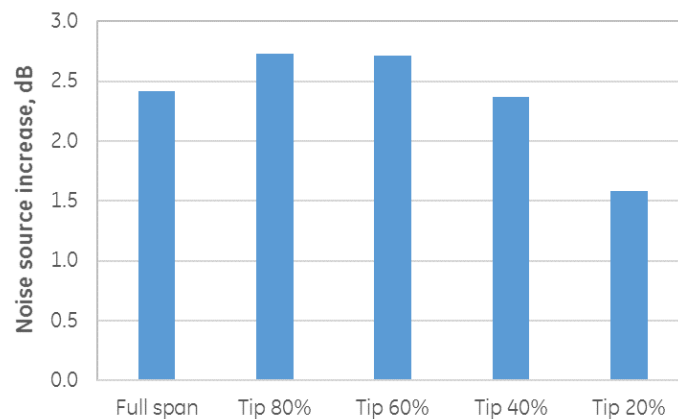
Figure 39.—Radially integrated broadband distortion noise sources at main fan face.

4.3 CAA of Fan Tone Noise Shielding at Approach

A CAA of the fan tones with wing shielding is performed to verify the assumed shielding benefit of 10 dB. A simple plane wave propagating upstream from the fan at various frequencies was studied to assess shielding benefits. It is too expensive to model the propagation of the acoustic wave within the nacelle as well as the external wing scattering. Therefore, the nearfield propagation of the acoustic wave in the presence of flow at angle of attack and a representative installation was first simulated in the frequency domain using GE's Linearized RANS solver. This is the same solver used in the other fan and installation studies in this Chapter. Subsequently, scattering and shielding from a simplified model of the wing is studied using the commercial Multiphysics solver COMSOL 5.2a. The COMSOL study includes propagation inside the nacelle as well, but is performed with a uniform flow at no angle of attack. While this study incorporates wing scattering, it does not have a realistic mean flow, so the nearfield Linearized RANS analysis serves to complement it.

4.3.1 Nearfield Propagation

Nearfield propagation is studied for a plane wave mode injected from the fan at the AIP into a model of the nacelle and installed flow field. Initially the mesh and geometry were identical to that used in the fan distortion study in Section 4.2. However, robustness issues were encountered in the linear solver due to grid spacing discontinuities caused by the need to resolve fine features around the aux door hinges that were essential to accurately capture distortion ingested by the fan. To improve solver robustness, the struts and the details around the aux door were removed and a CAA mesh regenerated. Since the study is focused on forward propagating fan noise, the vertical tail was also removed. This slightly modifies the radiation patterns emanating from the nacelle, however these modifications are not expected to change the shielding and scattering from the wing significantly. The mesh was further coarsened to 33MM elements to quickly assess nearfield propagation within a reasonable run time and iterate on frequencies. To put this in context, a well-resolved 1/3rd sector model of the isolated nacelle and farfield propagation in the N+2 Ph2 Ext. program had over 100MM elements. Thus, performing a fully resolved CAA of the entire wing and nacelle at a representative angle of attack is a significant undertaking. However, since we are modeling the wing scattering using COMSOL, this coarse grid analysis of the acoustics in and around the nacelle suffices to study the source physics.

The aircraft angle of attack is restricted to 6° (M = 0.25) to avoid potential robustness issues with vorticity dominated flows in the linear solver at higher angles of attack. Two frequencies (500 Hz and 1000 Hz) are considered. Due to the high fan tip speed and large blade count, these frequencies are well below the blade passing frequency, however simulating higher frequencies would have been very expensive. In any case, the COMSOL study extends to frequencies close to fan BPF.

Figure 40 shows the flow field around the aircraft and nacelle at this condition. Unsteady pressures around the nacelle at 500 Hz are shown in Figure 41. As expected, at this low frequency, much of the energy beams out axially through the inlet lip. The coarse grid resolution away from the nacelle attenuates the acoustics. Diffraction of the acoustics around the wing tip is also visible. These effects will be quantified in the next section.

Figure 42 shows the nearfield propagation for the plane wave tone at 1000 Hz. For this frequency, the acoustic wavelength is on the order of the aux door opening and a significant fraction of the energy beams out through the aux door. The residual power propagates forward although this is under-resolved by the coarse grid used in the study. The figure also shows the acoustics emanating from the aux door at an angle is reflected by the wing, so we expect that less of the power from the fan will diffract around the wing tip. So, we expect that as the frequency increases, more energy will reflect from the wing resulting in higher levels of shielding for frequencies that dominate the fan noise spectrum.
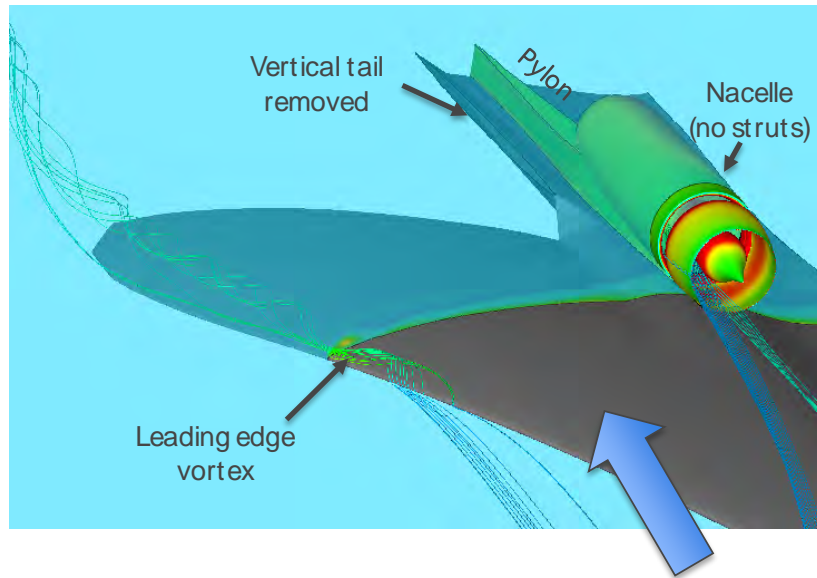
Figure 40.—Wing upper surface flow at M = 0.25 and 6° AoA. Key features of acoustic model shown.
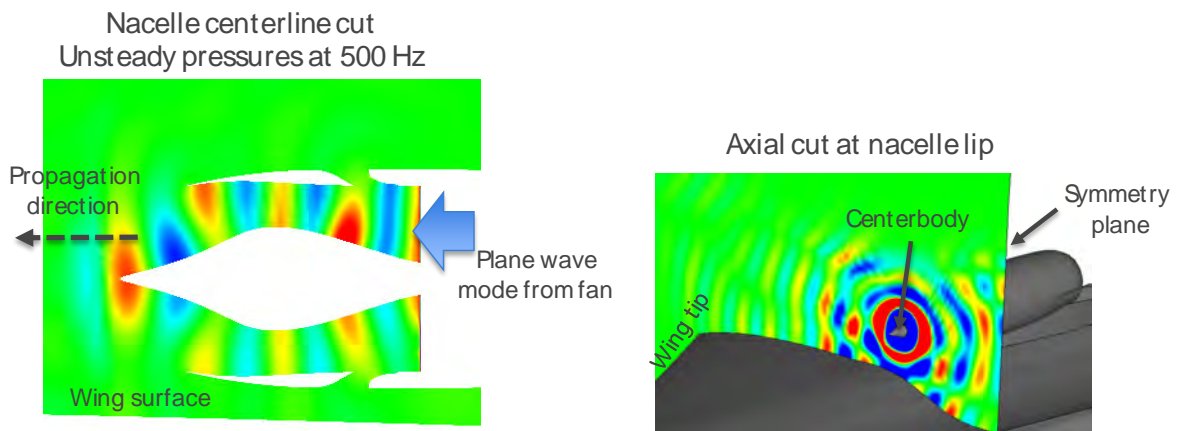
Figure 41.—Nearfield unsteady pressures at 500 Hz.
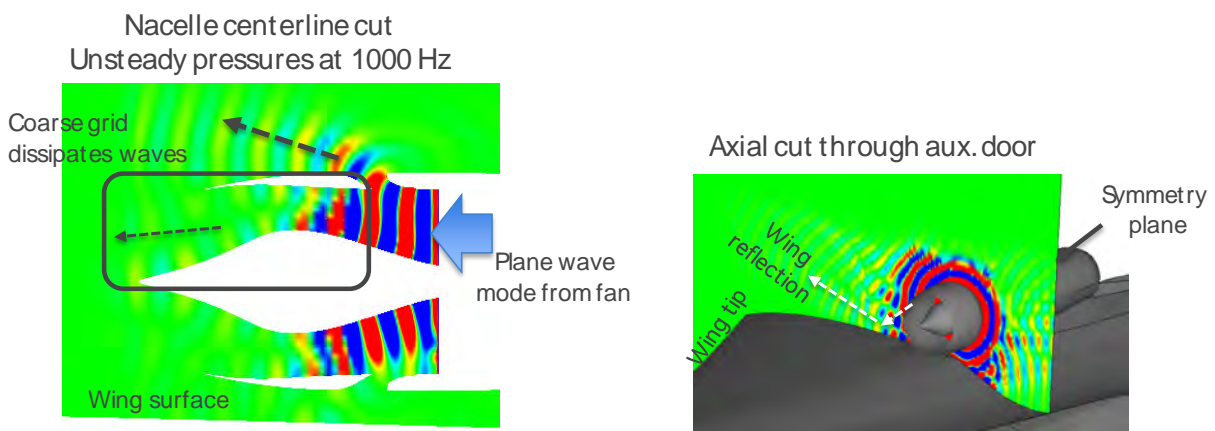
Figure 42.—Nearfield unsteady pressures at 1000 Hz.

4.3.2   Wing Scattering

Acoustic evaluations were performed at a uniform forward flight Mach number of 0.25 (no angle of attack). To estimate wing shielding, a three-dimensional model was built using COMSOL's acoustic module. The computational domain included the forward portion of the wing only, since aft noise is not significant relative to the jet. As shown in Figure 43, free-field radiation boundary conditions are imposed on the sides and the bottom of the domain, and a Perfectly-Matched Layer (PML) is imposed at the top of the domain to minimize spurious reflections from the numerical boundary. The wing was approximated by a triangle as shown in Figure 44, but the nacelle geometry was fully resolved as shown in Figure 45. The centerbody contour was simplified for ease of mesh generation but this is not expected to have any impact on the solution.
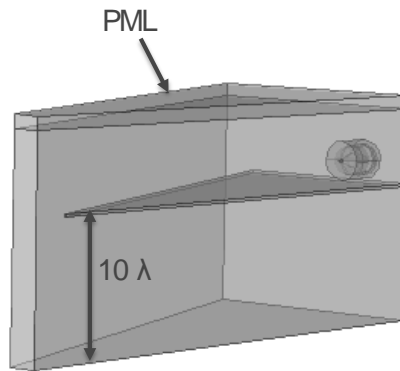
Figure 43.—COMSOL 5.2a CAA
domain for estimating tone shielding.
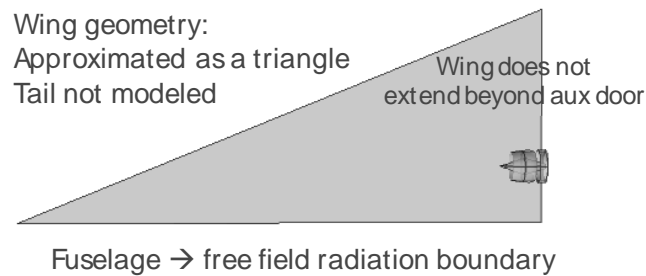
Figure 44.—Top view of wing and nacelle. Wing simplified
to a triangular geometry, and vertical tail is not modeled.
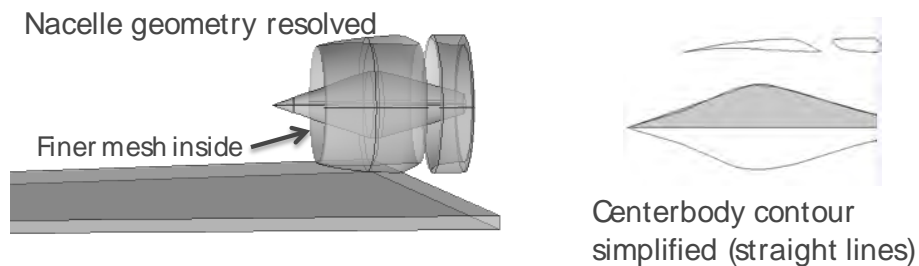
Figure 45.—Close-up view of nacelle and centerbody.

A plane single-harmonic wave with specified frequency was provided as input inside the nacelle at the AIP. Three frequencies were studied: 600, 1200, and 1800 Hz. To estimate shielding benefits, acoustic power levels (PWL) through the side surface (everything below the wing) and the bottom surface were computed for the cases with and without the wing as shown in Figure 46. The difference in PWL in dB provides total shielding benefits for all observer angles. Also, directivity plots for the observers below the wing located in the engine symmetry plane were computed and SPL for the cases with and without the wing are compared.

First, a check on the boundary conditions is performed. Figure 47 shows the acoustic field in a smaller domain and a corresponding larger domain at 1200 Hz. No reflections are observed from the free-field boundaries, validating the use of smaller domains for this study.
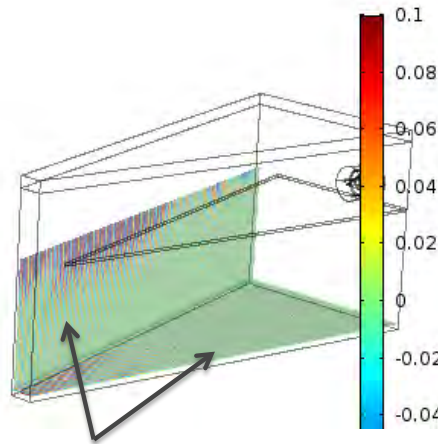
Acoustic intensity flux computed on wing side surface (below wing) and bottom surface

Figure 46.—Side and bottom surfaces used for acoustic power flux calculations.
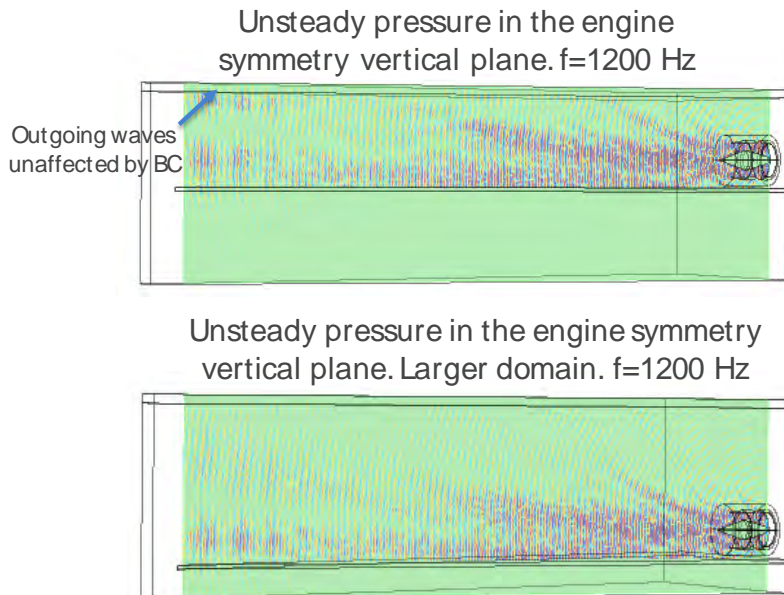
Figure 47.—Assessing impact of boundary conditions on acoustics. Larger domain shows no reflections from the outgoing waves on the top boundary.

Figure 48 shows the results for different frequencies. The first row of subplots shows that directly below the wing, the sound attenuation is on the order of 30 dB, but the attenuation becomes less severe in the region near the wing leading edge particularly at low frequencies. This is consistent with the more axial propagation of noise observed in the nearfield studies in Section 4.3.1. The second row of plots shows the reflections from the wing surface and confirms that the noise radiation is primarily forward, justifying omitting the scattering by the wing trailing edge.

Table 1 shows acoustic power reduction (ΔPWL, with PWL = $10 \cdot \log_{10}$(PWL/PWL$_{ref}$)) due to shielding for different frequencies. The overall noise shielding through the side and bottom surface at 1800 Hz is on the order of 10 dB or more. For lower frequencies, the shielding benefit is slightly lower, but 1800 Hz is on the order of the fan blade passing tone at engine scale, so shielding benefits at this frequency should be representative of the annoyance-relevant portions of the fan noise spectrum.

Finally, Figure 49 shows SPL directivity for an observer below the wing in the engine symmetry plane for the three different frequencies. Except for the far forward angles, shielding benefits are over 10 dB at all frequencies and angles. Note that for radiation at the shallow angles, noise reaches the observer when the aircraft is far away, so spherical spreading effects will reduce observed noise levels. The results of this study show that the assumptions in the preliminary assessments in Section 3.2 are thus validated.
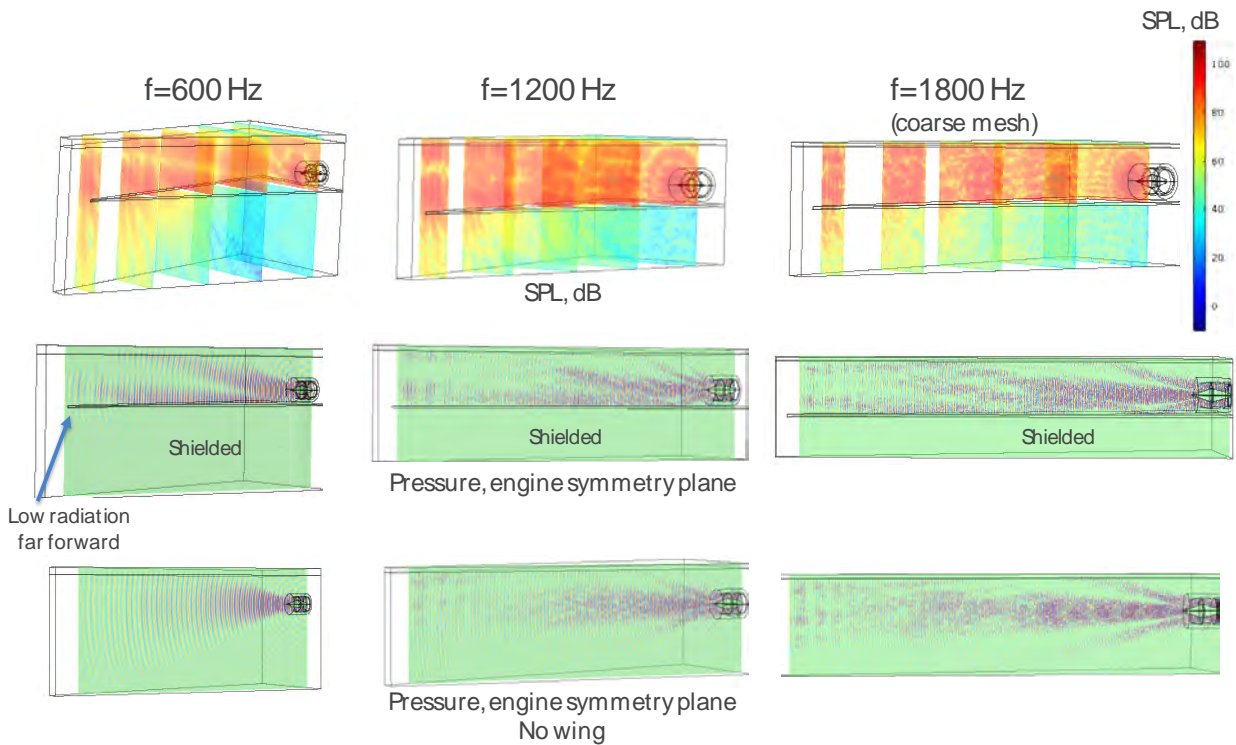
Figure 48.—Fan tone radiation contours for different frequencies. The first row of plots shows SPL in dB, the second row shows unsteady pressures (Pa) on a symmetry plane through the nacelle and the last row shows the unsteady pressures on the same plane without the wing.

TABLE 1.—DIFFERENCES IN THE TOTAL ACOUSTIC POWER
THROUGH THE SIDE AND BOTTOM SURFACE TABULATED

$$\Delta PWL = 10 log_{10} \frac{\text{Power}_{\text{no\_wing}}}{\text{Power}_{\text{wing}}}$$

	600 Hz	1200 Hz	1800 Hz (coarse mesh)
Side surface ΔPWL, dB	5.9	7.2	7.0
Bottom surface ΔPWL, dB	14.7	19.0	18.0
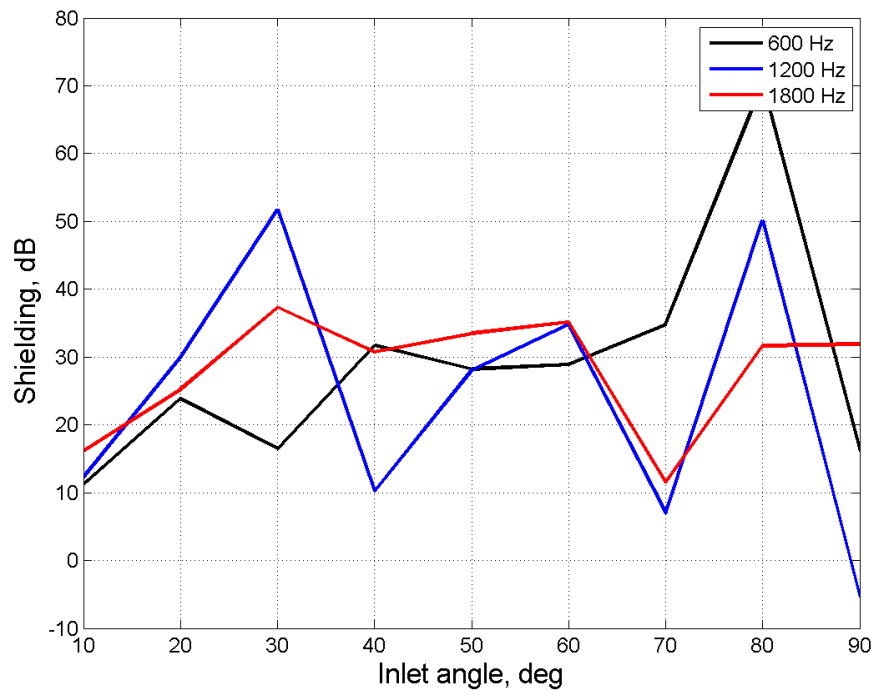
Figure 49.—Noise shielding directivity for an observer located 10 wavelengths below the wing in the engine symmetry plane.

5.0   Jet Exhaust Noise Reduction Studies

5.1   Installed LES Analysis of Jet Exhaust Shielding

Here, using Large Eddy Simulation (LES), we verify the jet exhaust noise shielding benefit by installing the engine over the wing. In Section 3.2, a preliminary estimate was made using the JSI model at the sideline and cutback operating conditions. But given the importance of the shielding benefit in achieving the noise goals, a detailed high-fidelity analysis is performed at the sideline operating condition for the baseline trajectory using the AFRL LES solver FDL3DI that has been validated internally within GE.

The details of the over-wing geometry chosen, were described in detail in Section 3.2.1. Figure 7 shows the above wing model where the exhaust nozzle lip is 5 diameters upstream (X/D = 5) of the wing trailing edge that is considered for the present analysis.

5.1.1   Operating Conditions

Acoustic evaluations will be performed at a forward flight Mach number of 0.38 and the baseline nozzle operating at the sideline thrust condition. Simulations have been performed for both isolated and installed configurations to predict the shielding provided by the over-wing installation.

5.1.2   LES Solver

The LES approach is based on high-order finite difference solutions for unsteady 3D compressible Navier-Stokes equations in curvilinear coordinates. Spatial and temporal discretizations are based on a 6th order compact finite difference scheme and a 2nd order Beam-Warming scheme respectively. An 8th order spatial filter is employed in place of sub-grid models to remove spurious waves at the high frequency end of the turbulence energy spectrum. This approach is commonly known as the implicit LES (ILES) method. It has been widely used for flow and acoustic problems and carefully validated for various applications, including exhaust jets, low Reynolds number wind turbine airfoils, film cooling and fan blades. Significant improvements have been made on the data structures, memory efficiency, and I/O efficiency to enable scalability for massively parallel simulations. Domain decomposition based on multiblock overset grids is used for parallelization and complex geometry adaptation. GE has previously demonstrated the ability of leveraging this LES based approach to predict the acoustic signature and examine noise source generation from canonical nozzles and passive noise control devices such as chevrons (Ref. 6). The same numerical approach was then expanded to examine the effects of installation including pylon and wing surface (Ref. 7).

5.1.3   Simulation Approach

A highly resolved structured overset mesh is generated to model the over-wing installed geometry along with the baseline three-stream nozzle in the sideline configuration. Starting with an initial solution that is interpolated from a prior RANS prediction, a time accurate simulation is performed using the LES solver described in the previous section. Time accurate data is then sampled on predefined surfaces that encompass the jet plume and the installed geometry. Having solved for the near field fluctuations in the jet plume using LES, the far-field noise is predicted using a permeable surface Ffowcs Williams and Hawkings (FWH) solver. This projects the near-field fluctuating quantities on the FWH integration surface to a far field observer location, alleviating the need to numerically solve for the flow quantities in the far field, resulting in significant resource savings. The far field solution will be computed based on surface integrals of the flow quantities evaluated on the control surface. A frequency domain formulation of the FWH solver is used in the present work (Ref. 6).

5.1.4 Computational Domain and Grid Metrics

Details of the computational domain are shown in Figure 50. To significantly reduce the computational cost of the simulation, the entire aircraft is not included in the computation domain. Rather, only features relevant to the jet exhaust flow development and noise generation are modeled. Only one engine is included (center engine is not modeled) and a symmetry boundary condition is used to model the second outboard engine. The inlet of the computational domain is located at the inlet of the three-stream nozzle. Only the aircraft geometry downstream of this location is included in the computational domain as shown in Figure 50. The axial extent of the computational domain is 75D. The radial extent of the domain is 15D at the nozzle inlet and expands to 25D at the domain exit.

A RANS simulation of the full aircraft at 8.1° AoA is first performed at M = 0.38. The solution is interpolated onto the LES domain to provide an initial flow field. In addition, the mean flow values interpolated onto the inlet plane are held constant as the inlet boundary condition. No inlet turbulence is provided as the turbulence generated in the jet plume is expected to be much larger that the boundary layer turbulence on the wall surfaces. In addition, sponge/buffer zone (Ref. 8) boundary conditions are applied at the exit and farfield boundaries to slowly force the solution to the RANS condition and ambient condition respectively with no reflections. Total temperature and total pressure inlet boundary conditions are specified at each of the three nozzle inlets, Figure 51.
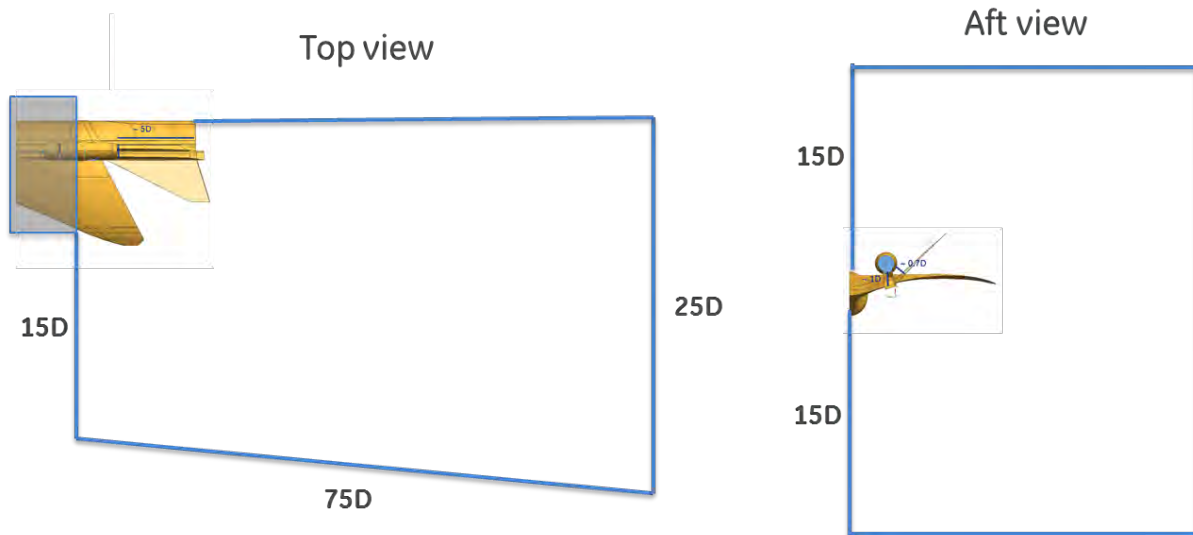
Figure 50.—Computational domain definition for the LES simulation.
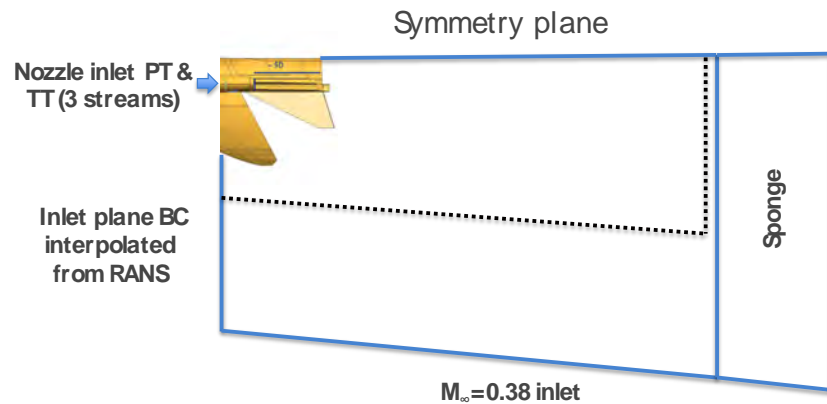
Figure 51.—LES simulation boundary conditions.

An overset approach is used to model the complex installed geometry. An example of this is shown in Figure 52. LES best practices developed by GE are used to generate the grid. The near wall resolution at all wall surfaces is y+~1. Near nozzle walls, the off-the-wall stretching ratio was chosen to be ~1.08. The cell aspect ratio in the jet shear layer region was maintained at ~5 to 10. While best practices were used in the nozzle wall region and the jet plume, slightly higher wall stretching ratios and cell aspect ratios were used near the aircraft surface since modeling the wall boundary layers is not as critical as accurately predicting the jet turbulence and to keep the total grid count practical. This should have minimal effect on the prediction of exhaust noise or the impact of surfaces on the noise generated or propagated. Significant advantage was taken of hole cutting and block blanking to enable modeling of installation geometry including the tail and the partial wing.

The total grid count for the installed configuration was ~230MM points. Using the software Bellero, the various blocks in the computational domain were split into a total of 512 sublocks. Multiple iterations of sublocking were attempted to ensure that no block partition goes through a blanked region—a necessary condition for solver robustness. The simulation was performed on 512 cores on a Cray cluster. Solver scalability is not an issue as the solver scaling is more than 95 percent at the current levels. For acoustic sampling, an L-shaped surface that is aligned with grid lines (along multiple blocks) is chosen as the FWH surface (Figure 53). The surface is not closed at either the upstream or downstream ends. The grid spacing at the FWH surface is chosen to resolve acoustic waves up to a frequency of approximately 3.5 KHz at full-scale. Time accurate data is sampled on the surface to be used as input to calculate the far-field acoustics. Acoustic predictions will be made using just the sampled L-shaped surface, as well as a U-shaped surface (created by mirroring the L-shaped surface) to assess the sensitivity of the choice of sampling surface.
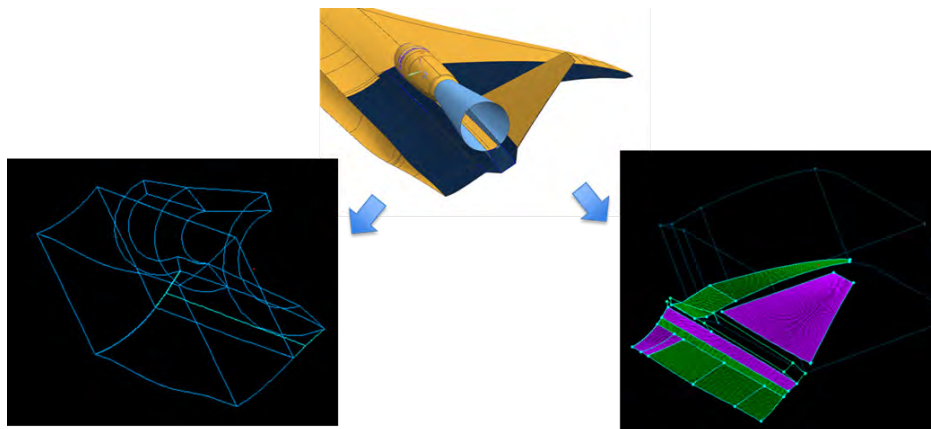
Figure 52.—Overset block topology for the above wing geometry.
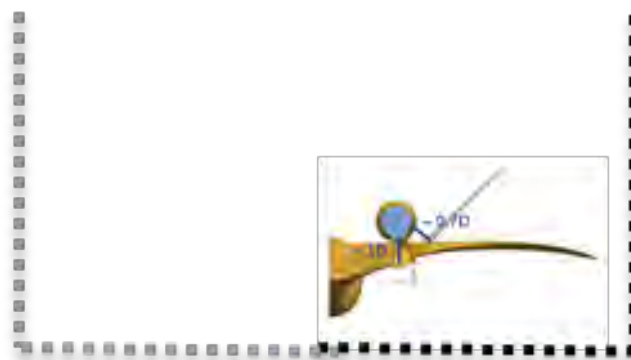
Figure 53.—Schematic of FWH surface (dotted lines).

5.1.5 Preprocessing

First, a RANS simulation was performed for the full installed configuration using GE's in house solver. The RANS simulation did not include the 3-stream nozzle and the jet plume. Instead a conical plume was used to simulate the presence of the jet, with the outer wall of the plume being treated as a slip wall. This flow field was then interpolated onto the LES grid to provide an initial flow field and inlet boundary condition to the LES computational domain. In regions where there is no flow present in the RANS solution (e.g., nozzle, jet plume), a uniform flow field was prescribed for the initial flow. A preliminary investigation of the solution showed some flow separation downstream of the pylon. This could possibly introduce numerical stability issues in the LES in addition to undesirable noise sources. To remedy this, the pylon geometry was modified as shown in Figure 54 where the pylon is tapered to avoid a blunt trailing edge. The LES grid was accordingly modified and the preprocessing steps repeated. A RANS simulation was once again performed on the fully installed configuration, but with the modified pylon geometry. This solution was then interpolated onto the LES computational grid to provide an initial flow field. As described earlier, the flow field at the inlet plane of the LES domain is held constant and is used as the inlet boundary condition (Figure 55). Only the mean flow values are used with no turbulence specification. This is a reasonable assumption as the turbulence levels in the jet shear layer should be significantly higher than the levels in the free stream or surface the boundary layer.
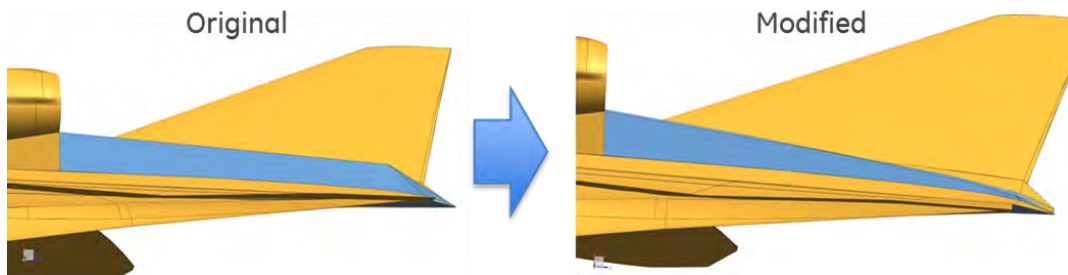
Figure 54.—Pylon modification to remove trailing edge separation.
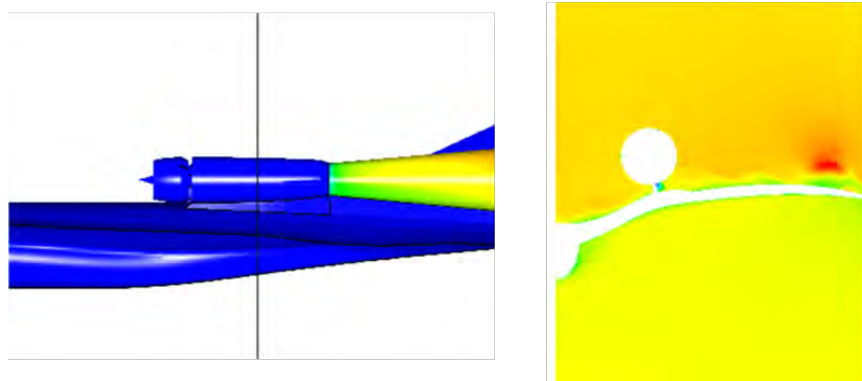
Figure 55.—The 2D inlet boundary condition (axial velocity shown) for the LES domain.

5.1.6   Solution

The LES simulation procedure is as follows. Unsteady simulations with the initial flow field obtained from a RANS solution are started using a second order filter. This is a strong filter that allows for solver robustness as initial transients, including regions of discontinuity between interpolated RANS solution and prescribed uniform solution, are allowed to flow out of the computational domain. A relatively large time step of 1e-5 sec is used during this phase of the simulation. The simulation is run for about 15 flow through time units (one time unit is the time taken for the freestream flow to travel the length of the domain), which should allow for a fully developed flow field. The filtering is then changed to 4th and finally 6th order in two steps. At each step the total simulation time is about 15 flow through time units till a fully developed stage is reached. The time step is also reduced to a lower value of 5e-7 sec to maintain stability.

5.1.7   Results

Once the flow field is fully developed, near-field fluctuations are sampled on the L-shaped surface as described in the previous section. The total run time, to obtain a fully developed flow field and for flow sampling, was approximately 14 weeks. The frequency domain FWH formulation is then used to predict the noise from the installed configuration at various observer locations.

To assess the sensitivity of the choice of FWH surface shape, predictions were made for an observer below the engine centerline using the data sample on the L-shaped surface and using a full U-shaped FWH surface that encompasses the simulated engine and the symmetrical outboard engine (using the symmetry plane boundary condition). Figure 56 shows the prediction from the two different surfaces at polar angles of 90° and 150°. As expected, when the sampled FWH surface is mirrored and predictions made using the U-shaped FWH surface, the predicted noise levels are ~5-6 dB higher than predictions made using a L-shaped surface. This is because we now assume two coherent noise sources propagating to the observer. In reality, the two exhaust plumes are independent. For our current purposes, i.e., estimation of surface shielding effects on a single engine, we could safely use just the L-shaped surface with no significant loss in accuracy. Hence all subsequent predictions for the installed configuration are made using only the actual sampled surface.

As mentioned earlier, simulations have been performed at the sideline operating condition for both the isolated and installed nozzles. Figure 57 shows the far field acoustic predictions from both simulations for a sideline observer. Comparisons are shown for four different polar angles. It should be noted that while the simulations were performed at model scale, the results presented here are at engine scale. It is observed that the installed configuration provides a significant shielding benefit across almost all frequencies for the upstream angles. As we move to the downstream observers, wing shielding does provide benefit at mid to high frequencies, but as expected there is no noticeable difference at the low frequencies. In fact, the peak noise level increases by approximately 1.5 dB for the furthest downstream observer. The spectral plots show a drop off at high frequencies. This is because the grid for the installed and isolated cases is designed to resolve up to ~3.5 KHz at the engine scale, and higher frequencies are under-resolved.
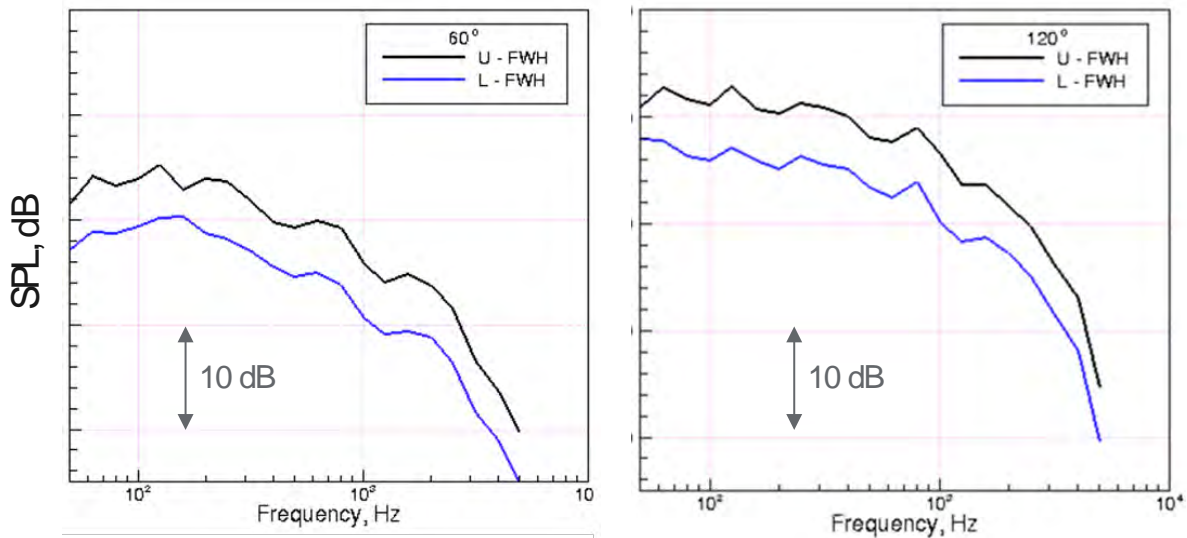
Figure 56.—Comparison of predicted farfield noise using two different FWH surfaces.
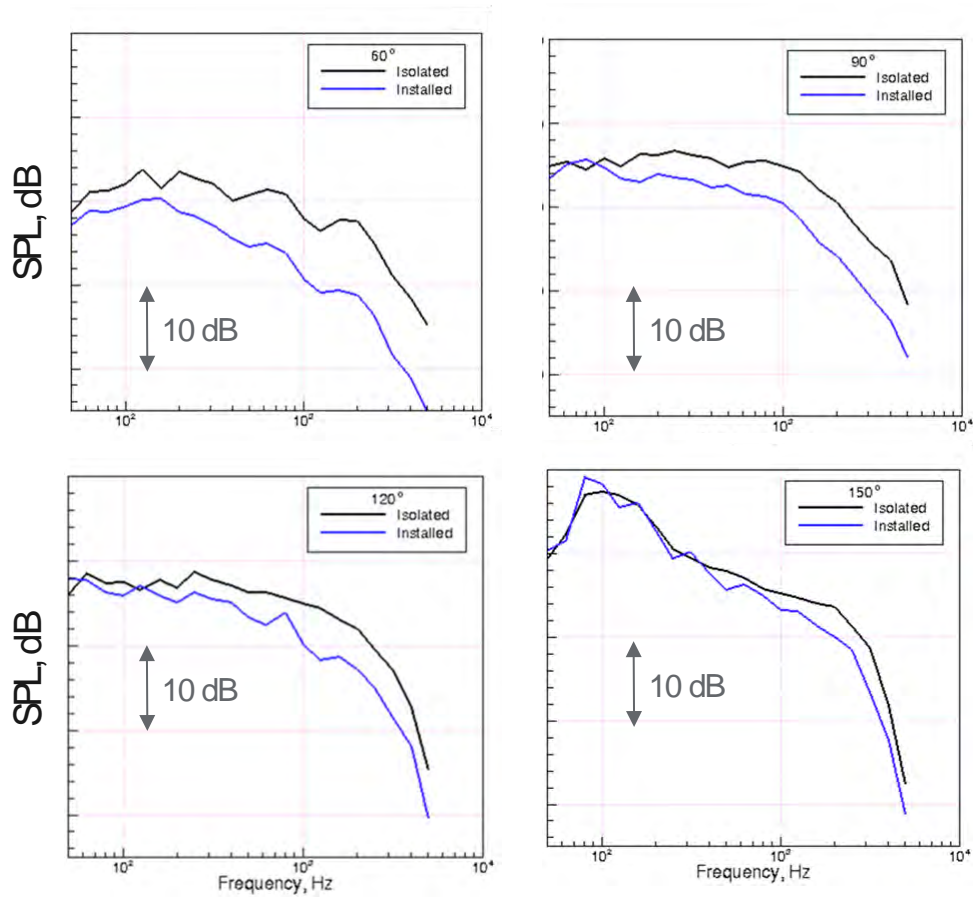
Figure 57.—Comparison of farfield predictions at sideline observer for isolated and installed configurations.

Figure 58 shows the net shielding impact for the above wing configuration for a sideline observer. This is compared to preliminary estimates of shielding benefit predicted by the Jet Surface Interaction (JSI) model that was used in the system noise studies. At upstream angles, LES predictions show a trend similar to JSI in terms of overall benefit at mid-to high frequencies, but the LES predicts approximately 20 to 40 percent higher benefit. At the furthest downstream location, we assumed zero benefit in the shielding conceptual studies. But the LES shows that even at such angles the wing/tail surfaces seem to prove a small amount of shielding. There is also a small increase observed at low frequencies. It is not clear if this is a numerical issue or a real effect. Significantly larger sampling time and effort would be required to refine the predictions in the very low frequency range. However, the low frequencies shown do not affect EPNL significantly.

To assess the impact of shielding at the flyover observer location, FWH far-field acoustic predictions are also made for an observer at the flyover location (symmetry plane). Figure 59 shows the predicted spectral benefit at four different polar angles suggesting that for the same pressure ratio, more benefits are observed directly beneath the aircraft (e.g., flyover, approach conditions). Also, note that for the sideline observer, shieling is provided by some combination of the aircraft wing and the side tail, but for the flyover observer, the shielding is primarily due to the aircraft wing. Overall, it is observed that the predicted shielding benefits in the symmetry plane is higher for almost all the polar angles when compared to the sideline observer.
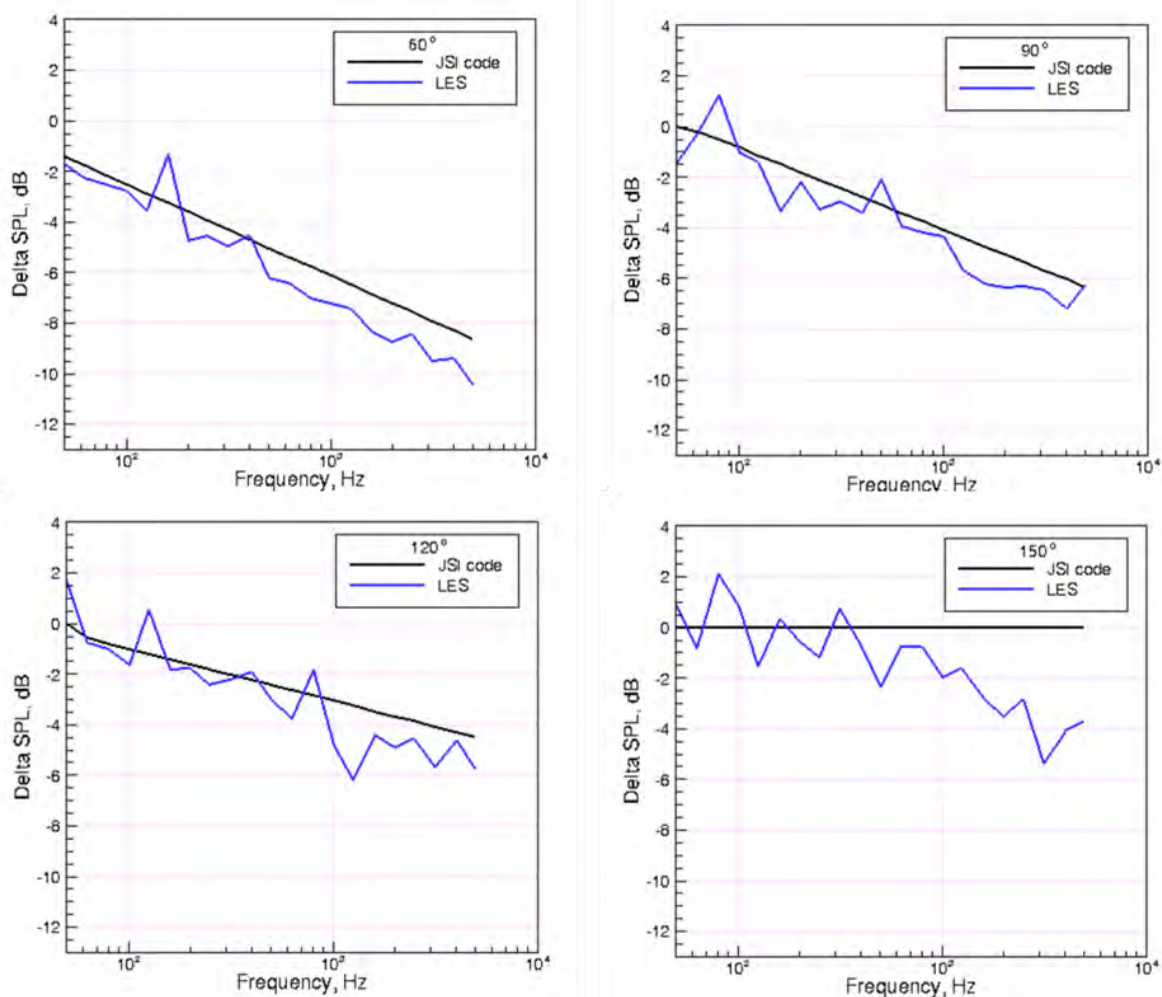
Figure 58.—Comparison of shielding benefit as predicted by NASA's JSI code and LES approaches.
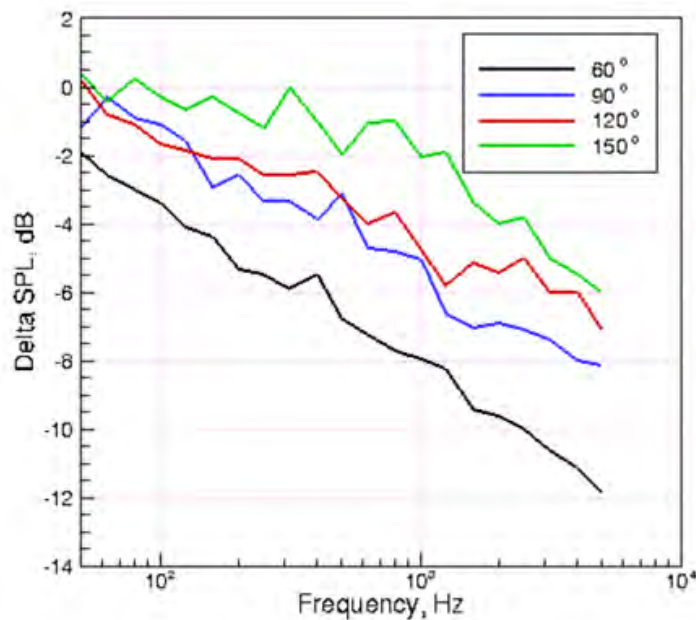
Figure 59.—Shielding benefit predicted by LES for observer in
the symmetry plane, below the aircraft (Flyover observer).

Based on the results of this LES, it is expected that the preliminary assessment of jet noise shielding benefits made in Section 3.2 are somewhat conservative. Thus, the over wing mount configuration could provide a larger net acoustic benefit than anticipated by the shielding studies. However, this conservatism is acceptable considering the preliminary nature of these studies.

5.2 Chevron Design Exploration

5.2.1 Background

The chevrons tested in the N+2 Ph2 Ext. program reduced low frequency noise but did not provide any cumulative noise benefit. The objective of this study is to explore the design space systematically in more detail to improve noise benefit similar to subsonic applications (Ref. 9).

We hypothesized that the tested chevrons showed no cumulative noise benefit because:

- These chevrons were designed to reduce noise under isolated conditions. This means that the low-frequency benefits are weighed against the high frequency penalty to ensure overall noise improvement. There is no accounting for capability to absorb high frequency penalties (by physical shielding), to help achieve additional low frequency benefits.
- The frequency at which the tested chevrons cross over from low frequency benefit to high frequency penalty is too low to take advantage of the high frequency shielding provided by the wing surface.

To assess the potential system noise impact of an improved chevron design, we considered two conceptual chevron acoustic spectrums that were derived from the tested chevrons with the following assumptions:

- Scale the chevron benefit to move the low frequency benefit/high frequency penalty crossover point to higher frequencies
- Assume twice the low frequency benefit, but with no change in the high frequency penalty region

Suppression tables were generated for the two conceptual chevrons and fed into the system noise analysis. It is observed that these spectral modifications can provide an additional 0.8-1.2 EPNdB benefit at just the sideline condition. This suggests that significant cumulative noise improvements could be achieved if these spectral changes can be effected.

5.2.2 Analysis Approach

Two approaches will be used to explore chevron designs. The first approach, described below, involves direct investigation of the chevron-modified flow field and noise sources. The second approach is described in Section 5.2.3. By studying the areas with increased or reduced levels of turbulence kinetic energy, coupled with the turbulent length scales, it is possible to predict directly from the computed flow field which frequencies will have higher or lower noise. It is well-known and validated in tests that RANS-modeled jet mean flows can give a quantitatively correct picture for the fine-scale turbulence noise sources (Ref. 10). By plotting the noise sources for different frequencies, one can directly see and evaluate the noise impact of chevrons as well as visualize the spatial noise source distribution, which helps evaluate chevron benefits in concert with shielding. Figure 60 shows the computed noise sources for the baseline nozzle at sideline for three frequencies: low, medium and high, corresponding to Strouhal numbers of 0.02, 0.2, and 2. The noise spectrum peaks near a Strouhal number of 0.2. As expected, the lower-frequency sources are located far downstream the nozzle, peak-frequency sources are located near the end of the jet potential core, and high-frequency sources are located close to the nozzle exit, making them more amenable to shielding.

5.2.3 Geno

The second approach for evaluating the effects of chevrons is to use a GE-developed jet noise prediction tool, GENO (Ref. 4). At the core of the GENO code lies the MGBK model which has been an industry standard noise prediction method for many years. Using this tool consists of two steps: (a) Computing the jet mean flow using a RANS model, and (b) Propagating sound to the far-field using a nonaxisymmetric Green's function. The GENO code has been extensively tested and validated on conventional single and dual-stream nozzles. The application to three-stream nozzle with chevrons will be new. A combination of mean flow and noise sources investigation using the GENO tool should provide design guidance for chevrons.
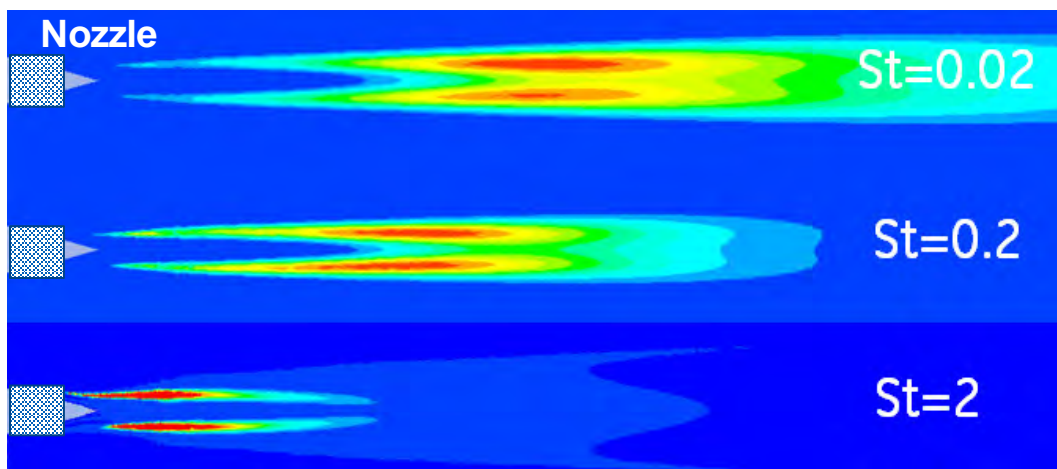
Figure 60.—Noise sources for the baseline nozzle at sideline at three different frequencies.

5.2.4   Chevron Design Approach

To identify the most promising chevron designs with shielding, sensitivity studies will be performed (at the sideline operating condition) on the chevron design parameters such as extent of chevron penetration, number and size of chevrons, and the position of chevrons.

The design process starts with the CAD model modification, followed by CFX RANS computation for the mean flow, followed by noise source quantification and flow field evaluation and finally, GENO propagation to the farfield. The SST turbulence model is used to compute the flow field since it has proven to be an adequate tool for resolving jet mean flow and turbulence for both cold and heated jets. To expedite design iterations, an extra-fine unstructured mesh is used to resolve the flow, Figure 61.

The nozzle along with the jet is encapsulated into a cone with the mesh fine enough to resolve local velocity gradients and the highest acoustic frequencies of interest. A sensitivity study on the mesh count was performed. Mesh sizes of 18, 25, and 80 million nodes were evaluated, with mean flow results virtually identical between the last two grids. In the interest of accurately resolving the noise sources however, the 80 million node mesh is chosen since it is at the limit of what can be analyzed quickly in a design loop. In the far field, opening boundary conditions are prescribed in CFX to allow for jet entrainment. By iterating between CAD, CFX, GENO and source analysis, several promising designs can be quickly evaluated.

5.2.5   Validation of Methodology

To validate the approach, the four nozzle designs (baseline plus three chevrons) for which noise data from the prior N+2 program are available, were first evaluated using noise source maps and GENO predictions.

The baseline nozzle has no chevrons. The second configuration designated PCHVR, has chevrons only at the top of the primary nozzle. The third configuration designated ACHVR, has chevrons at the bottom on the shield nozzle exit and on the top of the primary nozzle exit. And the fourth configuration, SCHVR, has chevrons only at the bottom on the shield nozzle exit.

Figure 62 shows contour maps of the turbulence kinetic energy (TKE) for the four configurations. The scale is the same for all cases, with red color corresponding to high TKE levels. It is well-known that for a jet, higher levels of TKE generally correlate with higher noise levels. Everything else being equal (geometry and operating conditions), a jet with a higher TKE level will be noisier at some part of the spectrum.

As can be seen in Figure 62, there is a distinct trend between the presence of the chevrons and the TKE levels: adding chevrons leads to higher TKE levels near the nozzle exit (top stream for PCHVR and ACHVR, and bottom stream for SCHVR), but removes the large red region in the baseline nozzle midway to the end of the jet potential core (top of the PCHVR, bottom of the SCHVR and top and bottom of ACHVR). The region near the nozzle exit corresponds to small length scales and high frequencies. Adding chevrons leads to higher TKE levels in that region, known as the chevron high-frequency penalty. The shield stream has lower total pressure and lower velocity, therefore the gradients between the shield stream and the ambient flow are lower, which is why the high-frequency chevron penalty for the SCHVR configuration is less pronounced compared to the PCHVR and ACHVR nozzles. The region of large TKE near the end of the jet potential core corresponds to radiation at the frequencies where the noise spectrum peaks at side angles, and it is obvious that chevrons tend to reduce the TKE levels, and one would expect noise reduction at the dominant part of the spectra.

Based on the TKE and noise source maps, and keeping in mind that the high-frequency penalty region is above the wing and will be partially shielded, one would expect that the ACHVR configuration is the most promising for jet noise reduction although the chevron design must accommodate the pylon. Figure 63 shows the contour maps of the noise sources at 200 Hz, approximately where the full-scale jet noise spectrum peaks, and here we see a picture similar to Figure 62. In all cases studied, the peak noise source maps for the fine-scale turbulence correlated with the TKE levels, so we will focus on the TKE maps for simplicity.
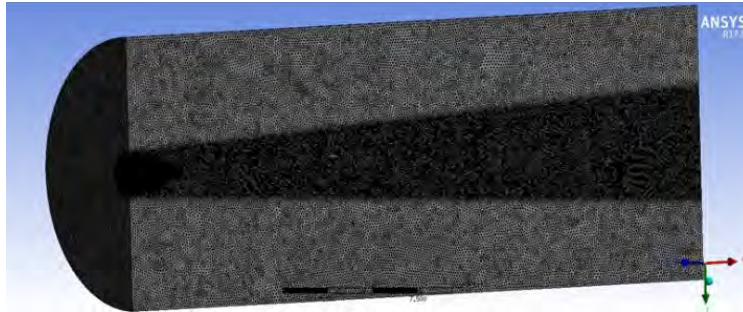
Figure 61.—Typical grid topology for the jet mean flow computation.
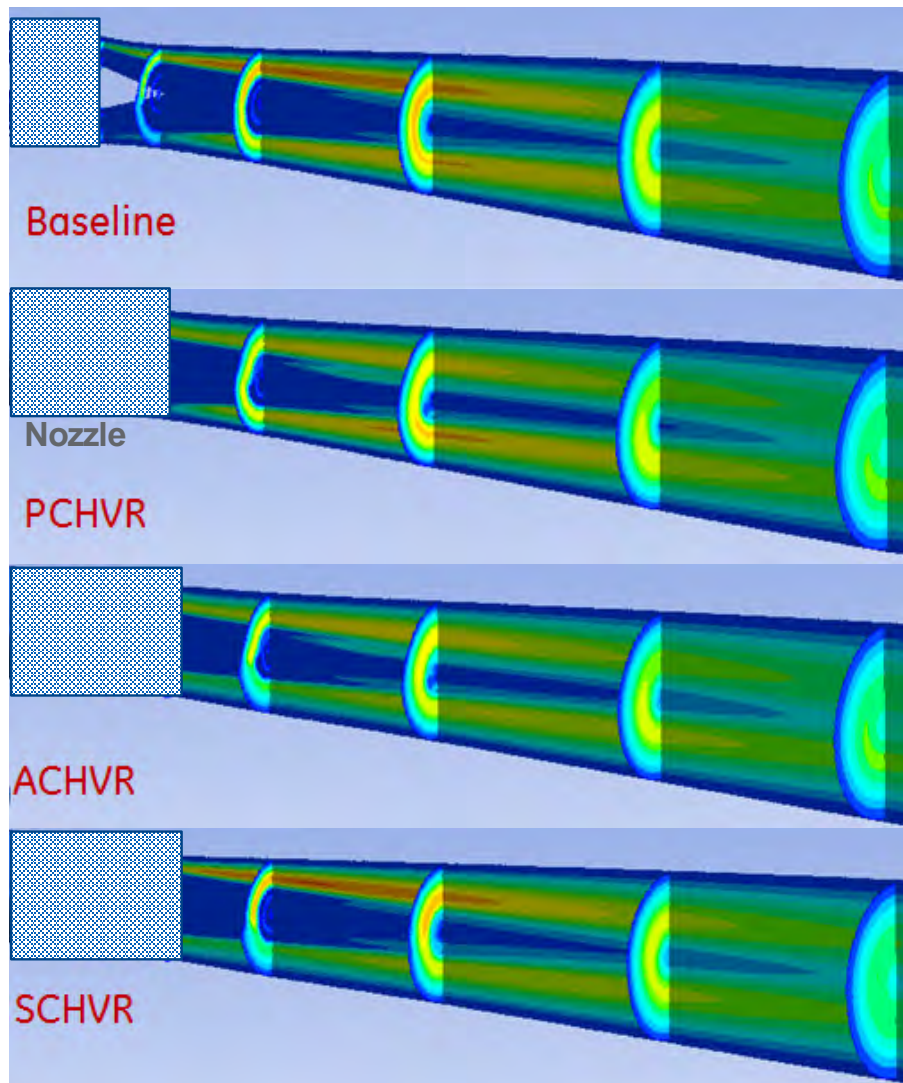
Figure 62.—TKE distribution for the four tested configurations.
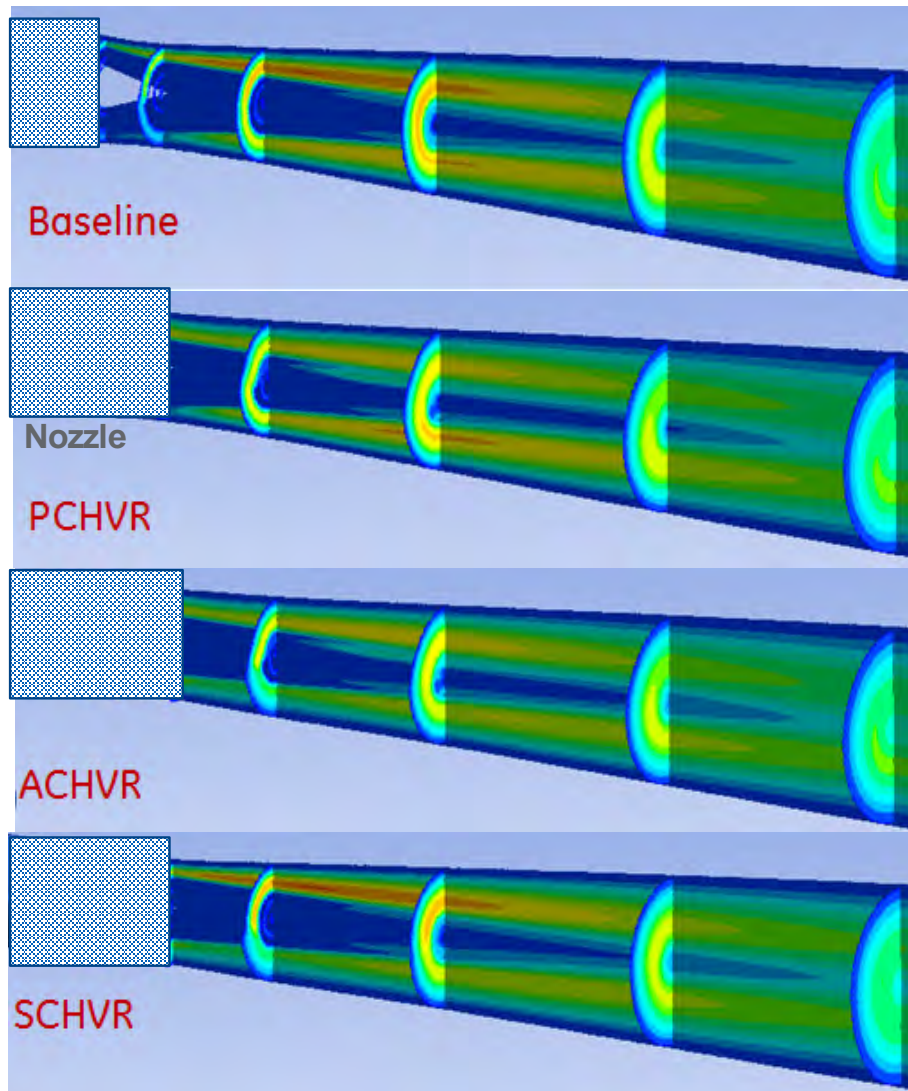
Figure 63.—Noise source distribution for the four tested designs at 200 Hz.
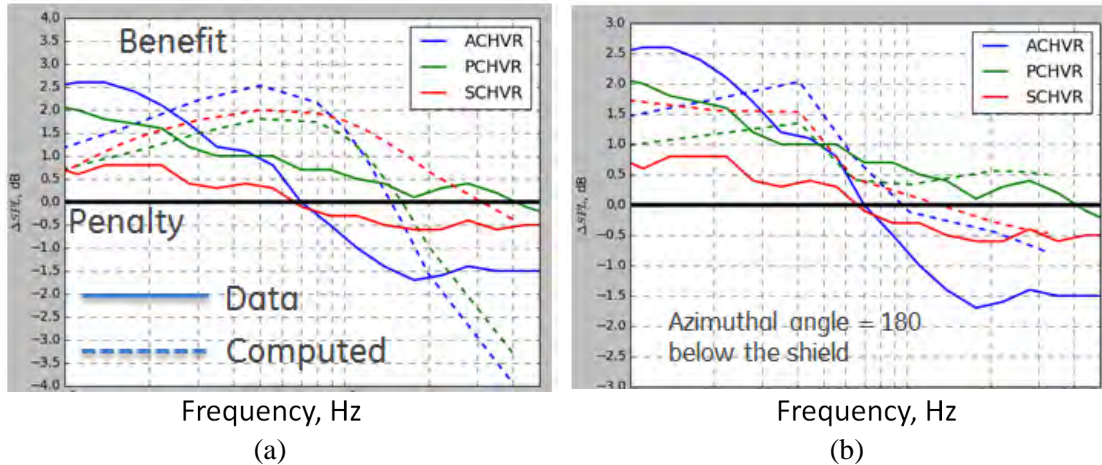
Figure 64.—Full scale spectra of delta SPL vs baseline spectrum for all 3 chevrons at polar angle 90°: (a) Noise sources volume integrated, and (b) GENO predictions for the observer located below the shield. Positive delta means noise benefit; negative delta means chevron noise penalty.

Figure 64 shows computed delta SPL relative to the baseline nozzle for the three tested configurations. The computed spectra for the PCHVR, ACHVR sand SCHVR configurations are subtracted from the baseline spectrum. Figure 64(a) shows the trend for the volume integrated noise sources at engine scale, and Figure 64(b) shows the GENO predictions. If delta SPL is positive, it means that the given design is quieter than the baseline, i.e., there is benefit from adding chevrons at this frequency, and if the delta SPL is negative, then the chevron is louder. Solid lines are computed spectra and dashed lines are the measured data. As can be seen, the computed spectra follow the measured spectra trend-wise in general—where we see a penalty in the measured data, we also see a penalty in predictions, and where we see a benefit in the measured data, we see a benefit in the predictions. The discrepancy at very low frequency around 100 Hz can be partially explained by the fact that for frequencies below 100 Hz the computational domain must be large enough to completely capture all the sources contribution which would make the domain and mesh size very large. Near 100 Hz, the noise levels are almost 5 dB below the peak, and frequencies below 50 Hz are not relevant, so limiting the computation domain to 2.5 jet core lengths was deemed adequate here. From previous experience, the accuracy of GENO is no better than 0.5 dB, therefore it is challenging to accurately resolve the difference between the different designs on unstructured meshes. Nevertheless, there is value in examining the GENO spectra, as they should in general predict strong trends, and together with the flow turbulence and source maps direct us towards quieter designs.

5.2.6   Chevron Improvement Study

Before studying the effects of the chevron count and penetration on noise, the placement of chevrons was studied. In particular, it is not obvious whether one should keep the chevrons on the shield only or remove the shield chevrons but add chevrons at the bottom of the primary nozzle, or retain chevrons everywhere on all nozzles. To better understand chevron placement choices, four configurations with different permutations of chevron position were studied using the approach outlined in the previous section. This study showed that the ACHEVR design is best from a positioning perspective. Starting with this (ACHEVR) design, four more configurations were analyzed with different counts and penetration angles. The primary intent here was to increase low and mid-frequency benefits with the understanding that high frequency penalties (if limited) would be shielded.
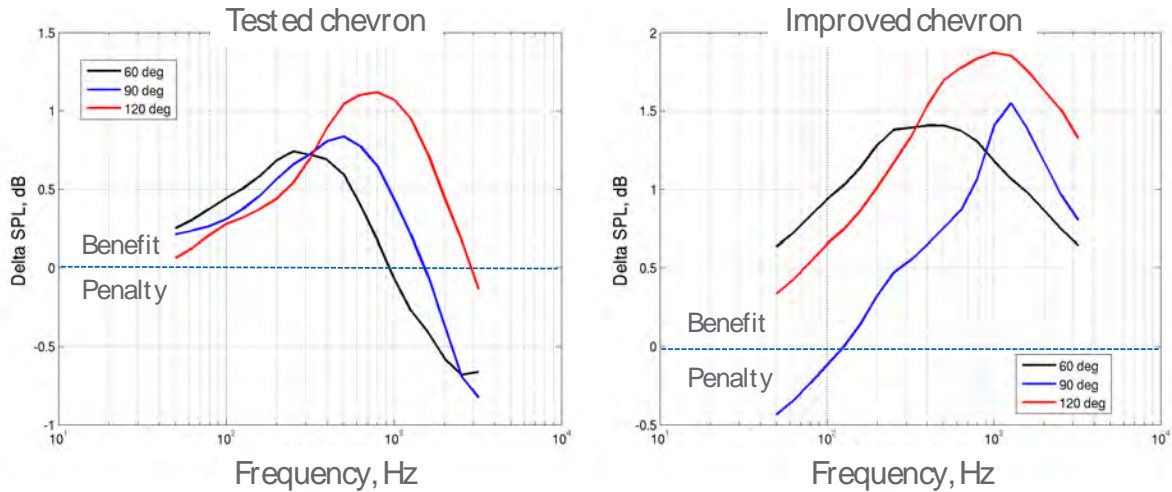
Figure 65.—Farfield noise trends relative to baseline nozzle at engine scale as predicted by GENO.

In Figure 65, spectral benefits predicted by GENO at an azimuthal angle of 90° (side) are plotted for the tested ACHEVR and the best design from this study. Three curves are shown in each plot for inlet angles from the jet axis of 60° (upstream), 90°, and 120° (downstream) with the latter being of most interest. The new design gives benefit across almost the entire frequency range. Note also that for frequencies beyond 1 KhZ, shielding benefits become significant, so high frequency penalties are not weighted significantly.

To compute the EPN benefit of the new design, spectral trends as a function of angle were input as user-defined suppression arrays into the baseline system noise model. Benefits were assumed to be zero for frequencies higher than that shown in Figure 65. Additionally, chevron benefits for downstream angles greater than 120° were assumed to be the same as 120°. This is a conservative assumption but adequate for design differentiation. Shielding benefits from the JSI code for a nozzle position 5 diameters upstream of the wing trailing edge were also included. The resulting exercise shows that the new design provides over 1.2 EPNdB relative to the baseline nozzle at the sideline operating condition. Accounting for some realization of the noise benefit of these improved chevrons at flyover and approach, it is estimated that chevron technology will yield upwards of 2 EPNdB noise reduction.

While the chevrons show a noise benefit in these assessments, one must recall that the accuracy of the GENO tool is within ±0.5 dB, so the noise benefits may not be realized in testing. Additionally, these designs were evaluated in an isolated fashion and the impact of installation is uncertain. These uncertainties must be factored into any technology maturation effort. Furthermore, the noise benefits must be traded against the performance impact to be considered for product optimization.

6.0 Sonic Boom and Cruise Performance Study

Lockheed Martin performed sonic boom and cruise performance assessments on the installed geometry with the outboard engines at the most upstream location feasible within vehicle balance constraints. The analysis shows similar boom loudness potential for either engine location, with perhaps a dB or two better potential near the edge of the sonic boom carpet for engines over the wing. However, the L/D impact of engines over the wing was significant (–7 percent) primarily due to the loss of propulsion-induced lift compared to underwing nacelles. Preliminary estimates show that this penalty could be mitigated by increasing the nacelle fineness ratio, however that requires a more detailed study that takes into consideration engine diameter and accessory placement trades.

Details of the analyses are described in the Lockheed Martin report.

7.0 N+2 Aircraft System Noise Status and Technology Options

The goal of this program was to evaluate low noise technologies for low boom aircraft to achieve an aggressive community noise goal of Chapter 14 minus 10 EPNdB. Targeting this goal, we investigated over-wing installation, flight path optimization procedures such as takeoff PLR and steep approach, and improved chevron designs. In this chapter, we summarize the results of these investigations as well as the risks and additional considerations that need to be addressed.

The baseline N+2 trajectory (with aggressive PLR) and 3° Approach glideslope is shown to nominally meet Chapter 4. Therefore, additional technology is needed to meet the noise goal. Table 2 shows the potential noise benefits as well as the risks assessed for each of the noise reduction approaches investigated in this study to attain the program goal. It is clear that flight path optimization procedures are very powerful means of community noise reduction. Furthermore, from GE Aviation's analysis some level of PLR (currently not allowed by regulation) is needed for the aircraft to meet the sideline noise constraint for Chapter 3. And while the impact of PLR or steep approach on the design of the aircraft system itself may not be very detrimental, regulatory and safety considerations need to be assessed.

The improved chevron design from Chapter 5.2 was predicted to achieve over 1.2 EPNdB at the sideline condition with shielding. Accounting for some realization of the improved chevrons at the flyover and approach conditions, it is estimated that chevron technology will yield upwards of 2 EPNdB but at some cruise performance cost. Since the benefits are attractive and there is room for improvement, acoustic validation of the chevron design with shielding in the NASA Glenn AAPL facility is recommended to guide design optimization studies.

7.1 Wing Shielding Considerations

Wing shielding is by far the most transformative technology for noise, yielding at least 6 EPNdB cum. benefit for the engine mounted near the wing trailing edge and upwards of 10 EPNdB cum. benefit for the most upstream engine position. Moving the engine further aft to improve vehicle balance will reduce the noise benefit.

Lockheed Martin assessed a –7 percent impact to L/D for the current installation due to loss of propulsion-induced lift force for over-wing nacelles. However, nacelle fineness ratio improvement by improved accessory placement and engine design was identified as a possible solution to negate the performance impact. In addition, starting from a clean-sheet configuration design would offset some of the negatives. Thus, shielding benefits need to be considered in the context of such system trades and potential improvements.

Finally, fan distortion and noise is a critical piece of the puzzle for over-wing installations. We assessed a penalty of 3 dB for fan distortion at Approach that is not accounted for in the shielding estimates. Also, while distortion was assessed, its impact on fan operability was not evaluated. Distortion degrades operability, so this must be considered as well in future studies.

TABLE 2.—NOISE REDUCTION APPROACHES EVALUATED IN THIS PROGRAM

Technology	Benefit	System impact	Comments
Takeoff procedures	3-4 EPNdB	Low	Regulatory issues
Steep approach	>4 EPNdB	Low	Safety/regulation
Shielding	6-10+ EPNdB	Med-High	Needs redesign to mitigate
Chevrons	2+ EPNdB	Low-Med	Needs validation

7.2   A Potential Noise Scenario

Figure 66 shows a potential noise scenario using the noise benefits assessed in this program. Results shown are nominal projections (50 percent confidence) with no implied guarantee or commitment on the part of GE. No technology realization factors have been applied. A $M = 1.7$ low boom commercial supersonic transport with under-wing installation and advanced variable cycle engine with mid-term technology levels does not meet current subsonic regulation without flight path optimization procedures or further noise reduction technology. Increasing the rotation speed to take advantage of the aircraft's low speed drag characteristics improves the situation somewhat. With PLR, an additional 3 EPNdB of noise benefit is realized, allowing the aircraft to nominally meet Chapter 4. However, this is contingent on regulatory approval of PLR. Increasing the approach glide slope to 4.5° adds approximately 5 EPNdB of margin provided the airplane is certified for the steeper approach.
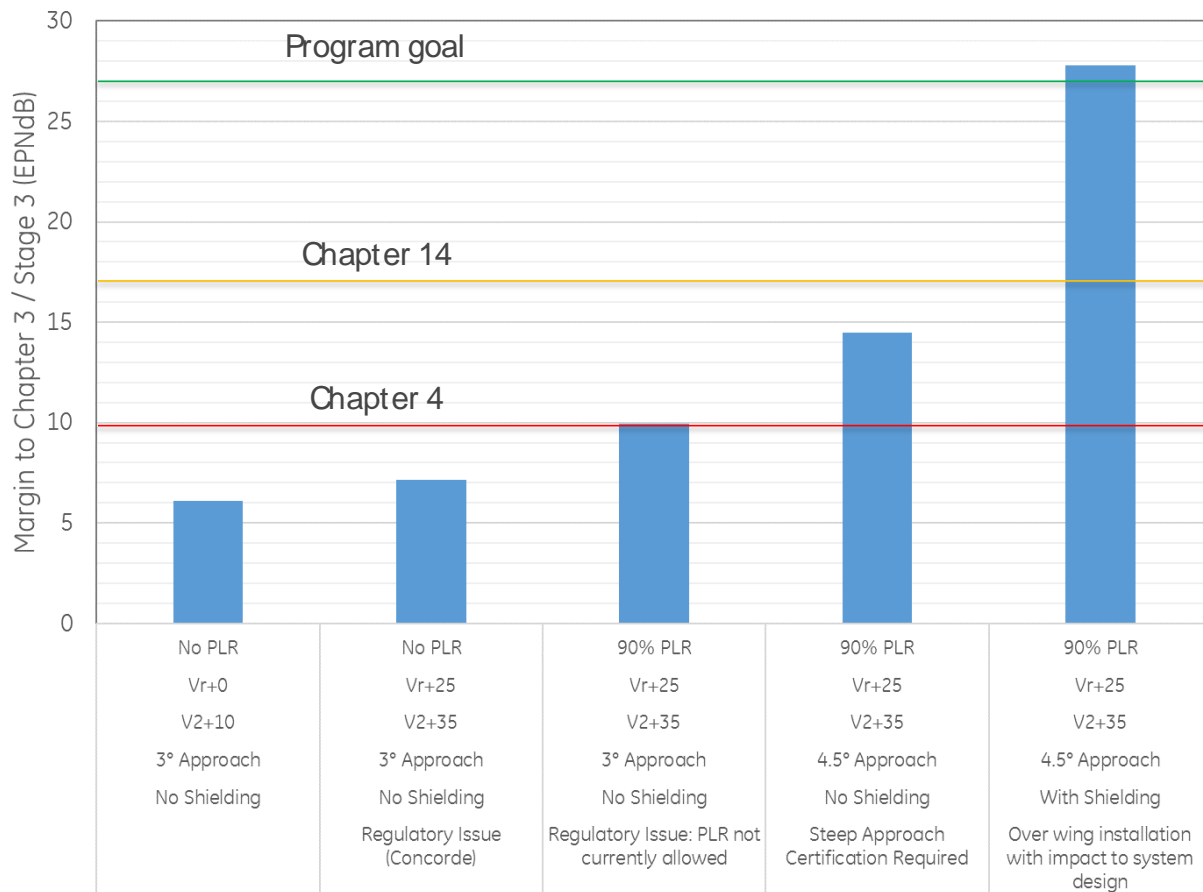
Figure 66.—Example noise scenario. Nominal projections (50 percent confidence) shown with no technology realization factors applied.

The figure does not show any chevron or other propulsion noise technology benefits. It is conceivable that with the addition of relatively high TRL propulsion noise technologies such as chevrons, the aircraft would meet Chapter 14 nominally. However, it would still have no margin for risk during an engine development program. On the other hand, with wing shielding, it is possible to attain the program goal of Chapter 14 minus 10 EPNdB. This level of noise margin may not be needed for a product, so some shielding benefit may be traded against procedures that require regulatory approval such as PLR. But over-wing installation comes with the performance challenges described earlier. So, a balanced approach considering system trades and the regulatory framework is needed to solve the supersonic noise problem.

7.3   New Technology Developed in This Program

In this program, we studied the effect of wing shielding on a mid-term, low sonic boom commercial supersonic transport using an advanced variable cycle engine. System noise benefits of the installation were assessed comprehensively and verified using higher fidelity CAA approaches with key features included in the modeling. In particular, the installed LES analysis performed to verify shielding benefits for exhaust noise is a significant extension of the modeling capability developed and validated for canonical configurations to a realistic aircraft geometry. Risks such as distortion and impact on cruise performance/sonic boom were also assessed. This effort therefore significantly enhances understanding of installation effects on noise for commercial supersonic aircraft and recommends directions for further study.

8.0   Suggested Future Work

Based on the work conducted in this program some suggested follow-on activities are listed below:

- More detailed engine-airframe integration studies including weight, performance and noise trades for over-wing installation:
  - Configuration studies with shielding as an integral consideration
  - Evaluate simpler engine architectures/cycles such as Mixed Flow Turbofans
  - Focused study on improving engine installation to improve L/D and performance
- Fan wind tunnel test with a supersonic inlet with auxiliary doors to validate the high-fidelity distortion, operability, and noise assessments
- Acoustic testing of improved chevron nozzles with shielding and follow on high-fidelity validation studies. Tests with Mixed Flow Turbofan nozzles (baseline/chevrons) are also recommended to quantify jet noise benefits for simpler cycles.
- System noise and trade studies for identifying the best combination of technologies/procedures to mitigate community noise.

Evaluation of Low Noise Integration Concepts and Propulsion Technologies for Future Supersonic Civil Transports

Prime Contract (GE Global Research) NNC15CA02C

GE Aviation

Michael Martinez and Muni Majjigi

1.0   System Noise Assessment—Process

For the trajectory study, GE Aviation used the in-house community noise projection process that is employed for all GE proprietary noise assessments. This process uses a combination of noise source predictions and measured data projected to a single segment flight path defined by an altitude, flight path angle, angle of attack, airspeed, and engine thrust. Cycle points are interpolated to the required thrust point per engine specified in the flight path trajectory. Inlet fan noise is predicted using HiFan which is GE's version of the published NASA/Heidmann method (Referenced in NASA TM X-71763). Only fan inlet noise is accounted, with fan exhaust noise assumed to be suppressed sufficiently due to the relatively long aft fan duct and potential to add liners to suppress it below other sources. The jet noise source is scaled from model scale data taken in NASA Glenn's AAPL in March 2014. The jet noise data is further adjusted for the thrust difference between the measured points and the thrust required at each trajectory point. Airframe noise uses a generic airframe spectra adjusted to the target EPNL provided by Lockheed Martin. The full scale spectra are then flown along the N+2 Ph2 trajectory and the fan, jet and airframe noise components are summed spectrally to compute the aircraft system noise.

Ground reflection effects as well as Extra Ground Attenuation (EGA) and Doppler shift due to source motion are included. Corrections for fan liner attenuation or installation penalties are accounted for by user supplied suppression arrays on the noise components as a function of third octave band center frequencies and angle. No installation penalty is applied for the jet. Note that although jet noise data was acquired at $M = 0.3$, it is flown along a trajectory at a takeoff speed corresponding to the trajectory. EPNLs are obtained by integrating the PNLT time history of the entire aircraft system from the peak to 10 dB down levels in half second intervals and accounting for the duration correction.

Table 1 lists the study assumptions. The following sections will provide details on each of the assumptions.

TABLE 1.—ASSUMPTIONS FOR SYSTEM NOISE ASSESSMENT

	System Noise Assessment Assumptions
Flight Path Points	As provided by Lockheed Martin SL extrapolated from pre-cutback trajectory to 984 ft alt Single Segment flight paths
Cycle Points	N+2 Ph. 2 cycle and engine interpolated to required thrust/engine for each flight path trajectory point. No difference in conditions assumed for differences in cycle velocity points and flight path velocity
Fan Noise Inlet only (Primary & Flade)	Fladed fan predicted with HiFan code (NASA/Heidmann method in NASA TM X-71763): Broadband, BPF tones, Combination Tones included; no distortion flag used. Inlet suppressions applied accounting for treatment area scaling from typical commercial turbofan experience (documented in GE Global Research's report)
Fan Noise Shielding	Body and wing shielding assumed to be 10 dB benefit as documented in the GE Global Research report
Jet	Model scale jet noise data from test in AAPL (March 2014) Specific test point selected from closest pressure ratio point Scaled to engine size $40*\log_{10}$ thrust correction to account for thrust difference between flight point and data point
Jet installation and Flight Effect	Flight effects included in test data. Spectral shielding obtained from JSI code as described in GE Global Research's report.
Airframe	Generic airframe noise prediction adjusted to target airframe noise provided by Lockheed Martin (3° glide slope for AP)

2.0   Flight Path

Lockheed Martin provided several flight path trajectories in support of this study to evaluate the impact of Program Lapse Rate (PLR) on aircraft system noise levels (in terms of EPNL) at the Sideline, Flyover (with Cutback) and Approach flight conditions. Although current subsonic noise certification procedures do not permit PLR, this study is investigating the noise reduction potential of PLR for potential use in community noise certification of supersonic aircraft. The details of the trajectory are described in Lockheed Martin's report. The system noise analysis for Sideline and Flyover (with Cutback) focused on sensitivity to PLR and improved takeoff procedure combinations. Trajectories A-C have no PLR but different takeoff rotation speeds while trajectories D-F include PLR. Trajectories G and H utilize improved takeoff procedure combinations.

As delivered to GE Aviation, the takeoff trajectories detailed the aircraft path from brake release, through steps of rotation, reduction to climb thrust, reduction to cutback power and push over to noise cutback and continued initial climb. The aircraft in several cases initiated the noise cutback below the sideline altitude for max "full power" EPNL. For all the takeoff trajectories, this sideline certification point was assumed to occur at 984 ft altitude, with the noise assessment done at 1476 ft (650 m) from the ground projection of the flight path centerline. To obtain the sideline trajectory information required for the system noise assessment, the flight path needed to be extrapolated from the trajectory points just prior to cutback initiation. For this study, a linear extrapolation of velocity and thrust was made from several points along the flight path where the flight path angle and angle of attack were constant.

For the Flyover with Cutback certification point, the noise assessment was made at the regulatory point, 21325 ft (6500 m) from brake release. In this case, the flight path information provided to GE Aviation specified the required information at the exact Flyover noise certification point.

In addition to the takeoff trajectories, three approach cases were provided for system noise evaluation: A baseline 3° glideslope Approach case and two steep Approach cases, at 4.5° and 6° glideslopes. As provided, the Approach velocity and thrust were provided at 394 ft altitude. However, per the regulations, the approach certification point occurs at 6561 ft (2000 m) from the runway threshold. This results in different altitudes for each approach condition. It was assumed for this study that no appreciable change to thrust required or airspeed results from the difference in altitude: the thrust required is due to the change in glideslope. Also, no change in airframe noise levels was assumed even though airframe noise may change if safe steep descent requires additional control devices, which was not investigated.

3.0   Cycle Model Points

The engine cycle used was created for the N+2 Ph2. study and used without modification for this study. Due to the limited scope of the effort, no modifications were made to account for the differences in flyover altitude and airspeed, and in sideline altitude between the earlier study and the flight path altitudes and airspeeds from this study.

The cycle points needed for this study are the corrected fan RPM, Primary and Fladed fan mass flow, primary and secondary jet nozzle pressure ratios and jet velocities. For the shielding corrections, the mixed velocity, mixed nozzle pressure ratio and mix total temperature are also needed.

4.0 Component Noise Modeling

4.1 Fan Module

Fan noise for this multistage fan was predicted using a GE Proprietary noise module "HiFan" (developed during the HSR program) which uses the Heidmann fan noise module (NASA/Heidmann method in NASA TM X-71763) akin to ANOPP2. This tool was used to estimate only the inlet radiated noise. As mentioned earlier, aft radiated fan noise was considered negligible for this study.

Consistent with the CFD predictions from the N+2 Ph2 Ext. program, the source models show that the noise from the primary fan is dominant over the FLADE stream.

4.2 Jet

Jet noise source data are taken from NASA GRC AAPL scaled model tests of the GE nozzles featuring an IVP and fluidic shield as part of the N+2 Ph2 Ext. program. Test data were acquired at various nozzle pressure ratios and forward flight Mach numbers and with chevrons. For this study, only the IVP and fluid shield with the shield in between the nozzle and the microphones was used at the nozzle pressure ratios corresponding to the flyover and sideline thrust settings that cover the range of thrusts from the given trajectory.

No attempt is made to baseline these source levels to a parent engine database or flight test data. This could be a refinement as part of a future study.

4.2.1 Model Scale Jet Data Adjustment

The data from the facility is first scaled to a 1 ft lossless arc after correcting for jet refraction effects at the microphones. This is then scaled to full scale and atmospheric attenuation is accounted for.

The various trajectories provide engine thrusts that do not align with the equivalent thrust settings of the model scale data. In particular, the thrust for the Approach condition is well below the equivalent thrust of the lowest data point acquired. Therefore, an extrapolation to the jet noise component is required to account for the difference in thrust (and hence, pressure ratio) between the trajectory point and the model scale data. To determine the correction, the model scale data were flown to the N+2 trajectories for Approach and Cutback, and EPNL calculated. The results were compared based on equivalent gross thrust and jet velocity as shown in Figure 1 and Figure 2, respectively.
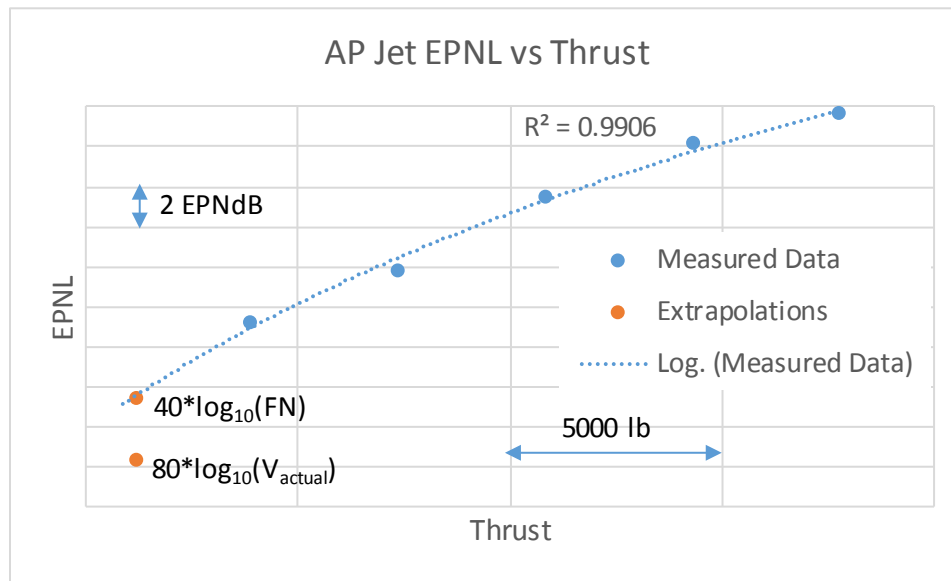
Figure 1.—Jet noise EPNL as function of thrust.
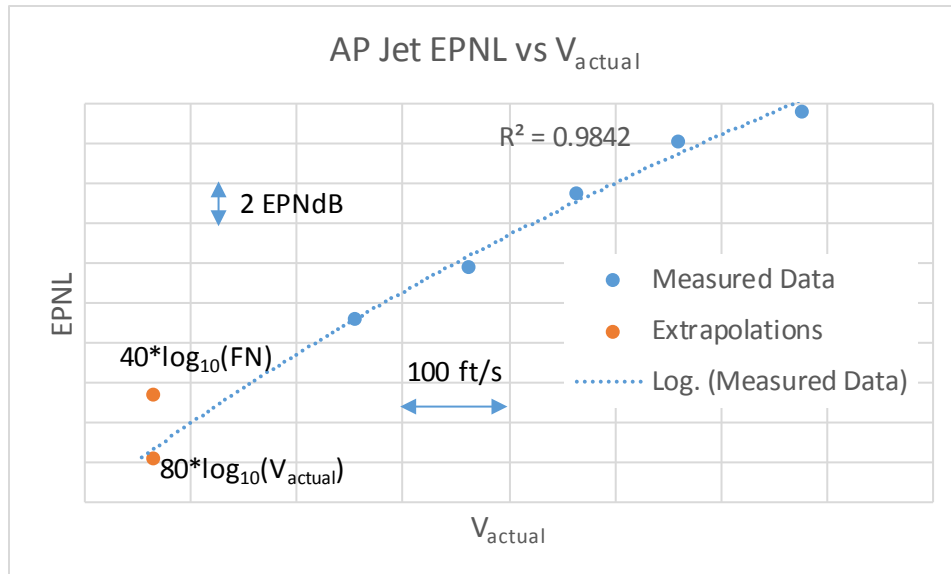
Figure 2.—Jet noise projected to approach point EPNL as function of jet velocity.
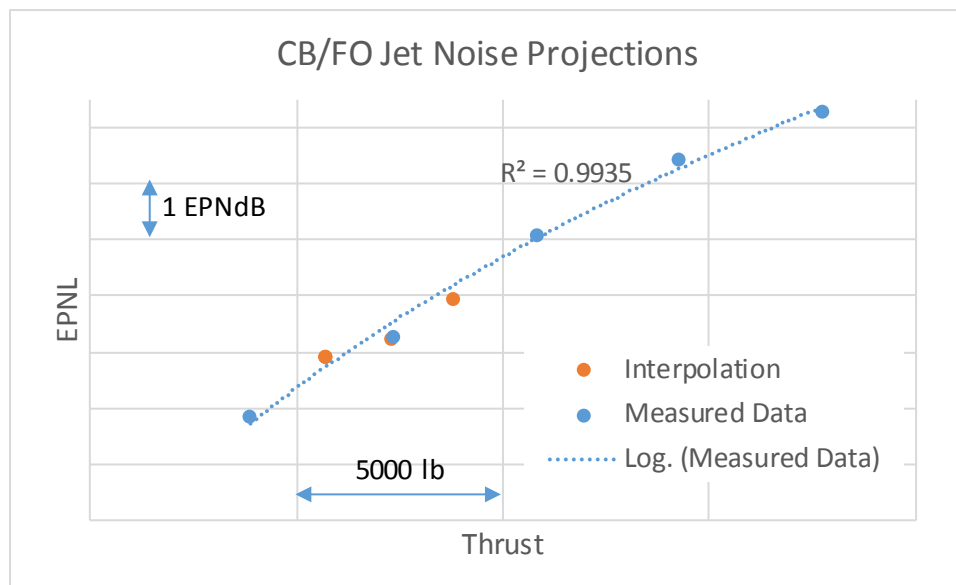
Figure 3.—Jet noise projected to flyover point EPNL as function of thrust.

The extrapolation points mark the equivalent thrust and jet velocity points from the N+2 Ph2 Approach trajectory. Whereas the results would indicate that either the thrust based curve or the velocity based curve would suffice, the thrust based curve, rounded up to a $40*\log_{10}(FN)$ correction for jet, was adopted based on these results due to the slightly higher R^2 value of the curve fit. Figure 3 shows a similar plot for Flyover with Cutback point indicating interpolation based on thrust is reasonable.

4.3 Airframe

To achieve the airframe levels provided by Lockheed Martin on a spectral basis for inclusion in the trajectory analysis, GE applied uniform suppressions to the GE airframe prediction model and projected to flight on the 3° Approach glide slope, with a few iterations needed to match the specified value. This suppression value was retained for the analysis of the steeper Approach glide slopes. Projecting the airframe noise model to the 4.5° and 6° glideslope trajectories result in lower airframe noise than the target, assuming no additional drag devices are employed to meet the steep approaches.

The target airframe noise values for Sideline and Flyover with Cutback are very small compared to the Fan and Jet noise components. Therefore, airframe noise is not included in the analysis for those points.

4.4 Shielding

An additional system noise assessment of the benefits of shielding the inlet and jet by placing the engines above the wing was conducted. For fan inlet noise, a 10 dB benefit across all frequencies and angles was applied at each certification point as described in the GE Global Research report that was verified subsequently using the wing scattering CAA analysis. The jet shielding was computed for the nozzle exit location to be 5 nozzle diameters forward of the trailing edge using the NASA-JSI code and is described again in the GE Global Research report. Jet shielding was also verified for the Lockheed installation using LES—in fact the assumed shielding was conservative compared to the high-fidelity prediction.

It is important to note that for this part of the study, no impact to trajectory or engine cycle is assumed for placement of the engines above or below the wing. This strictly shows the impact of shielding without additional installation benefits or penalties. One point worth noting is that the effect of distortion on fan noise is not included as a penalty since shielding benefits were shown to be higher than 10 dB from the CAA performed by GE Global Research.

5.0 Results

Approach noise levels are summarized in Figure 4. Without shielding, Fan inlet noise is at the same noise level as jet noise, with airframe noise nearly 10 EPNdB lower. The fladed fan inlet noise component is also significantly lower than the primary fan and jet noise sources. On the steep Approach flight paths, system noise levels are substantially lower (–4.5 and –7.6 EPNdB) due to the increased altitude and lower thrust required. As mentioned earlier, because of the assumption that no additional drag devices are employed, the prediction for the 6° glide slope trajectory is optimistic.

At departure, the system noise results show that in general, PLR provides a benefit in sideline noise at the expense of a penalty on the Flyover with Cutback noise. Figure 5 summarizes the unshielded trajectory study results on Sideline noise and Flyover with Cutback noise. The unshielded impact to Cumulative noise of a PLR takeoff, using the standard 3° glideslope for Approach, is shown in Figure 6.

Finally, applying shielding to the PLR Trajectories and the 3° glideslope approach, Figure 7 shows the benefit of the shielding on the Cumulative Noise.
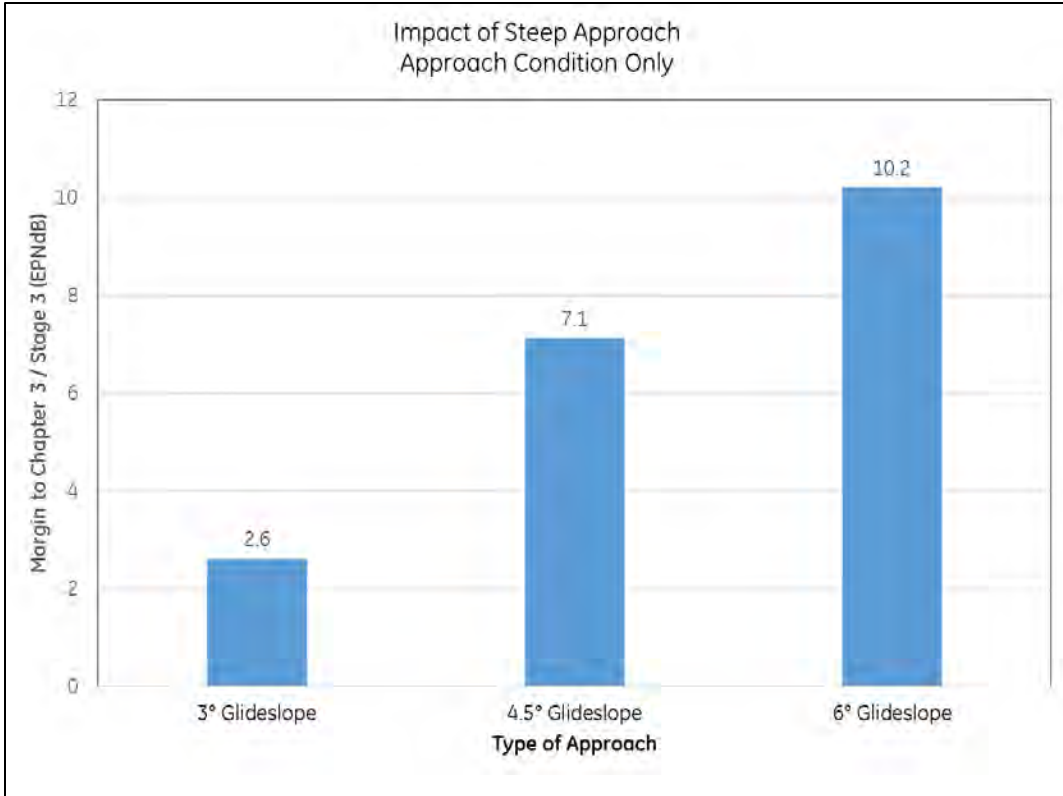
Figure 4.—Impact of glideslope angle on approach noise.
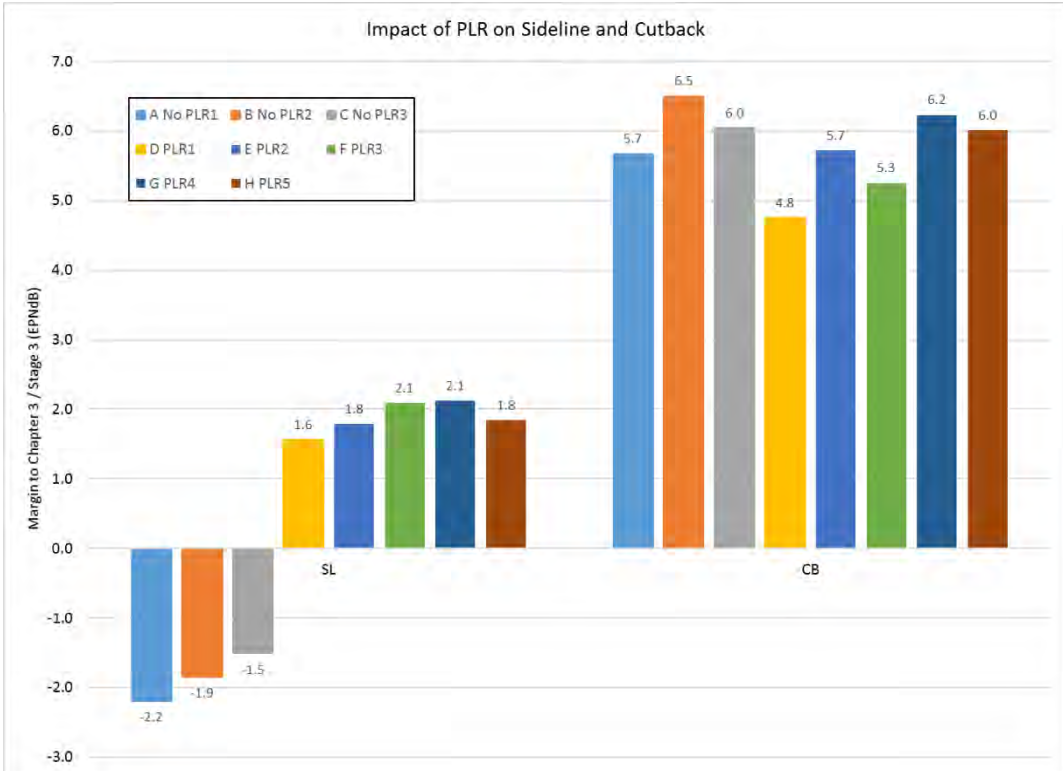
Figure 5.—Results of trajectory study on sideline and flyover with cutback noise.
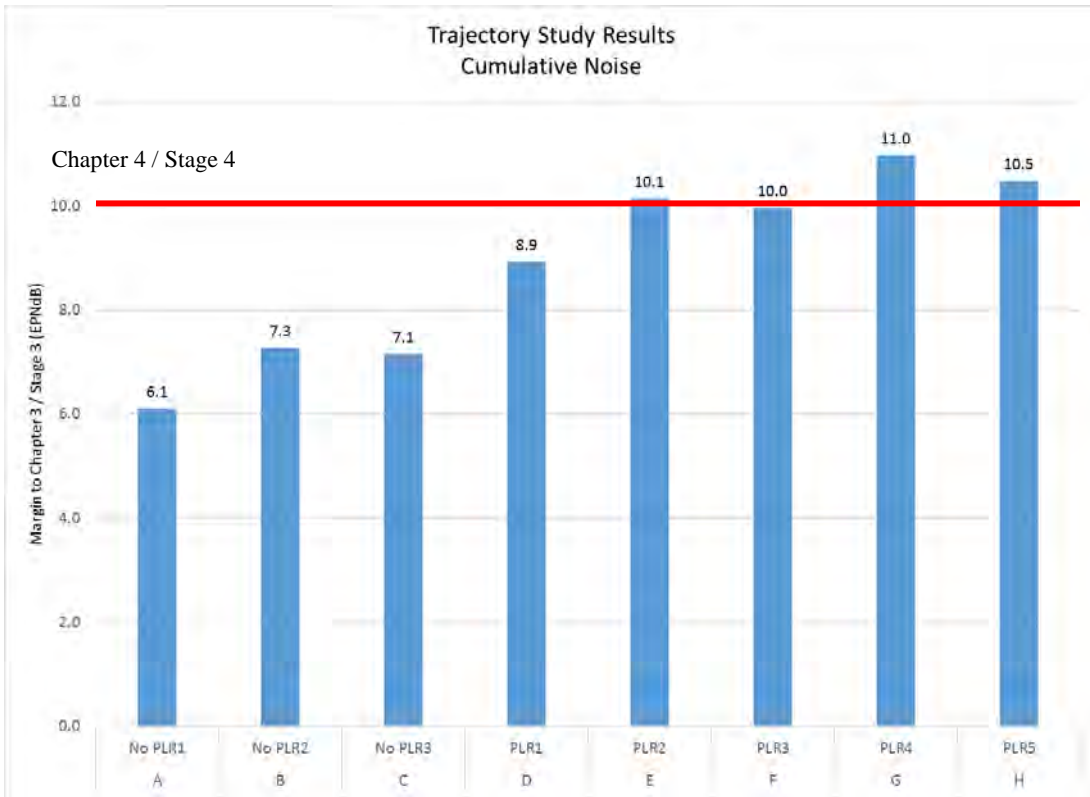
Figure 6.—PLR trajectory study impact on cumulative noise (using 3° approach).
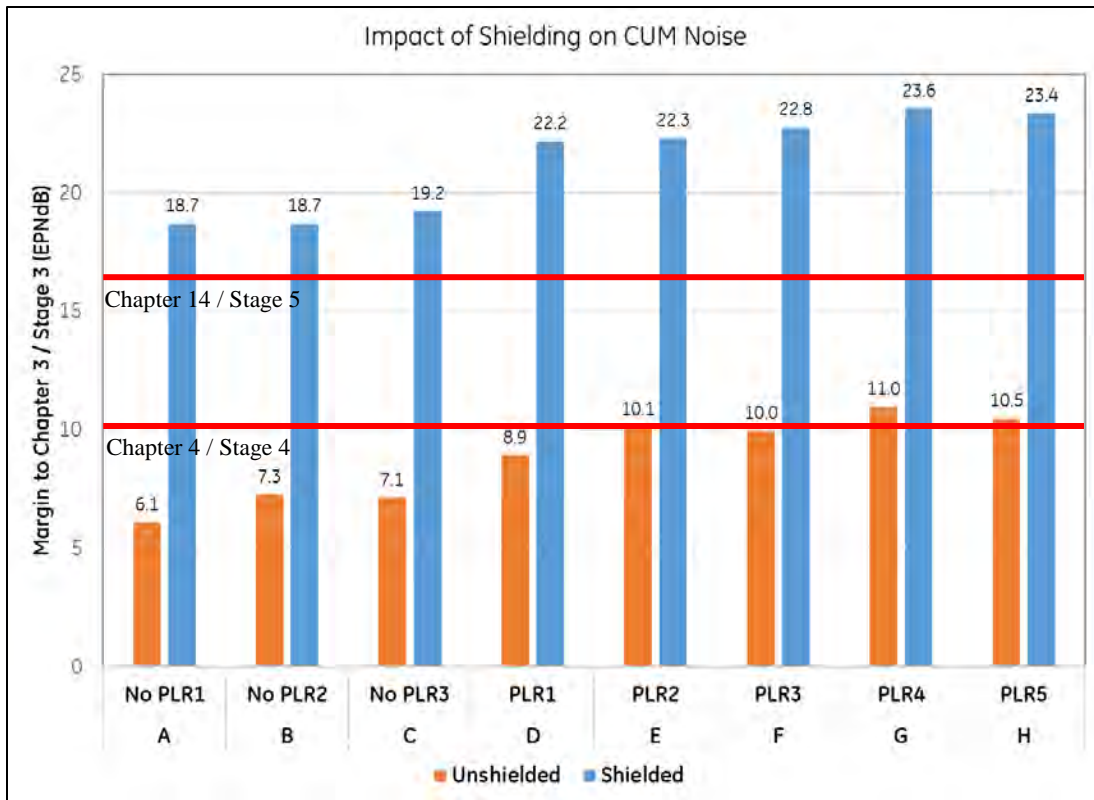
Figure 7.—Impact of applying shielding on cumulative noise for the study trajectories.

6.0 Summary

The trajectory study shows that both the increase of the Approach glideslope and the use of PLR for takeoff significantly reduces the noise of the N+2 aircraft. The best results on takeoff for this airplane and engine combination occur with improved takeoff procedure combinations with a PLR thrust reduction on climb out, until the standard initiated cutback occurs. The impact on Sideline noise improves from having a negative margin to the rule without PLR to having a positive margin to the rule for the PLR cases. In general, the PLRs lead to lower altitudes for the Flyover with Cutback point. However, by employing improved takeoff procedure combinations, the PLR penalty on Flyover with Cutback can be reduced and potentially eliminated. Note that these results are nominal (50 percent confidence) preliminary design data with no implied guarantee or commitment on the part of GE Aviation.

On Approach, the steeper the glideslope, the higher the airplane over the microphones, the lower the thrust required, and the lower the noise level. However, airframe noise may increase more than indicated in this study if safe steep descent requires additional control devices, which was not investigated.

Significant noise reduction results from placing the engine system above the wing and using the wing and body to shield the inlet and jet noise. Even though the noise benefits are impressive, caution is urged regarding relying on these benefits prematurely. Only a simplified aircraft design analysis was performed with no engine cycle changes. Further, a very large performance impact needs to be mitigated to insure these benefits can be realized. More work needs to be done to retire the risks of such an installation before noise benefits from shielding are fully realized.

The following studies are recommended, resources permitting:

a) System noise studies assuming more realistic steep approaches, including airframe noise and safety
b) System noise studies using Mixed Flow Turbofan cycles
c) Trade studies to identify best technologies to close the gap to future noise goals.

Appendix B.—Lockheed Martin Report

LOCKHEED MARTIN CORPORATION
LOCKHEED MARTIN AERONAUTICS COMPANY—PALMDALE

GE Global Research's NASA Prime Contract NNC15CA02C "Evaluation of Low Noise Integration Concepts and Propulsion Technologies for Future Supersonic Civil Transports"

Low Noise Technologies for Low Boom Aircraft: Achieving Chapter 14 Minus 10 EPNdB
CDRL 001: Initial Assessment of Cruise Efficiency/Sonic Boom
CDRL 002: Report of Findings/Recommendations
CDRL 003: Report of Findings/Recommendations of Trajectory Optimization Studies

Technical Point of Contact:

Dr. Anthony Pilon

Email: tony.pilon@lmco.com

Phone: (661) 572–7197

Fax: (661) 572–5798

1011 Lockheed Way

Mail Zone: 1100

Palmdale, CA 93599-1100

Principal Investigator: John Morgenstern
Additional Investigators: Dr. Anthony Pilon, Dr. Michael Buonanno

1.0 Vehicle Performance Assessment With Top Mounted Engines Versus Below Wing Engines

1.1 Airport Noise

1.1.1 Targeting the Chapter 14 limit –10 EPNdB for Supersonic Airplanes (i.e., Stage 4 –17 EPNdB or Stage 3 –27 EPNdB)

Chapter 14 is the new noise standard that is coming into effect in December 2017 for large airplanes (MTOW, maximum take-off weight, greater than 55 metric tons). The goal of this study is to identify noise technologies to achieve a 10 dB margin to Chapter 14 to allow for potential compliance (with margin) with subsonic regulations for a future EIS (Entry into Service) of a commercial supersonic transport.

To put the difficulty of this target noise level into perspective, Concorde's certification numbers were a cumulative +45 EPNdB relative to Stage 3 (reference in section 5.1.1), and thereby, +62 EPNdB relative to the new Chapter 14 limits. The target of Chapter 14 minus 10 EPNdB translates to a 72 EPNdB cumulative reduction from Concorde, or an average reduction of 24 EPNdB at each measurement point.

1.1.2 Supersonic Noise Expected to be Equivalent to Subsonic

In on-going international standards meetings (like International Civil Aviation Organization's SuperSonic Task Group i.e., ICAO's SSTG) there is a popular expectation that supersonic transportation should be no louder than subsonic. Any request to allow greater noise from new supersonic transports is being met with strong opposition. Even if a good case were made and louder limits were enacted for supersonic noise certification, such airplanes would likely be constantly challenged with widespread restrictions to airport access and operations, which greatly reduces vehicle value. The capability for Chapter 14 minus 10 EPNdB would be the final break though providing viable new supersonic transportation.

1.1.3 Achieving Chapter 14 Minus 10 EPNdB With Efficient Performance

Subsonic airplane efficiency and noise has improved greatly since Concorde's first flight in 1969. The improved materials and designs developed to improve propulsive efficiency (e.g., higher bypass ratio) also reduced noise. Advancing subsonic noise standards have caused earlier adoption of new technologies and earlier retirement of older airplanes. Even with this acceleration, subsonic noise standards are met without incurring a massive performance penalty for compliance. Meanwhile, commercial vehicles optimized for supersonic flight (Concorde and TU-144) were louder before noise limits began, and following designs with propulsive improvements were not pursued for either of these vehicles. Meeting subsonic noise standards would result in a massive performance penalty for a supersonic airplane if better means for improving noise are not developed.

This contract is investigating and integrating many unique and new features of supersonic transport design to find better means of improving noise. The current Lockheed Martin (LM) design features strong noise shielding when all engines are mounted on top of the vehicle. However, past investigation of this arrangement has indicated a possible severe loss in vehicle performance due to the engines inducing a loss of lift, whereas, bottom mounted engines produced a lift increase. New methodology and designs can change such an outcome, so we are reassessing top mounted engine performance potential. For this initial investigation, we performed a single analysis case without optimization; and focused on understanding causes and estimating ideal performance potential. While our analysis case did have a large aerodynamic efficiency loss, it indicated the source of the loss along with a possible means of negating it and even a possible means for increasing aerodynamic efficiency with engines located on top of the vehicle.

1.2 Sonic Boom Noise

A standard defining acceptable sonic boom noise is being worked; however, its completion will require human response data from shaped boom flights. Quiet shaped sonic boom designs are predicated on this standard to enable supersonic flight over land. Having supersonic over land capability would particularly boost the market, and thereby number of potential sales, of shorter range and single owner business jets that are likely to be the first products.

1.2.1 Market Multiplier Depending on Performance

With two thirds of subsonic jet traffic flying over land, the market advantage of supersonic over land is clearly present. However, shaping boom to be acceptably quiet could penalize performance enough to reduce or negate the advantage. With Lockheed Martin's 1044 baseline design, we have not run an exhaustive back-to-back optimized N-wave boom design versus optimized shaped boom design to conclude that our shaped boom performance does yield an advantage. However, we do believe our results indicate that a net advantage can be achieved with a shaped sonic boom design.

1.2.2 Engine Location Effect on Boom Loudness and Performance

For the engines above the wing instead of under the wing, we want to understand both:

- if shaped boom is quieter or louder
- if performance with that shaped boom is better or worse.

Boom shaping depends on an integration of all vehicle components with many interactions, so it is not practical to analyze all the interactions involved in this conceptual assessment. Off-track boom with engines under the wing tends to degrade a little from optimum due to the engine alignment change at different roll angles, while engines on top of the wing may generally have less degradation. Boom loudness seems to have a comparable potential for both engine locations and a dB or two better off-track boom may be easier to achieve with the engines on top.

The performance impact for shaping boom is very complex. From this nonoptimized design, we do not see any reason for a substantial difference in performance impact for shaping boom with the engines on top. In summary, the boom shaping potential seems similar for both engine locations. Specifically, a similar loudness potential for either engine location, with perhaps a dB or two better potential near the edge of the sonic boom carpet for engines on top.

1.3 Cruise Efficiency and Range Performance

1.3.1 Supersonic Performance Success (Versus Subsonic)

Good supersonic efficiency and range capability are essential characteristics for supersonic transportation viability. The absolute level needed for viability is a complicated determination, but incremental changes can be limited to fewer characteristics and are sufficient for assessing differences due to engine location. Increased range allows more market and larger time savings for greater passenger value. Better range efficiency means lower fuel burned. And the fuel savings is compounded because it also reduces the vehicle weight needed to carry the fuel. The value of saving a pound of fuel on a supersonic transport is twice the value of saving a pound on a subsonic transport. This higher value on weight savings requires the selection of more expensive materials and requires great emphasis on maximizing cruise efficiency.

1.3.2 Range Performance From Aerodynamics, Propulsion and Weight

Range performance is assessed with mission analysis codes that calculate airport to airport range performance including reserve fuel. Supersonic transport range is dominated by cruise efficiency. It can be understood and well estimated by the Breguet range equation: velocity * L/D * 1/SFC * $\ln(W_{MTOW}/W_{[MZFW+reserve\ fuel+misc]})$, where SFC is specific fuel consumption (lb_{thrust} / lb_{fuel}), MTOW is maximum takeoff weight full of fuel, (divided by) MZFW maximum zero fuel weight + reserve fuel + miscellaneous fuel (for taxi, reduced climb efficiency and some ATC, air traffic control, allowance mostly for airport landing approach). For moving the engines from below the wing to above, nearly all the change is in the cruise L/D term. Propulsion SFC tends to be a barely significant amount worse due to higher flow velocity at the inlets (and its reduction of pressure recovery) and weight tends to be barely significantly lighter for the top mounting. So, the combined change in propulsion and weight efficiencies is insignificant. The change in L/D will be initially examined by a CFD comparison between the two locations, though the new engine location on top of the wing will be less optimized since the under-wing geometry was refined through multiple CFD iterations. This difference will be considered when making comparisons between CFD results for the engines on top versus previous results with the engines below from the prior study (NASA/CR—2015-218719). The CFD solution will also be run in a manner suitable for assessment of sonic boom changes, with the same nonoptimum comparison caveat stated above for L/D.

2.0 Engines on Top Effects

These section 2 assessments are based a combination of the analysis shown, experience with many iterations of related analyses and engineering judgement. Because the goal of this quick assessment was not to estimate the performance of the configuration shown; but rather, project the performance potential of the new engines on top location relative to the old engines on the bottom. The previous configuration had a certain amount of refinement and optimization iterations performed on the design shape. This new configuration had some careful and experienced layout to reduce flow constriction between the nacelles, but only this single analysis, without any design drag optimization or sonic boom reshaping. So, results are presented along with estimations of optimized performance and loudness potentials. Furthermore, additional analysis refinement was added later in the contract as shown in section 4.0.

2.1 Engines on Top CFD

The following is relative to CFD of the baseline with outboard engines mounted under the wing. The outboard engines on top of the wing CFD force prediction (same angle-of-attack or alpha) indicates that 9 percent of lift has been lost, but drag also got 2 percent worse, instead of getting better with the reduction in lift. This is actually a comparatively small lift loss, because scaling previous designs to this size and condition resulted in lift losses twice as big. In the top CFD picture of Figure 1, the high pressure compression (red) induced by the forward portion of the wing nacelles is now on top of the wing, instead of underneath it. Between the forces and this picture, it is clear that the reduction in aerodynamic efficiency is due to the induced lift loss. This CFD indicates a –9 percent change in L/D, obviously, an impact to be avoided. With more optimization and refinement effort, additional improvement options are likely to be discovered.

The baseline engines were located under the wing trailing edge so the strong compressive disturbance from their forward nacelle portion would reflect off the wing downward for increased lift. When the engines are moved on top of the wing, that disturbance reflects up, generating a loss of lift. This nacelle compression is stronger than any other vehicle feature because the nacelle area change is greater versus length. If the nacelle area change could be reduced, the induced lift-loss would diminish.

The wing nacelle and pylon geometry were refined but no further optimization was performed

The lower wing reflex was removed but no upper reflex was added and no re-area ruling performed
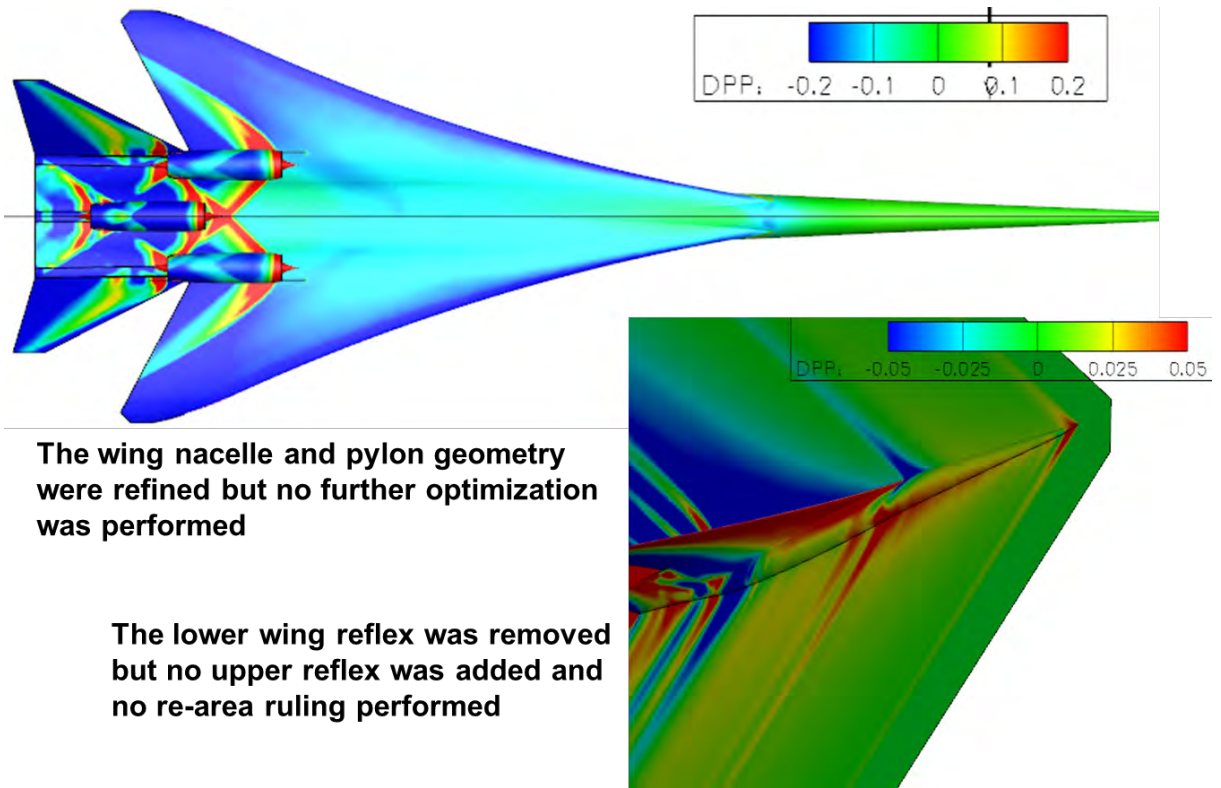
Figure 1.—CFD indicates good positioning for low drag, with perhaps some room for further improvement and some redesign needed for boom compliance.

2.2   Engines on Top: Sonic Boom

The CFD delta pressure data, which is extracted for sonic boom at a radius of 732 ft (18.3 semispans), is shown in Figure 2 for directly below the vehicle (undertrack). The disturbance is the same until the under wing nacelle shock is first evident at 150 ft back of the baseline 1044-02 signature. This pressures thereafter change quite a bit, which should be expected for moving the vehicle's component that causes the greatest DP/Ps. However, the lack of engines under the wing leaves a lower amplitude average aft pressure, which could have resulted in a slight aft shock reduction if its final expansion spike at 255 ft was not stronger than the baseline. Instead, the stronger final spike persists into a greater ground aft shock strength as shown in Figure 3.
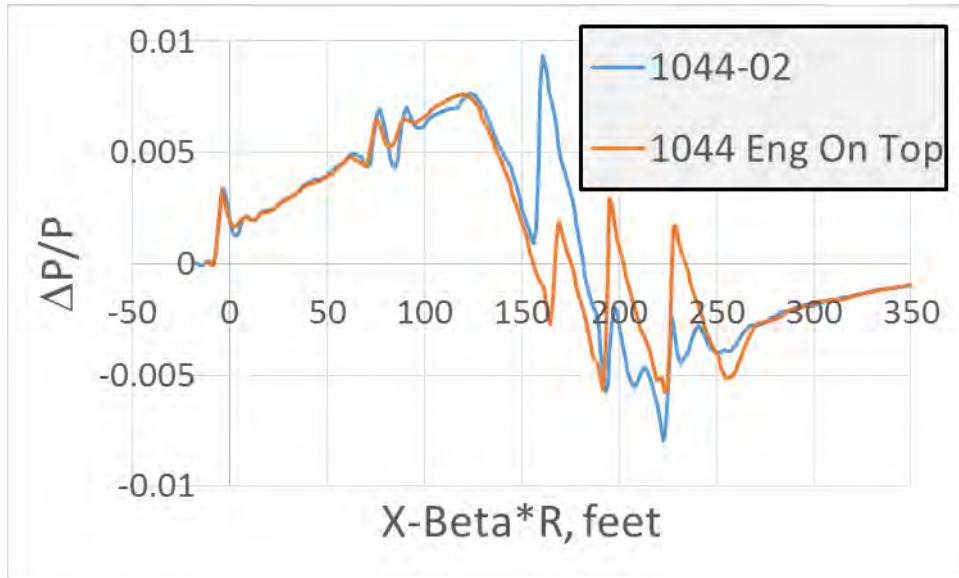
Figure 2.—Repositioning of the engines changes the vehicle's pressure disturbance shape.
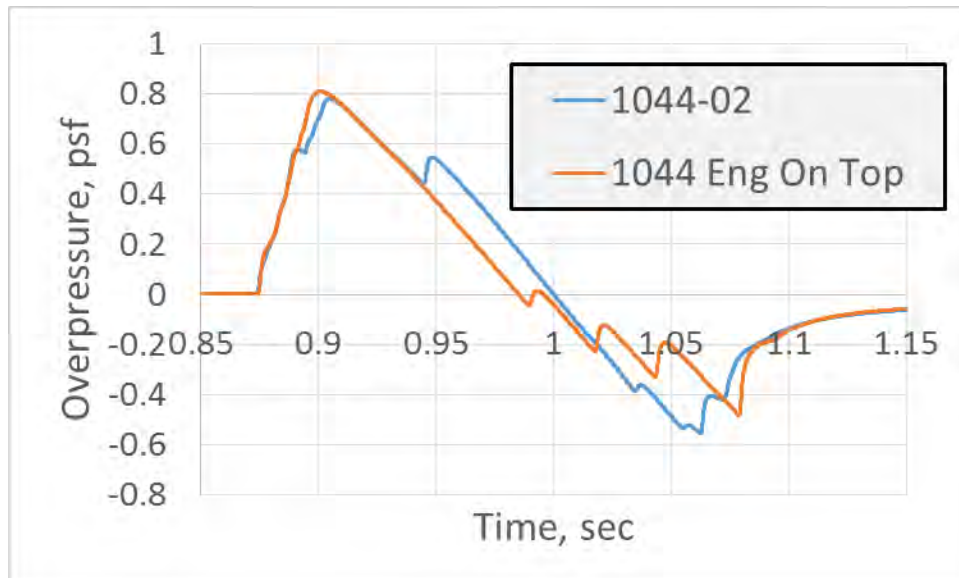
Figure 3.—The pressure disturbance shape change due to engines on top affects the ground sonic boom, but appears easily repairable.

The undertrack ground pressure signatures are shown in Figure 3 for the baseline and for the wing engines moved on top. The front ramp looks nearly the same, which is expectd since the geometries are identical until the nacelle under the wing disturbance begins. The slightly greater rounding of the front shock, rounding of the wiggles around 0.89 sec (80 ft in Figure 2) and greater average pressure from 0.89 to 0.90 sec (95 to 120 ft in Figure 2) are likely from the lower (Euler) grid resolution used in this quick assessment, but these differences did not affect the loudness of the front portion of this signature. The undertrack stronger aft shock for engines on top is responsible for 2 PLdB greater loudness and the engines on top is 1-3 PLdB louder throughout their carpets at cruise, but this is not a representative difference. After even much smaller changes to a design, a vehicle needs to be re-boom-ruled. It looks like some small and easy to integrate recontouring of the lower aft deck or fuselage below the deck could eliminate the 1-3 PLdB higher loudness across the carpet and perhaps even a dB or two more at some angles.

In summary, there is a potential to achieve nearly optimal full-carpet sonic boom with either the engines mounted below or above the wing.

2.3   Engines on Top: Performance

As discussed previously, moving the engines from below the wing to on top is not expected to affect the propulsion SFC or the weight of the vehicle much, especially compared to the aerodynamic effect. Aerodynamically with the engines on top, we had cases with –7 to –20 percent in L/D before optimization. The reduction is caused by the propulsion induced lift effect for underwing nacelles being lost and induced downforce for nacelles above the wing. There was some very successful maximization of induced lift for nacelles under wings, but it should be beneficial to minimize induced lift loss for engines on top. The CFD analysis of the upper aft deck, with the shock waves bouncing between the nacelles, gives indications that wave drag can be reduced a little by varying nacelle fore-aft locations and refining their pylon shapes. The nacelles are a very significant portion of the vehicle's wave drag.

3.0   Considerations for Achieving Airport Noise Shielding and High Cruise L/D

Supersonic wave drag and its consequential more than halving of cruise L/D versus subsonic transports causes supersonic transports to struggle in economic competition with subsonic ones. Despite their shorter time burning fuel countering most of their higher drag (twice the fuel burn rate for half the time would result in matching fuel usage) and despite the higher value of their productivity and time savings, because engine efficiency also degrades in supersonic flow. Supersonic SFC increases the fuel flow rate by about a 1.5 factor beyond just the amount of higher drag, resulting in additional fuel weight to carry, along with the additional propulsion weight needed for the greater thrust. Therefore, improving supersonic L/D provides a compounded benefit (section 1.3.1 sizing growth factor) to supersonic efficiency.

An ideal vehicle would integrate airport noise shielding benefits, quiet shaped sonic boom (without a significant performance penalty) and the highest range efficiency possible. Trading shielding for L/D would ideally be avoided. While some positions are worse than others, a nacelle causes a lot of drag anywhere it is located. Additional work reducing the sources of nacelle drag should be particularly beneficial for a shaped sonic boom vehicle.

4.0 Refined Assessments of Nacelles on Top Shaped Sonic Boom and Performance

Additional refinement of the nacelle positioning and on-top shaped boom and performance was performed.

4.1 Nacelles on Top Shaped Sonic Boom Optimization

For airport noise shielding, the wing engines were moved to the top of the vehicle inside of the V-tails. To create well optimized nacelles on-top positioning without needing a lot of funding for time-consuming geometry refinements, faster linear optimization was used. The optimization resulted in improved shaped boom weight capability and quieter boom, increasing the weight to match previous takeoff noise studies and reducing sonic boom loudness from 81.8 to 78.9 PLdB at the maximum carpet loudness point, which were both undertrack in Figure 4.

These linear analysis results were first calibrated, with a difference function, to match the previous CFD results, as illustrated below in Figure 5. The linear analysis was then used, with the difference increment, for an incrementally linear optimization. Given that the difference function was small and the optimization changes were also small area changes, it is believed that similar results and improvement potential would be found with higher fidelity tools. For this application, it was important to show that a well-optimized result would achieve similarly quiet sonic boom.

4.2 Nacelles on Top Aerodynamic Optimization

4.2.1 Nacelles on Top Position Refinement

The linear optimization resulted in an outboard nacelle position that was 1 ft forward of the original CFD analyzed position shown in Figure 55. There was a slightly better position aerodynamically, which had the center nacelle moved aft a few feet, but that location would reduce the shielding that this program was pursuing, so it was not further pursued. The nacelles below/above to wing difference is substantially the same. Versus nacelles below the wing, above the wing nacelles reduced the cruise L/D (re-trimmed) by 7 percent, which reduces maximum range by 8 percent. Overall, a significant reduction that should be avoided.

The main reason for the L/D reduction, as mentioned previously, is the removal of nacelle induced lift below the wing and its partial re-occurrence as induced lift loss above the wing. If the nacelle maximum radius increase of 7 in. could be reduced to 3 in., the 7 percent L/D penalty would go away, along with most of the difference in drag between the two locations. (Further details are in the updated section 3.0.)
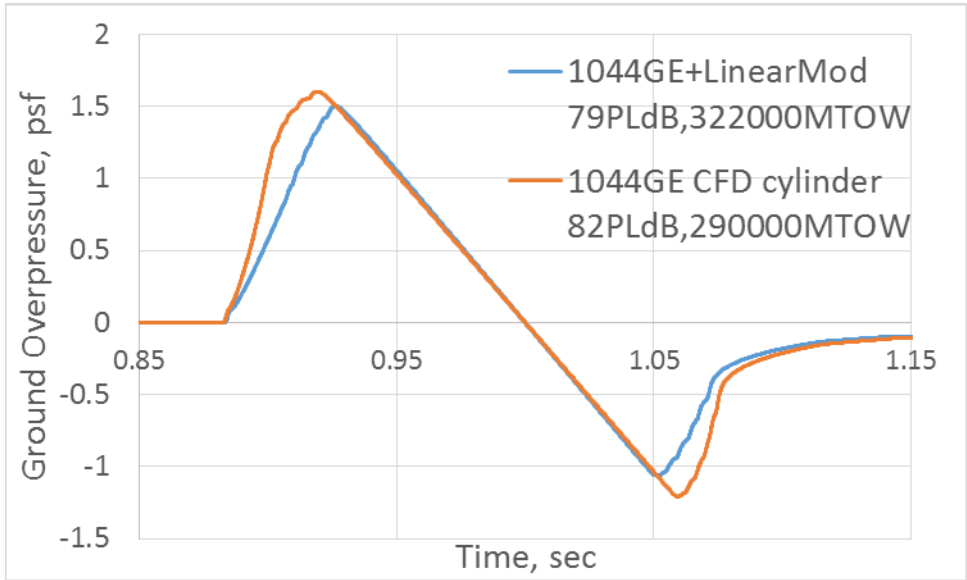
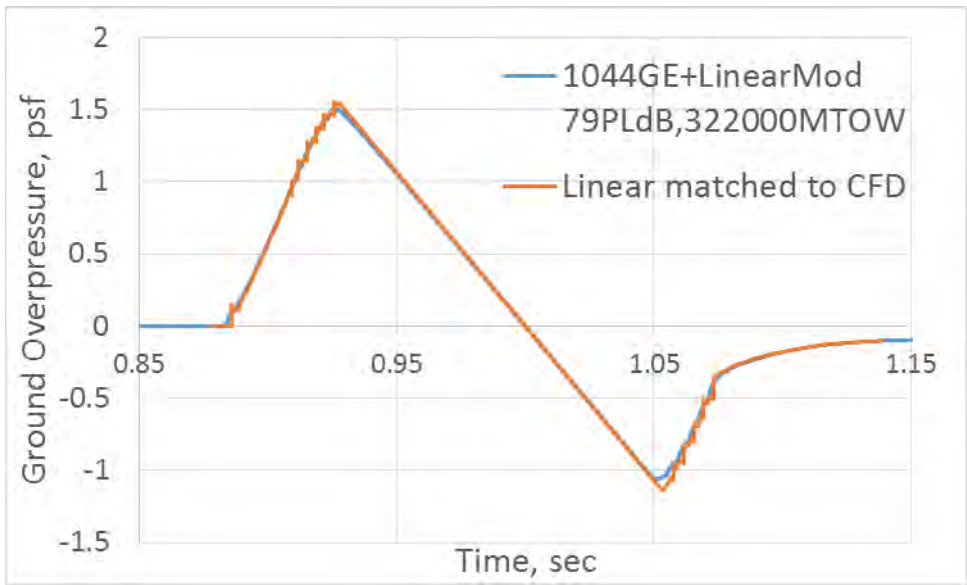Figure 4.—Optimization resulted in improved weight capability and quieter boom.

Figure 5.—The linear analysis used in Figure 4, was first calibrated to match the previous CFD results.

5.0   Trajectory Optimization

5.1   Background

5.1.1   Concorde Noise and Trajectory Speed

Based on preliminary noise assessments by GE in Year 1 of the program, both LM and GE recommended a trajectory optimization study as part of Year 2 tasks. Based on prior technology research, various techniques have been developed for reducing noise of supersonic aircraft using trajectory variations in speed and throttle. The Concorde was designed just before noise regulations went into effect. Noise reduction technology was limited and noise measurements were just beginning as it went into service, so we know its cumulative noise of +44.9 EPNdB relative to Stage 3 (112.0 = SL+11.9, 119.5 = TO+17.8, 117.0 = AP+15.1 from the FAA website's file "Turbojets_ForeignCert.xls"). In flight testing, they quantified that the Concorde was worse than any other subsonic transport, and they worked to mitigate its noise levels. They found a small benefit by exploiting a unique characteristic of its design, specifically that its drag reduced significantly as it accelerated faster than its takeoff speed because its minimum drag speed was about 350 KCAS (knots calibrated air speed). The Concorde was assessed for noise at V2 + 35 (KCAS) instead of the usual V2 + 10 (KCAS) subsonic typical practice. This speed profile resulted from the Concorde's unique drag versus speed characteristic and matched the AEO (all engines operating) speed gain that was used operationally.

Higher speeds were previously investigated for our N+2 design (NASA/CR—2013-217820, NASA/CR—2015-218719) and in work done for previous business jet studies. This is particularly effective for a delta-wing design because its modest takeoff flap deflections without slots, create very little drag or lift down the runway until they rotate, whereas a 3-4 engine subsonic airplane's high-lift system drag may be almost as high in drag before rotation as after. (Twin-engine subsonic aircraft fall between these extremes, because they tend toward bigger wings and less extreme high lift drag to counter their 50 percent drop in thrust with an engine-out.)

5.1.2   Low Drag Systems for Low Speeds (Like Subsonic High Lift)

Designs utilizing low aspect ratio, delta-type wings, like Concorde, substantially improve in L/D as they accelerate to a V2 + 35 (KCAS) climb-out speed. This was particularly true for Concorde because it's ogive planform was shaped to maximize LE (leading edge) vortex separation and strength to generate additional lift; however, the additional vortex lift comes with much more drag (without LE suction, reference Polhamus, E.C.; "Predictions of vortex-lift characteristics by a leading-edge suction analogy", Journal of Aircraft, Vol. 8, No. 4 (1971), pp. 193–199.) reducing the low L/D even further, and increasing the thrust required. The weight savings of a smaller wing was justified by Concorde's high thrust-to-weight ratio propulsion solution. Their zero bypass-ratio afterburning turbojet engine entered service 40 years ago, but had a higher thrust-to-weight than (quieter) supersonic propulsion solutions currently under consideration. But an afterburning turbojet's high thrust-to-weight results from exhaust velocities 2 1/2 times higher than today's subsonic engines—and jet noise increases to the 6th to 8th power of that velocity.

The LM airframe and GE engine developed for NASA's N+2 Supersonic study (NASA/CR—2015-218719) was designed for quiet sonic boom and quiet community noise limits (section 1.1.1). To meet subsonic noise limits, it employs LE flaps, which on a high sweep LE are designed to suppress vortex separation and thereby "reduce drag"—not generate "high lift" like subsonic LE flaps & slats. (By reducing vortex separation, the LE flap actually reduces lift.) The N+2 design used in this study employs a vortex suppressing LE flap, so its drag at lower speeds increases less severely than Concorde's.

5.1.3 Programmed Lapse Rate

NASA's large effort in their High Speed Research (HSR) program of the 1990's, targeted a noise goal of meeting the FAA's Stage 3 limits plus a margin considered adequate by potential engine and airframe builders. One procedure that was particularly popular was known as PLR for Programmed Lapse Rate. PLR means that the engine controls automatically (the variation always occurs, it is not selectable) reduce the output of the engines by –10 percent (in velocity at a constant mass flow) after clearing the takeoff obstacle height. This aided the noise at the most difficult sideline certification condition. (Sideline noise peaks as an airplane flies through altitudes around 1000 ft. Below 1000 ft, the ground attenuates noise to a greater and greater extent until a maximum attenuation is reached at the ground.) This extra thrust would also be available for use in any emergency situations and automatically restored in engine-out situations.

5.1.4 Takeoff Noise Study

This takeoff noise study uses the N+2 quiet shaped sonic boom airplane with its wing engines relocated on top for engine source noise shielding. This study combines the effects of takeoff parameter variations and their effect on noise. LM-proprietary improved takeoff procedure combinations, termed PVR#, are also shown. The goal is to find the best combinations for achieving low noise with high efficiency. These variations are performed stepwise into a final integrated combination, quantifying their individual effectiveness along with their effectiveness in combination.

5.1.5 Approach Procedures for Reduced Noise

Approach noise of subsonic transports tends to be dominated by fan noise and airframe noise, as fans have become quieter. Supersonic vehicles tend to have lower BPR's and more room for noise absorbing liner in the inlet ahead of their fans, which both tend to lower fan noise. Auxiliary inlet flow can sometimes be reduced to near choking (sonic) to reduce fan noise from propagating out of the inlet. Supersonic airframe noise should also benefit from far lower flap loadings (or even no flaps, like Concorde) without slots and without other flow separations. However, higher drag and higher exhaust velocities can result in jet noise being significant on approach for supersonic configurations. Several procedures can be used but the most straightforward and effective tends to be higher approach glide slope angles, which have the double benefit of reducing thrust needed and increasing height above the noise measurement point. Higher slopes of 6.0° and 4.5° are assessed in addition to the standard 3.0°. Higher slopes are likely to provide negligible improvement because thrust is already close to idle at 6.0°. While there are safety issues involved in higher glide slope approach angles, there are many technologies that may be developed to address such issues.

5.1.6 Study Limitations

Another design technique for increasing low speed L/D is increased span. Implementation is usually through higher AR, often with a lower sweep outboard wing. Such a modification mitigates low speed drag (like HSR's PTC design), but increases high speed drag a little and significantly increases wing weight. For this study, airframe variations such as an initial design with higher span and shaped sonic boom quieter than 80 PLdB were not available. Creating such an airframe design is an expensive task, but should eventually be explored. Likewise, resizing the engine offers many trade possibilities for reducing noise. For the variations investigated in this study, the resulting designs retain their quiet shaped boom loudness. This study was completed at an extremely low funding level by carefully limiting the trades to variations that would not require resizing of the shaped boom vehicle. All the noise improvements achieved by the trajectory variations have no negative effect on the vehicle's mission performance, range, fuel burn, etc., meaning there was no vehicle or engine re-sizing (sized 100 percent). Unfortunately, optimizing a shaped boom design is much more laborious. Care must be taken to use only optimized designs for trend and sizing sensitivities or inaccurate values will result.

5.2 Trajectory Optimization Results

Figure 6 shows the landing and takeoff trajectory of the N+2 vehicle from the prior study (NASA/CR—2015-218719). This trajectory was used by GE for the baseline noise assessments.
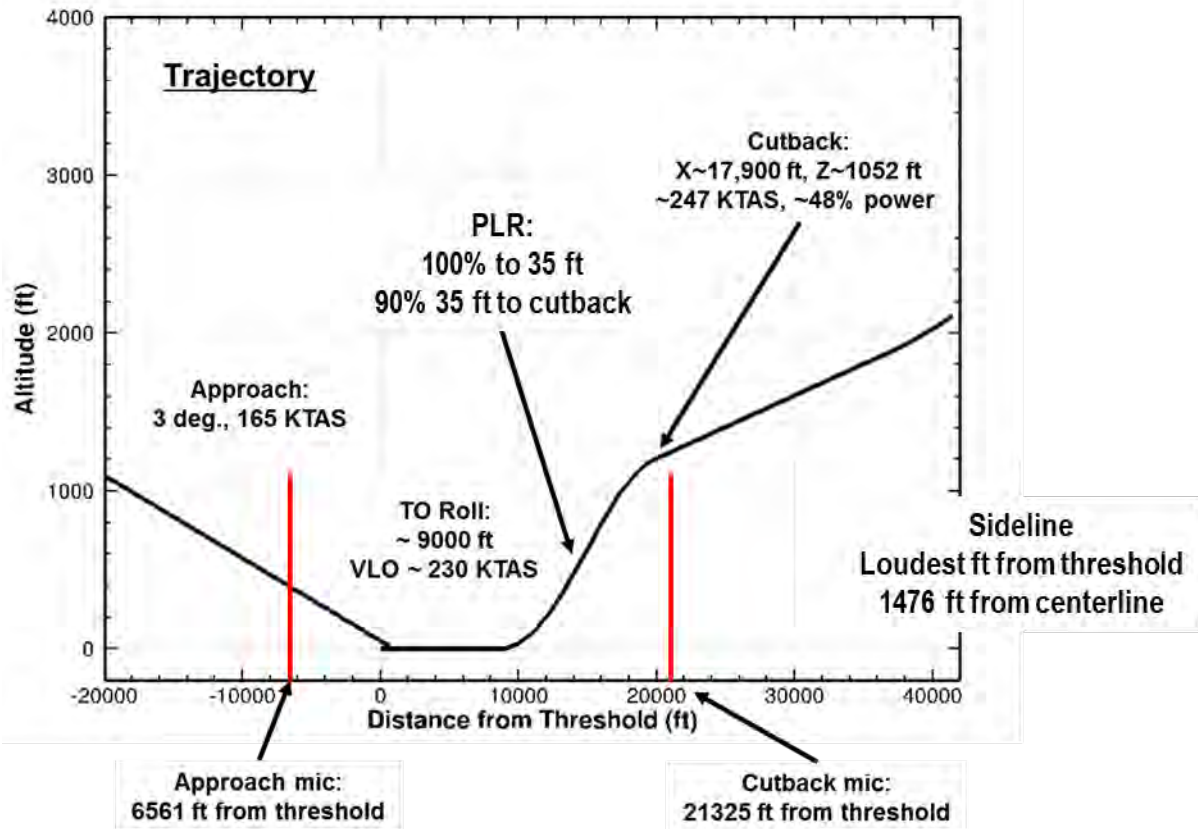

Figure 6.—The takeoff trajectory used for sizing and noise analysis of this N+2 vehicle from the prior study (NASA/CR—2015-218719).

Trajectory optimization considered procedures such as PLR (section 5.1.3) and PVR (company proprietary variation procedures) with different levels of automatic thrust cutback or runway over-rate at different rotation speeds. Steeper glide slopes than 3° (4.5° and 6°) at Approach were also investigated. The takeoff trajectories are summarized in Table 1. The results were run step-wise:

A-C   speed steps no PLR
D-F   speed steps w/PLR
G   PVR1
H   PVR2
I-K   PVR1 with later takeoff cutback (I same as G)
L-N   PVR3 with later takeoff cutback (L improves upon H)
C-I-L These compare PLR, PVR1, PVR3 at the same V2+35 KCAS

TABLE 1.—TAKEOFF PARAMETER VARIATIONS FOR TRAJECTORIES
AND GE'S NOISE ASSESSMENTS

	Sized	Climb	Cutback	h (ft)	KCAS	Comment
A.	100%	100%	57.8%	1362	V2+10	no PLR
B.	100%	100%	53.2%	1300	V2+20	no PLR
C.	100%	100%	48.4%	1162	V2+35	no PLR
D.	100%	90%	57.7%	1250	V2+10	−10% PLR
E.	100%	90%	53.1%	1203	V2+20	−10% PLR
F.	100%	90%	48.2%	1082	V2+35	−10% PLR
G.	100%	PVR1	PVR1	PVR1	PVR1	PVR1
H.	100%	PVR2	PVR2	PVR2	PVR2	PVR2
I.	100%	PVR1	PVR1	PVR1	PVR1	Base10.0° to CB
J.	100%	PVR1	PVR1	PVR1	PVR1	18.0° to CB mic
K.	100%	PVR1	PVR1	PVR1	PVR1	24.0° to CB mic
L.	100%	PVR3	PVR3	PVR3	PVR3	Base10.0° to CB
M.	100%	PVR3	PVR3	PVR3	PVR3	18.0° to CB mic
N.	100%	PVR3	PVR3	PVR3	PVR3	24.0° to CB mic
I-J-K, L-M-N compare later cutback throttle reduction					
C-I-L compare PLR, PVR1, PVR3					
G same as I					

Noise analysis for trajectories A-H are documented in the GE section of the report. This study found that takeoff procedures, like PLR and PVR, provide large improvements and should be included in the optimization of all supersonic designs.

References

1. Morgenstern et al., "Advanced Concept Studies for Supersonic Commercial Transports Entering Service in the 2018-2020 Period Phase 2," NASA/CR—2015-218719.
2. Brown, C., "Developing an Empirical Model for Jet-Surface Interaction Noise," *AIAA-2014-0878*.
3. Thomas et al., "Hybrid Wing Body Aircraft System Noise Assessment with Propulsion Airframe Aeroacoustic Experiments," *AIAA-2010-3913*.
4. Cheung et al., "Fine-Scale Turbulent Noise Predictions from Non-Axisymmetric Jets," *International Journal of Aeroacoustics*, Volume 14, Issue 3–4, 457–487, August 2015.
5. Heidmann, M., "Interim Prediction Method for Fan and Compressor Source Noise," *NASA TM X-71763*.
6. Paliath, U., Shen, H., Avancha, R., and Shieh, C, "Large Eddy Simulation for Jets from Chevron and Dual Flow Nozzle," *AIAA-2011-2881*.
7. Paliath, U., Premasuthan, S., "Large Eddy Simulation for Jet Installation Effects," *AIAA-2013-2137*.
8. Bodony, D.J., "Analysis of Sponge Zone for Computational Fluid Mechanics," *Journal of Computational Physics*, 212, 681–702 (2006).
9. Martens, S., "Jet Noise Reduction Technology Development at GE Aircraft Engines," *ICAS 2002 Congress*.
10. C.K.W. Tam, N.N. Pastouchenko, R.H. Schlinker, "Noise Source Distribution in Supersonic Jets," *Journal of Sound and Vibration*, 291: 1–2, 192–201 (2006).